Experimental and Numerical Investigations into Fundamental Mechanisms Controlling Particle Transport in Saturated Porous Media

Po-Chieh Liu

Submitted in partial fulfillment of the
requirements for the degree
of Doctor of Philosophy
in the Graduate School of Arts and Sciences

COLUMBIA UNIVERSITY

2016

ABSTRACT

Experimental and Numerical Investigations into Fundamental Mechanisms Controlling Particle Transport in Saturated Porous Media

Po-Chieh Liu

This dissertation presents the results of a series of experimental and numerical studies designed to advance knowledge of the fundamental mechanisms controlling colloidal particle transport in saturated porous media. That colloidal particles facilitate contaminant transport in porous media, or act as contaminant sources, is well known, and also widely recognized as important to environmental and health issues around the world. Many prior and ongoing studies are aimed at understanding particle transport and deposition behavior in saturated porous media, and these studies have generated a broad range of knowledge regarding particle fate and transport mechanisms. However, the prediction of particle transport behavior still remains challenging, not least because the particle transport processes themselves still include many unknown factors. The goal of the work reported in this dissertation, was to advance understanding of the influence of varying flow velocity conditions, flow direction, particle size and mixed particle populations on particle transport processes. In order to meet this goal, a new numerical model for particle transport was developed, and standard laboratory column test protocols were modified to enable the imposition of varying flow conditions during a test, as well as visualization of particle concentrations within the interior of a column. In addition, and in collaboration with other researchers, numerical modeling work was also undertaken to provide insight into the processes governing particle transport at an instrumented field site.

Numerical models have been used extensively to investigate a wide variety of

engineering and applied science problems, including those involving colloidal particle transport in saturated porous media. For the research presented in this dissertation, a new numerical model, termed the Kinetic Colloid Transport Model (KCTM), was developed and implemented using the Matlab platform. The KCTM is based on a one-dimensional (1-D) advection-dispersion-sorption equation coupled with different kinetic sub-models for simulating particle interactions with the solid phase of a porous medium, including irreversible and reversible attachment mechanisms, as well as two-attachment site and two-particle population behaviors. The KCTM is capable of directly simulating particle transport behavior for a given set of initial and boundary conditions, and also inversely solving for the sub-model kinetic parameters based on particle concentrations observed during column or field experiments. To validate the KCTM, KCTM results were compared with analytical solutions generated by the STANMOD program and numerical solutions generated by HYDRUS-1D. Simulation of particle breakthrough concentrations during a hypothetical column experiment with fourteen different case studies, involving a range of particle dispersion coefficients as well as attachment and detachment rates, was used for the validation. Agreement between the KCTM results and those generated by STANMOD and HYDRUS-1D, as defined by corresponding R^2 values (all above 0.999), was considered acceptable across all ten case studies. The KCTM has the advantage of modeling a range of particle transport mechanisms, many of which are not accounted for in current open-source or commercially available codes.

Fluctuating or varying velocity conditions are common under many real-world scenarios involving colloidal particle transport, yet are often neglected in laboratory column experiments designed to investigate particle transport behavior. To understand the influence of varying velocity conditions on particle transport, a series of traditional and modified laboratory column experiments was conducted. For the modified column experiments, a protocol was developed to enable the simulation of both increasing and decreasing velocity conditions during a test, as well as condi-

tions involving an increase followed by a decrease in velocity. Laboratory column experiments were performed to examine the downward transport of 2 micron diameter microspheres through a saturated bed of 100 micron diameter glass beads under both constant and varying velocity conditions. The KCTM was simultaneously fit to observed particle concentration breakthrough curves, as well as measured particle concentrations retained in the column at the end of each constant velocity experiment, to obtain a relationship between a dimensionless irreversible kinetic attachment coefficient K_i^* and transport velocity. This relationship was then used to model the results of the varying velocity tests, with limited success. A comparison of the K_i^* values obtained from direct fitting of the varying velocity tests using the KCTM, with the K_i^* values derived from the results of the constant velocity experiments, revealed a potential dependence of K_i^* on the rate of change of transport velocity, which is currently not accounted for in any particle transport model. Overall, the results of this experimental and numerical investigation pointed to the need for better understanding of how varying velocity conditions impact fundamental particle transport mechanisms.

A visualization technique was used to examine the effects of particle size and flow direction on particle transport in a saturated porous medium comprised of 500μm diameter glass beads. Packed column experiments with uniform (100% 1μm or 100% 6μm) and mixed (90% 1μm with 10% 6μm and 90% 6μm with 10% 1μm) polystyrene latex microspheres were performed in one-dimensional upward, horizontal and downward flow fields at a constant velocity of 1.7m/day. Particle concentrations were recorded over time in the interior of a column and at the column exit. Experimental results showed that upward flow conditions generally gave rise to higher retained particle concentrations and lower particle breakthrough concentrations than horizontal and downward flow conditions, indicating that gravitational settling decreases particle transport distances and enhances particle deposition mechanisms. Consistent with prior studies, results also showed increasing particle retention with increasing parti-

cle size. The 1μm particle tests results were successfully modeled using a first order, irreversible particle attachment model, indicating little filtration of this particle size within the glass bead columns. Modeling of the 6μm particle tests required a two-site kinetic modeling approach, that accounted for particle interactions with the surfaces of the glass beads as well as straining of particles at bead-bead contact points. The presence of a second particle population had little impact on the transport of the 1μm particles. For the 6μm particles, the presence of the second particle population had the most impact during downward flow conditions. Overall, the results of this study confirm that gravity, particle size and flow direction impact particle transport processes. The study also reveals that particle size heterogeneity could also impact particle transport under certain conditions. Both of these findings have implications for field-scale modeling of particle transport.

The up-scaling of results obtained from laboratory column experiments to predict particle transport at the field scale is generally reported to under-estimate particle transport distances observed in the field. The over-simplification of column experimental conditions, in comparison to field conditions, or the use of improper kinetic models are two possible reasons leading to such inaccurate predictions. In order to explore the possible hurdles to current up-scaling methods, the KCTM was used to analyze a series of *Escherichia coli* based column experiments using aquifer sand obtained from a field site in Bangladesh, which are described in the collaborative work presented in Appendix A. Four *E. coli* breakthrough curves (BTCs) and two profiles of spatially retained *E. coli* concentrations at the end of an experiment were generated by the column test series. The KCTM successfully modeled the BTC results using a two-population kinetic sub-model. Both one-site and two-site particle attachment sub-models failed to reproduce the observed BTCs. None of the kinetic sub-models could reproduce the observed particle retention profiles, although the two-population sub-model generated similar hyper log-linear profiles to those seem in the experiment results. Low mass recovery rates in the column experiments are one possible reason

why the KCTM failed to fit the retained profiles. The kinetic parameters obtained from the KCTM fits to the column experimental results were incorporated into a two-dimensional transport model, HYDRUS-2D, to predict *E. coli* transport observed at an instrumented field in Bangladesh. Predictions obtained using only irreversible attachments kinetics, reversible attachment kinetics and both reversible and irreversible attachment kinetics performed with RMSE values of 1158, 826, and 99, respectively. The dramatic decrease in RMSE with the application of the two-site kinetic model indicates that E. coli transport at the field site likely involves both reversible and irreversible attachment. An important conclusion of this work was the significance of designing laboratory column experiments that can enable the extraction of kinetic parameters relevant to field scale transport processes.

The numerical and experimental studies presented in this dissertation examined some factors that influence particle fate and transport in saturated porous media, which are commonly overlooked in many conceptual and numerical models of particle behavior. The results of these studies point to a need to better understand how varying velocity conditions, flow direction, particle size and mixed particle populations influence particle fate and transport. The results of these studies also prompt out several recommended future works. For the developed numerical model, current kinetic sub-models imperfectly reproduced experiment results, also inadequately described the particle transport in micro-scale observations, indicating the simplified first-order kinetics are inaccurate for describing actual particle transport behaviors. A non-log-linear kinetic sub-model and corresponding micro-scale experiments are needed for better predictions. Moreover, the effects of particle-particle interaction were proven significant in certain conditions, however, the processes is still unclear. Visualization technique introduced in this research is capable to explore the controlling mechanisms in micro-scale and further provides the foundations for developing non-log-linear kinetic model, quantifying the effects of particle-particle interactions, acceleration, and other uncovered physical/chemical factors on particle transport in

porous media. Advancing understanding of these factors has potential for improving the prediction of colloidal particle transport under real-world, field conditions, which can benefit many programs aimed at reducing the environmental and health impacts of colloid facilitated contaminant transport.

Table of Contents

List of Figures

List of Tables

Acknowledgments

It has been a great journey since I entered Columbia University Civil Engineering. Living and working in a foreign country is really challenging. The experiences over the past five years not only expanded my knowledge about science researches but also strengthened my mind and enlarged my view of the world. It is a very rare gift I can't get without the help from many people.

First and the most important, I am deeply grateful to my Ph.D advisor Professor Patricia J. Culligan who gave me the opportunity to study and research in one of the best universities around the world. Professor Culligan continuously provided helpful comments and suggestions that are vital for high quality academic results. Everything I learned from Professor Culligan is valuable asset to my life. I thank Professor Brian J. Mailloux for continuously showing me how to design and implement complicated experiments and encourage me to broaden my thoughts of my work. I am also indebted to Professor Alexander van Geen, Dr. Andrew S. Ferguson, and Dr. Peter S. K. Knappett for providing technical help and encouragement. I would also like to express my gratitude to my Ph.D committee members Professor Patricia J. Culligan, Pierre Gentine, Brian J. Mailloux, Steve WaiChing Sun, and Haim Waisman for their precious time and their review of the dissertation. I appreciate their cultivating me into an asset to the academia.

To my research group member, Jianqing Du, Robert Elliott, Rebecca Gibson, Diana Hsueh, Raha Hakimdavar, Nandan Shetty, and Ashley Wagner, thank you for your valuable feedback, help, and encouragement. I especially thank my particle transport research member Jianqing Du for his friendship in both work and leisure

life in New York.

I would like to thank my family for their moral support and warm encouragements while I was studying aboard. To my girlfriend, Yi-Chien Lee, thanks for your emotionally and practically support through the good and difficult times of the past years.

Least but not last, I would like to express my gratitude to staffs from Department of Civil Engineering and Engineering Mechanics and Robert A. W. Carleton Strength of Materials Laboratory. Thanks to Scott Kelly for helping me dealing with the complicate studying abroad problems. Thanks to Dr. Adrian Brugger, Dr. Liming Li, Travis Simmons, and Eric Sporer for their technical help and suggestions.

To my beloved family

Chapter 1

Introduction

1.1 Background and motivation of this research

Untreated groundwater is often considered to be a safe water resource [Leber *et al.*, 2011]. An estimated 2 billion people worldwide rely on untreated groundwater for their drinking water supplies. In addition, a significant portion of industrial and agricultural activities also rely on untreated groundwater [Morris *et al.*, 2003; Zektser and Everett, 2004]. Over the past several decades, multiple activities associated with human development, including industrialization, urbanization and population growth, have increased groundwater usage, leading to aquifer degradation and contamination[Foster and Chilton, 2003].

The spread of groundwater contamination via the mechanisms of advection, dispersion and diffusion has been the subject of a very large number of studies. More recently, however, the role of colloid transport in spreading aquifer contamination has received increased attention because of links with associated health risks [Feighery *et al.*, 2013]. For example, colloid transport mechanisms are responsible for the subsurface spread of fecal bacteria, which cause diarrheal diseases that kill an estimated 1.8 million people per year [WHO, 2004]. Colloid-facilitated transport also enhances the subsurface transport of dissolved radionuclides [Cvetkovic *et al.*, 2004;

Kurosawa *et al.*, 2006], and pesticides [McGechan and Lewis, 2002; Ngueleu *et al.*, 2013], both of which also pose significant human health risks. In addition, some emerging contaminants of concern, including nanomaterials, are believed to spread via colloid transport mechanisms.

Colloids are micron to sub-micron sized particles that can be generally categorized as abiotic or biotic particles, both of which are widespread and found in aquifers around the world [McCarthy and Zachara, 1989]. Examples of colloidal particles include silicate clays, iron/aluminum oxides, mineral precipitates, humic materials, viruses and bacteria [Auset and Keller, 2004; Kanti Sen and Khilar, 2006; Sen, 2011]. Although colloid-facilitated contaminant transport in aquifers and other porous media systems has been recognized as important to many environmental issues [Sen, 2011] the actual mechanisms governing colloidal particle transport in porous media still remain unclear. As a result, there continues to be a need for advancing understanding in this area. The work in this thesis contributes to this need through a combination of experimental and modeling approaches that seek to further knowledge on how colloidal particle size, groundwater flow direction and groundwater velocity fluctuations influence colloidal particle transport.

1.2 Mechanisms of colloid particle transport in saturated porous media

Colloid particle transport, often simply referred to as particle transport, in saturated porous media is generally agreed to be governed by diffusion, dispersion, advection and sorption processes [Sen, 2011].

Diffusion is a process via which a particle moves from a higher concentration area to a lower concentration area in accordance to Fick's first and second laws [Logan, 2001]. Particle transport rates due to diffusion in groundwater systems are usually much lower than rates associated with advection and dispersion [Fetter, 2001].

Dispersion is a mixing mechanisms arising from a combination of molecular diffusion and hydrodynamic dispersion. Advection describes particle transport at an advective velocity, whose magnitude is governed by the distributions of hydraulic gradient and hydraulic conductivity within the subsurface [Logan, 2001; Auset and Keller, 2004].

The particle sorption or "filtration" process in porous media is currently thought to be governed by three primary mechanisms: (1) mechanical filtration (2) straining filtration, and (3) physicochemical filtration [McDowell-Boyer *et al.*, 1986].

Mechanical filtration occurs when the particles moving in a medium's liquid phase are larger than the pore channels they encounter within the medium and, as a result, the particles are blocked from further transport. Straining is a form of mechanical filtration that occurs at grain-to-grain contacts within a medium, and involves physical blocking of particle transport at the grain-to-grain contact points [Yavuz Corapcioglu and Haridas, 1984; Ginn *et al.*, 2002; Stevik *et al.*, 2004]. The ratio of diameter of particle (dp) to the diameter to the grain media (dm) is used to indicate whether the straining effect is significant or not. Bradford et al. suggested that when the dp/dm ratio is greater than 0.0017 straining should be accounted for, and when the dp/dm ratio becomes greater than 0.005 straining becomes significant. Straining also has been put forward as one reason for why particle filtration behavior has been observed to vary with particle transport distance [Bradford *et al.*, 2006a]. Although numerous studies have investigated factors that might affect the straining filtration of particles, including medium grain size, particle size, shape, and particle clogging mechanisms, the characteristics of the straining mechanism and the relative contribution of straining to the total particle filtration process remain unclear [Sen, 2011].

The traditional approach used to describe the physiochemical filtration process assumes that particles deposit from the medium's liquid phase onto a solid surface in the medium at constant rate that is irreversible (i.e., once deposited on a solid surface, the particles do not re-enter the liquid phase). The particle filtration coefficient, or rate, is assumed to be related to several forces, which can be independently quantified

as force coefficients, and include fluid drag, diffusion, gravity and colloidal particle-solid surface interaction forces. The particle-solid surface interaction forces, which include the Van der Waals and electric double layer interactions, and are usually described by DLVO theory [Verwey and Overbeek, 1947; Derjaguin and Landau, 1993].

The irreversible attachment approach to physiochemical filtration has been shown to successfully describe spheroidal colloid transport behavior in homogeneous porous media systems under favorable electrostatic conditions. However, favorable electrostatic conditions are unusual in the natural environment. Specifically, in the natural environment both the abiotic particle and grain media surfaces are usually negatively charged [Molnar *et al.*, 2011]. In addition, common biotic colloids such as bacteria [McClaine and Ford, 2002; Bradford and Bettahar, 2006; Foppen and Schijven, 2006], virus [Ryan *et al.*, 1999; Schijven and Hassanizadeh, 2000; Jin and Flury, 2002; Schijven and Simnek, 2002], and engineered nanoparticles [Petosa *et al.*, 2010; Tian *et al.*, 2010; Li *et al.*, 2011; Xiao and Wiesner, 2013] also exhibit negatively charged surfaces. When both the colloidal particles and the solid phase within a porous medium are negatively charged, electric double layer repulsion occurs between the particles and solid phase, and this is normally referred to as unfavorable conditions. Nonetheless, particle filtration is still observed under unfavorable electrostatic conditions. Some researchers attribute this to particle deposition in secondary energy minimum, particle straining at grain-to-grain contact points (described above), and/or particle filtration as a result of surface charge heterogeneity [Tufenkji, 2007; Redman *et al.*, 2004; Tufenkji and Elimelech, 2005]. Under unfavorable electrostatic conditions particles can be released from the medium's solid phase and reenter the liquid phase, leading to reversible particle filtration behavior.

Heterogeneities among a particle population and also within a porous medium itself can also induced complex particle transport behavior. For example, the irregular shape of a granular medium might generate low or high fluid velocity zones, which

may further enhance particle filtration or create preferential pathways for enhanced particle transport. Particle populations with mixed sizes and/or surface charge will also behave in a different manner than homogenous particle populations. In addition, heterogeneities associated with solid phase grains within a porous medium, including grain shape, size, and surface roughness may also impact particle transport and filtration mechanisms. For example, *Yoon* and colleagues found that in porous media comprised of smooth glass beads, the dominant particle filtration mechanism was straining at grain-to-grain contact points. However for rough glass bead packs, particle filtration was also observed on the surface of the glass beads as a result of physical immobilization of particle in the vicinity of surface asperities [Yoon *et al.*, 2006; Basha and Culligan, 2010]. Although some mechanistic models have been adapted to address these complex scenarios [Ma *et al.*, 2009; Long *et al.*, 2010]., further research is still needed to fully understand all of the processes influencing particle transport in saturated porous media.

1.3 Mathematical models of particle transport in saturated porous media

The mathematical modeling of particle transport in saturated porous media usually incorporates the following aspects of particle behavior: (1) transport in the liquid phase due to advection and hydrodynamic dispersion, (2) exchange between the liquid phase and the solid phase (due to attachment and detachment of particles on the solid phase, where the inclusion of detachment is often necessary to model unfavorable electrostatic conditions), and (in the case of biotic particles) (3) inactivation, grazing or death [Tufenkji, 2007]. The attachment of particles to the solid phase of a medium encompasses all aspects of particle filtration, with irreversible attachment termed irreversible filtration and reversible attachment termed reversible filtration.

Various forms of advection-dispersion-sorption equations are used to describe par-

ticle transport in saturated porous media. A simplified form for one-dimensional transport in a homogeneous porous medium is:

$$\theta\frac{\partial c}{\partial t} + \rho_b\frac{\partial s}{\partial t} = \theta D\frac{\partial^2}{\partial x^2} - v\frac{\partial c}{\partial x} - \mu_w\theta_c - \mu_s\rho_b s \tag{1.1}$$

where c $[M/L^3]$ is the mass concentration of particles in the liquid phase at a distance x $[L]$ and time t $[T]$, s $[M/M]$ is the solid phase mass concentration, D $[L^2T^{-1}]$ is the hydrodynamic dispersion coefficient, v $[L/T]$ is the interstitial velocity, θ $[-]$ is the porosity, ρ_b $[-]$ is the dry bulk density of the porous media, and μ_w $[T^{-1}]$ and μ_s $[T^{-1}]$ are the inactivation or decay rates for biotic particles in the liquid and solid phase, respectively.

Particle filtration from the liquid phase to solid phase is often described as:

$$\rho_b\frac{\partial s}{\partial t} = \theta k_a c - \rho k_d s \tag{1.2}$$

where k_a and k_d are the first order kinetic attachment and detachment rates, respectively, and s is the solid phase mass concentration. Note, that although particle filtration processes occur at a microscopic scale, the attachment and detachment rates are described at the macroscopic level.

Various mathematical approaches have been developed to evaluate equation 1.1 and 1.2. Some of these approaches are discussed in the following section.

1.3.1 Colloid filtration theory

The classical colloid filtration theory (CFT) is the most commonly used approach to estimate particle filtration in saturated porous media. *Yao et al.* were the first to develop a "collector efficiency equation", which describes how particles interact with a single, solid grain "collector" within a porous medium, where the collector is described by an isolated sphere [Yao *et al.*, 1971]. CFT estimates the colloid removal efficiency via the superposition of three analytical solutions for particle deposition on the collector surface, including deposition due to interception (particles follow streamlines that

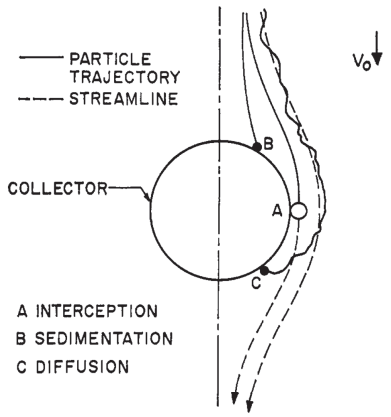

Figure 1.1: Basic transport mechanisms in water filtration (from Yao et al., 1971)

bring then in contact with the collector surface), deposition due to sedimentation or gravitation forces (particles diverge from the streamline they are following due to gravitational forces, and this divergence brings them in contact with the collector surface), and deposition by diffusion (i.e., as a result of random Brownian motion). Figure1.1 graphically illustrates basic processes via which CFT assumes that particles interact with a solid. The assumptions of CFT were validated by *Prieve and Ruckenstein* [Prieve and Ruckenstein, 1974]. Later on, *Rajagopalan and Tien* improved the model via the use of a numerical trajectory analysis for particle deposition involving interception and gravitational forces, which considered the London van der Waals force and hydrodynamic retardation. However, the diffusion mechanism in *Rajagopalan and Tien's* model was adopted from *Yao et al.* In addition, *Rajagopalan and Tien* replaced the CFT isolated sphere assumption with *Happel's* sphere-in-cell porous media model, in order to incorporate medium porosity and Stokes flow field effects [Happel, 1958; Rajagopalan and Tien, 1976].

CFT assumes that the removal of particles from the fluid flow field is irreversible. Upon this assumption, k_a equation1.2 is referred to as k_i, the irreversible attachment co-efficient, and k_d is zero. For steady-state conditions with a constant influent particle concentration co at $x = 0$, the analytical solutions of equation 1.1 and 1.2 at time

t for a uniform, porous medium initially free of particles are:

$$\begin{cases} \frac{c(x)}{c_0} = exp(\frac{-k_i}{v})x \\ s(x) = \frac{t\theta k_i c_0}{\rho_b} exp(\frac{-k_i}{v}x) \end{cases} \tag{1.3}$$

The irreversible attachment rate, k_i, can be derived from mass balance considerations within the porous media [Logan *et al.*, 1995] viz:

$$k_i = \frac{3(1-\theta)v}{2d_{50}}\eta_0\alpha \tag{1.4}$$

where d_{50} is the average grain size of the porous medium, η_0 is the single collector removal efficiency, which can be calculated using CFT, and α is the collision efficiency, which is an experimentally determined coefficient that takes into account the fact that removal efficiencies estimated using CFT are often higher than those experimentally observed. The value of $\eta_0\alpha$ is sometimes referred to as the "filtration" efficiency and it describes the fraction of particles in the liquid flow field that are actually irreversibly removed via interaction with the medium's solid phase.

Tufenkji and Elimelech improved *Rajagopalan and Tien's* model by considering all particle deposition mechanisms simultaneously, in particular they incorporated the effect of hydrodynamic retardation on the diffusion coefficient [Tufenkji and Elimelech, 2004a]. However, *Tufenkji and Elimelech's* model neglects particle rotation, which is considered in *Rajagopalan and Tien's* model, in their calculations of hydrodynamic retardation. In addition, *Tufenkji and Elimelech* used an isolated sphere model instead of *Happel's* sphere-in-cell porous media. *Tufenkji and Elimelech's* equations for the diffusion, interception, and gravitational removal efficiencies of particles are:

$$\begin{cases} \eta_D = 2.4A_S^{1/3}N_R^{-0.081}N_{Pe}^{-0.715}N_{vdW}^{-0.052} \\ \eta_I = 0.55A_S N_R^{1.55}N_{Pe}^{-0.125}N_{vdW}^{0.125} \\ \eta_G = 0.22A_S^{-0.24}N_R^{1.11}N_G^{-0.715}N_{vdW}^{0.053} \end{cases} \tag{1.5}$$

where A_s is a porosity-dependent parameter obtained from *Happel's* sphere-in-shell model, N_R is the ratio of particle diameter to collector diameter, N_{Pe} is the Peclet

number characterizing ratio of advective transport to diffusive transport, N_{vdW} is the *Van der Waals* number characterizing ratio of Van der Waals interaction energy to the particle's thermal energy, and N_G is the gravitational number represented the ratio of the Stokes settling velocity to the approach velocity. The value of η_0 in equation 1.4 is the sum of the η_D, η_I, and η_G values described by equations 1.5.

Long and Hilpert, *Ma et al.* and *Nelson and Ginn* have also worked separately on improving the CFT model. *Long and Hilpert* improved the Brownian diffusion expression by estimating the diffusion removal efficiency for a random packing of uniform spheres, but kept the interception and gravitation removal efficiency estimation from *Tufenkji and Elimelech* [Long and Hilpert, 2009]. *Ma et al.* and *Nelson and Ginn* improved prior CFT models by incorporating hydrodynamic retardation caused particle rotation [Ma *et al.*, 2009; Nelson and Ginn, 2011]. *Nelson and Ginn* kept the *Happel's* sphere-in-cell model. In contrast, *Ma et al.* used a hemispheres-in-cell model for estimating particle removal efficiency via straining at grain-to-grain contact points.

1.3.2 Alternative models and approaches

Numerous studies have reported that the classical filtration theory (CFT) fell short of predicting colloid transport in both laboratory column experiments and field tests under unfavorable condition [Tufenkji and Elimelech, 2004b]. In many cases this is attributed to particle and/or collector surface heterogeneities, including surface charge heterogeneities, that give rise to both "fast" and "slow" colloid deposition rates within a medium. An alternative approach commonly used to overcome the numerous variations of surface properties of both particles and collectors is the use of macro-scale coefficients, generally obtained from direct observations, instead of micro-scale collision efficiencies. In addition, some researchers have proposed the use of a statistical distribution function to replace the common assumption of constant attachment rates. For example, power-law, bimodal, and lognormal attachment coef-

ficient distributions have been proposed to describe the measured profiles of retained colloids [Baygents *et al.*, 1998; Redman *et al.*, 2001; Tufenkji *et al.*, 2003].

Another, alternative approach is the use of a "two-site" approach to describe "fast" and "slow" colloid deposition activities. Two-site models are formulated in terms of two different collector sites or two different particle populations, each of which has its own deposition rate. This approach has successfully described colloid transport in some studies [Schijven and Hassanizadeh, 2000; Schijven *et al.*, 2002; Tufenkji and Elimelech, 2005; Basha and Culligan, 2010].

Various alternative approaches to CFT have been used to model particle filtration via straining mechanisms. For example, *Bradford et al.* assumed that straining can be described by a first-order, irreversible attachment rate that is path-length dependent, and mostly leads to particle filtration at the column inlet during laboratory column experiments [Bradford *et al.*, 2003a]. In contrast, *Foppen et al.* reported that, for their column experiments, particle straining occurred throughout the column and exhibited a linear decrease in the particle filtration process with column length [Foppen *et al.*, 2007]. Recently, many studies have reported that straining is not only affected by the particle and collector sizes, it is also affected by the flow velocity, the particle inlet concentration, solution ionic strength and that shape of the particles [Bradford and Bettahar, 2006; Bradford *et al.*, 2006b; Shen *et al.*, 2008; Xu *et al.*, 2008].

Blocking and ripening effects are caused by particle-particle interactions. Blocking is when the particle deposition rate rapidly decreases because attachment sites on the collector surface are covered by particles, which prevents the attachment of further particles. Ripening is an alternate process whereby attached particles act as additional collectors for other particles, which increases the overall particle deposition rate [Camesano *et al.*, 1999]. Blocking and ripening effects have been proposed by some researchers as one reason why CFT predictions deviate from observations made during column experiments [Nascimento *et al.*, 2006]. Recently, several studies have applied a random sequential adsorption function to investigate blocking effects

[Ko and Elimelech, 2000; Loveland *et al.*, 2003; de Kerchove and Elimelech, 2008; Adamczyk *et al.*, 2013], and the results of these studies have all indicated that approach velocity, ionic strength and deposition particle sizes are impact particle filtration by blocking. *O'Melia and Ali* first reported ripening in their tests, and stated the head-loss caused ripening in their system. Their work inspired the development of a "ripening model" [Tare and Venkobachar, 1985; Vigneswaran and Tulachan, 1988; Tobiason and Vigneswaran, 1994].

1.4 Experimental methods of particle transport in saturated porous media

Particle transport in saturated porous media has traditionally been studied by researchers using bench-scale column experiments. In general, artificial groundwater containing either engineered particles or cultured biotic colloids is introduced into packed columns of glass beads, quartz sand, or natural sediments to simulate particle transport within a saturated porous medium. Typically, monitoring of the suspended effluent particle concentration exiting the column provides data that are then used to evaluate particle transport and filtration mechanisms [Tufenkji, 2007]. Findings from laboratory such column studies have been used over the years to verify theoretical models and further elucidate the factors controlling particle transport in saturated porous media. Recent investigations indicate that only monitoring the particle effluent concentration can be inadequate for identifying the particle transport mechanisms. Instead, combining effluent data with data on the spatial distribution of particles retained within a column at the end of an experiment provides a more accurate picture of particle transport behavior [Li *et al.*, 2004; Li and Johnson, 2005].

In general, well-controlled laboratory studies provide important insight into the fundamental mechanisms controlling particle transport and deposition activities. Sev-

eral physical and chemical conditions have been evaluated using this approach, including investigations into the influence of collector size and shape [Brown and Jaffé, 2001; Sandler, 2011; Syngouna and Chrysikopoulos, 2011; Chalk *et al.*, 2012], collector types or surface properties [Bolster *et al.*, 2001; Foppen and Schijven, 2005], fluid velocity [Gannon *et al.*, 1991; Tan *et al.*, 1994; Camesano and Logan, 1998; Hendry *et al.*, 1999; Becker *et al.*, 2004], solution ionic strength composition and pH [Ryan and Gschwend, 1994; Li and Logan, 1999; Walker *et al.*, 2005b; Choi *et al.*, 2007; Torkzaban *et al.*, 2008; Walshe *et al.*, 2010; Li *et al.*, 2011], and particle concentration [Tan *et al.*, 1994; Camesano and Logan, 1998; Camesano *et al.*, 1999; Bradford and Bettahar, 2006]. In addition, several abiotic and biotic particle factors have also been examined, such as particle surface macromolecule length and composition [Rijnaarts *et al.*, 1996a; Williams and Fletcher, 1996; Abu-Lail and Camesano, 2003; Walker *et al.*, 2004], cell motility [Camper *et al.*, 1993; Becker *et al.*, 2004; de Kerchove and Elimelech, 2008; Hidalgo *et al.*, 2011; Liu *et al.*, 2011; O'May and Tufenkji, 2011], particle size and shape [Elimelech, 1991; Mitropoulou *et al.*, 2013; Ngueleu *et al.*, 2013; Yu *et al.*, 2013; Chrysikopoulos and Syngouna, 2014], organism type [Hornberger, 1992; Rijnaarts *et al.*, 1996b; Hendry *et al.*, 1999], and the influence of growth phase on bacterial transport and deposition kinetics [Clement *et al.*, 1997; Walker *et al.*, 2005a; Walker *et al.*, 2005b; Sgountzos *et al.*, 2006; Tufenkji, 2007].

Since the inherent physical, chemical and biological heterogeneities in the real world are too complex to simulate during a laboratory scale test [Ginn *et al.*, 2002], field-scale observations and experiments are also needed to further the development of predictive tools and analyses. In most cases, the results of research conducted at the field scale confirm the dominant influence of inherent heterogeneity on particle transport processes. Examples include observations made at the US Geological Survey's Cape Code site, MA [Harvey *et al.*, 1993], and the Narrow Channel area of the South Oyster Site, VA [Hubbard *et al.*, 2001; Johnson *et al.*, 2001; Dong *et al.*, 2002; Fuller *et al.*, 2001; Scheibe *et al.*, 2011; Scheibe and Chien, 2003].

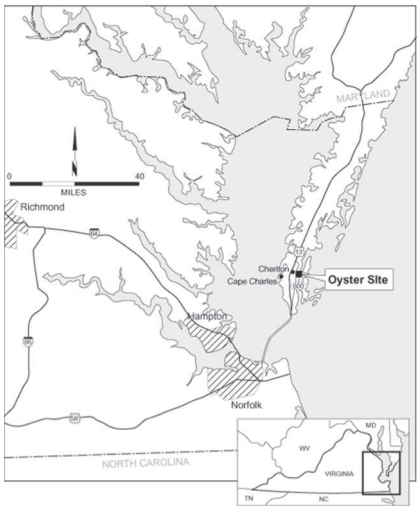

Figure 1.2: Location map of the South Oyster Site [*Scheibe and Chien, 2003*].

1.5 Organization of the dissertation

This dissertation is organized into five chapters and one appendix. This first chapter provides an over-view of the problem domain the research work was designed to address, and a literature review of prior work relevant to the topic. Chapter 2 presents the details of the one-dimensional particle transport model that was developed for the numerical investigations of the research. Based on a finite difference scheme, the numerical model, which contains multiple sub-models for describing particle interactions with the solid phase of a porous medium, was devised to analyze the results of the column experiments that were conducted as part of the research work. Chapter 3 describes a series of laboratory column experiments under taken to investigate the influence of varying velocity conditions on particle transport mechanisms, while Chapter 4 describes an investigation into the influence of particle size, flow direction, and particle-particle interactions. Chapter 5 presents a summary of the key findings of the dissertation and a discussion of future work that is needed to further advance understanding of the fundamental mechanisms governing particle transport in porous media. Appendix A of the thesis presents collaborative work that sought to

understand the relationship between laboratory investigations into particle transport behavior and field-scale behavior. Referenced sources are available at the end of the manuscript.

Chapter 2

Particle Transport Modeling

2.1 Introduction

Mathematical models are used extensively by researchers to describe and predict many scientific and engineering processes, including those associated with particle/ colloid transport in saturated porous media. In the case of particle transport, the most common mathematical models consist of mass balance equations that consider the fate and transport of particles in a representative elemental volume of a uniform, saturated medium. The analytical solution of such models usually requires several assumptions to be made to simplify the complexity of most real-world situations. For example, many analytical solutions are derived for an infinite or semi-finite domain containing a homogeneous and isotropic medium subjected to steady state flow conditions [Genuchten *et al.*, 1982]. In order to analyze more realistic problems, including the transient flow conditions considered by the research presented in Chapter 3 of this thesis, the mathematic models are approximately solved using numerical modeling techniques [Swanton, 1995].

This chapter presents the modeling work underpinning the research described in Chapters 3 and 4 of this thesis, as well as Appendix A. A numerical program, termed the Kinetic Colloid Transport Model (KCTM), was developed to simulate

one-dimensional particle transport through a saturated porous medium. Modeling of particle deposition on, and release from, solid surfaces in the porous medium, is included for both steady and non-steady velocity conditions. Different sub-models describing the kinetics of particle deposition onto, and/or release from, solid surfaces are embedded in the KCTM, including irreversible, reversible and two-site models. Model validation was undertaken via the comparison of KCTM results with results from analytical solutions and HYDRUS-1D, a well-known, open-source numerical model for predicting contamination fate and transport.

2.2 Mathematical model and numerical methods

2.2.1 Particle transport equations

Particle transport in saturated porous media is usually described by modified advection-dispersion-sorption (ADS) equations [Tan *et al.*, 1994; Loveland *et al.*, 2003; Massoudieh *et al.*, 2010; Li *et al.*, 2011; Rezaei *et al.*, 2013]. The ADS equation describes particle (or colloid) behavior within the liquid phase of a porous medium (i.e., the advective-dispersive transport), as well as particle interactions with the medium's solid phase (sorptive behavior). Particles deposition onto and release from a solid surface in a porous medium are usually referred to as attachment and detachment activities, respectively. Such activities are expressed by kinetic attachment or detachment coefficients in the ADS equation. Classical filtration theory (CFT) was the first approach developed to estimate particle attachment coefficients [Yao *et al.*, 1971]. CFT considers particle attachment (or sorption) to be described by a first order kinetic attachment model, with zero particle detachment. The CFT attachment coefficient is based on the surface properties of both the particles and the porous medium. However, as noted in Chapter 1 of this thesis, numerous studies have reported that CFT can only describe particle transport under very limited conditions [Tan *et al.*, 1994; Tufenkji *et al.*, 2004; Tong and Johnson, 2007]. Following the introduction of CFT,

other theories or hypothesis, including DLVO theory, blocking, ripening, and straining activities, have been put forward to explain CFT deviations from laboratory and field observations [Tobiason and Vigneswaran, 1994; Rijnaarts *et al.*, 1996b; Camesano *et al.*, 1999; Bhattacharjee *et al.*, 2000; Bradford and Bettahar, 2006; Bradford *et al.*, 2006a]. These theories were also described in Chapter 1.

For the research presented in this thesis, the following general, one-dimensional ADS was adopted [Johnson *et al.*, 2007b]:

$$\begin{cases} \theta\frac{\partial c}{\partial t} + \rho_b\frac{\partial s}{\partial t} = \theta D\frac{\partial^2 c}{\partial x^2} - v\frac{\partial c}{\partial x} \\ \rho_b\frac{\partial s}{\partial t} = f(c) \end{cases} \tag{2.1}$$

where c is the liquid phase particle concentration $[ML^{-3}]$, s is the solid phase particle concentration $[MM^{-1}]$, ρ_b is the bulk density of the solid matrix $[ML^{-3}]$, D is the hydrodynamic dispersion coefficient $[L^2T^{-1}]$, v is the pore velocity $[LT^{-1}]$, θ is the porosity [-].

The exchange function $f(c)$ describes the particle exchange between the liquid phase and solid phase. Based on different mechanisms, the exchange function can be expressed in different forms [Tufenkji, 2007]. For first-order, irreversible attachment kinetics, the exchange function becomes:

$$f(c) = \theta k_i c \tag{2.2}$$

where k_i is the irreversible attachment coefficient $[T^{-1}]$.

For first-order, reversible attachment kinetics, the exchange function becomes:

$$f(c) = \theta k_a c - \rho_b k_d s \tag{2.3}$$

where k_a and k_d are the reversible attachment and detachment coefficients $[T^{-1}]$, respectively.

For particle straining at grain-grain contact points, the KCTM assumes reversible attachment kinetics with depth-dependent parameters, and uses the following exchange function [Bradford *et al.*, 2003b]):

$$f(c) = \theta k_{a,str} \Psi_a c - \rho_b k_{d,str} \Psi_d s \tag{2.4}$$

where $k_{a,str}$ and $k_{d,str}$ are the reversible attachment and detachment coefficients $[T^{-1}]$, respectively, and Ψ_a and Ψ_d are depth-dependent power functions defined as:

$$\begin{cases} \Psi_a = \frac{(L+x)^{-a})}{L} \\ \Psi_b = \frac{(L+x)^{-b})}{L} \end{cases} \tag{2.5}$$

where L is the column length $[L]$, x is the distance from the column inlet $[L]$, a and b are dimensionless fitting parameters that control the shape of the kinetic coefficients as a function of transport distance.

For a two-site model, the collector (i.e., solid surface) is considered to have two types of interaction sites, so the exchange function becomes:

$$f(c) = \frac{\partial s_1}{\partial t} + \frac{\partial s_2}{\partial t} \tag{2.6}$$

For a dual mode or two-population model, it is assumed that there are two particle species, or populations, each of which has different kinetic characteristics. For this model, an ADS is written for each population and the following mass balance equation is employed to link the two ADS equations:

$$c = wc_1 + (1 - w)c_2 \tag{2.7}$$

where c is the total liquid phase particle concentration, w is the portion of first population, and c_1 and c_2 are the first and second population concentrations, respectively.

For dual mode modeling, the first and second populations are usually represented by a two-site and irreversible kinetic approach, respectively. The governing equations

are thus expressed as:

$$\begin{cases} \theta\frac{\partial c_1}{\partial t} + \rho_b\frac{\partial s_{1,1}}{\partial t} + \rho_b\frac{\partial s_{1,2}}{\partial t} = \theta D\frac{\partial^2 c_1}{\partial x^2} - v\frac{\partial c_1}{\partial x} \\ \rho_b\frac{\partial s_{1,1}}{\partial t} = \theta k_a c_1 - \rho_b k_d s_{1,1} \\ \rho_b\frac{\partial s_{1,2}}{\partial t} = \theta k_{i,1} c_1 \\ \theta\frac{\partial c_2}{\partial t} + \rho_b\frac{\partial s_2}{\partial t} + = \theta D\frac{\partial^2 c_2}{\partial x^2} - v\frac{\partial c_2}{\partial x} \\ \rho_b\frac{\partial s_2}{\partial t} = \theta k_{i,2} c_2 \\ c = wc_1 + (1-w)c_2 \end{cases} \tag{2.8}$$

where c_1 and c_2 are the liquid phase concentration $[ML^{-3}]$ of first and second population, $s_{1,1}$ and $s_{1,2}$ are the solid phase concentration $[MM^{-1}]$ of first and second site of first population, s_2 is the solid phase concentration $[MM^{-1}]$ of the second population, k_a and k_d are the reversible attachment and detachment coefficients $[T^{-1}]$, $k_{i,1}$ and $k_{i,2}$ are the irreversible attachment coefficients $[T^{-1}]$ of first and second population, respectively.

2.2.2 Numerical methods

In order to numerically solve the KCTM, the governing equations were implemented in a Matlab programing environment using finite-difference schemes to discretize the time and space derivatives. For the time derivatives, the implicit Euler and Crank-Nicolson schemes were employed. For the space derivatives, both upward and central difference approximations were employed [Hoffmann and Chiang, 2000a; Hoffmann and Chiang, 2000b]. The discretized forms of the particle transport equations are:

$$\begin{cases} \theta\frac{\partial c}{\partial t} \cong \theta\frac{c_i^{n+1} - c_i^n}{\Delta t} \\ \theta D\frac{\partial^2 c}{\partial x^2} \cong \theta D\left[\gamma\frac{c_{i+1}^{n+1} - 2c_n^{i+1} + c_{i-1}^{n+1}}{\Delta x^2} + (1-\gamma)\frac{c_{i+1}^n - 2c_n^i + c_{i-1}^n}{\Delta x^2}\right] \\ v\frac{\partial c}{\partial x} \cong v\left[\gamma\frac{\alpha c_{i+1}^{n+1} + (1-2\alpha)c_i^{n+1} - (1-\alpha)c_{i-1}^{n+1}}{\Delta x} + (1-\gamma)\frac{\alpha c_{i+1}^n + (1-2\alpha)c_i^n - (1-\alpha)c_{i-1}^n}{\Delta x}\right] \\ \rho_b\frac{\partial s}{\partial t} \cong \rho_b\frac{s_i^{n+1} - s_i^n}{\Delta t} \\ \theta k_a c - \rho_b k_d s \cong \theta k_a\left[\gamma c_i^{n+1} + (1-\gamma)c_i^n\right] - \rho_b k_d\left[\gamma s_i^{n+1} + (1-\gamma)s_i^n\right] \end{cases} \tag{2.9}$$

where n is the discretized time step index, i is the discretized space node index, $\gamma = 0.5$ for the *Crank-Nicolson* scheme and $\gamma = 1$ for the implicit *Euler* scheme, $\alpha = 0.5$ for the central difference scheme and $\alpha = 1$ for the upwind scheme.

The KTCM can directly simulate particle transport, or inversely calculate the kinetic parameters and particle population proportions from observed data by minimizing the error function. For the inverse calculation, the model employed a modified version of the Matlab optimization tool, the fminsearch fuction, which uses the *Nelder-Mead* simplex algorithm as described in *Lagarias et al.* [Lagarias *et al.*, 1998]. The inverse calculation used the optimization tool to minimize the objective function, which was the error function. The error function is the weighted sum of the squared error (i.e. the difference between the measured data and the modeled values) and was defined by *Simunek et al.* as [Simunek *et al.*, 2012]:

$$\begin{cases} R = \sum_j w_j (f^*(x,t) - f(x,t))^2 \\ w_j = \frac{1}{m_j \sigma_j^2} \end{cases} \tag{2.10}$$

where f^* and f are observed data and modeled values, respectively, while the weighting coefficient w_j minimizes differences in weighting between different data types, which is necessary because of the different absolute values and data points involved in some cases. For example, particle breakthrough concentrations collected during laboratory column tests usually comprise more data points than observations of retained particle concentration at the end of the test. The weighting coefficient is normalized by the measured data variance σ^2, and number of data m.

2.3 Model validation

There are no available analytical solutions to describe dual mode or two population particle transport. Thus, in order to verify the KCTM, the model outputs were compared to some well-defined analytical solutions as well as simulation results obtained from HYDRUS-1D, a well-known numerical model for groundwater flow and contam-

inant transport. The numerical simulation cases were adopted from previous study [Tosco and Sethi, 2009].

2.3.1 STANMOD and HYDRUS-1D

Several well-known computer programs have been developed to evaluate contaminant transport in porous media using analytical solutions of the advection-dispersion-sorption equation [Simunek *et al.*, 2012]. STANMOD (Studio of Analytical Models) is a public domain software package that integrates some of the most widely used transport models into a single software package. The first version of STANDMOD integrated the following one-dimensional transport models: CFITM, CFITIM, CHAIN, and CXTFIT. The second version included two more models, 3DADE and N3DADE, for analyzing multidimensional transport problems.

STANMOD was employed for validation of following simplified advection-dispersion-sorption (ADS) equation [Leij *et al.*, 2012]:

$$\begin{cases} \theta \frac{\partial c}{\partial t} + \rho_b \frac{\partial s}{\partial t} = \theta D \frac{\partial^2 c}{\partial x^2} - v \frac{\partial c}{\partial x} \\ \rho_b \frac{\partial s}{\partial t} = \theta k_a c - \rho_b k_d s \end{cases} \tag{2.11}$$

The CXTFIT code was used to provide an analytical solution of non-equilibrium solute transport under uniform flow conditions in a homogeneous, saturated porous medium. The CXTFIT model solves the following non-equilibrium solute transport model [Toride *et al.*, 1995]:

$$\begin{cases} \theta \frac{\partial c}{\partial t} = \theta D \frac{\partial^2 c}{\partial x^2} - v \frac{\partial c}{\partial x} - \frac{(\alpha \rho_b)}{\theta} \left[K_d - s \right] - \mu_c c \\ \frac{\partial s}{\partial t} = \alpha \left[K_d c - s \right] - \mu_s s \end{cases} \tag{2.12}$$

where α is a first order kinetic rate coefficient $[T^{-1}]$, Kd is an empirical distribution constant $[L^3 M^{-1}]$, μ_c and μ_s are the first order decay coefficients for liquid and solid phase, respectively.

For the KCTM model validation, it was assumed that there were no equilibrium exchanges and solute decay associated with either the liquid or solid phase. The

coefficients α and K_d can be expressed in term of the attachment and detachment coefficients of the particle transport problem, viz:

$$\begin{cases} \alpha = k_d \\ K_d = \frac{\theta k_a}{\rho_b k_d} \end{cases} \tag{2.13}$$

For the CXTFIT, the "Deterministic Non-equilibrium CDE" model was used with the corresponding dimensionless model parameters:

$$\begin{cases} R = 1 + \frac{k_a}{k_d} \\ \beta = \frac{1}{R} \\ \omega = k_d(R-1)\frac{L}{v_d} \end{cases} \tag{2.14}$$

where L is the column length $[L]$, v_d is the Darcy velocity.

HYDRUS-1D is a finite-element model able to simulate 1-D water, heat, chemical solute and particle transport in saturated or unsaturated media. HYDRUS-1D can be applied for both equilibrium and non-equilibrium conditions [Šimnek *et al.*, 2009]. For the particle transport simulation, the "Two Kinetic Site Model" of HYDRUS-1D, which is designed for simulating particle transport, was used for the validation exercise. In order to compare all three validation approaches (STANMOD-ADS, CXTFIT and HYDRUS-1D), the particle generation and inactivation rates, which are used for modeling biological particle behavior, were not considered in the HYDRUS-1D simulations. In addition, the second particle interaction site of the "Two Kinetic Site model" and the blocking function were also disabled.

2.3.2 Validation results

A hypothetical column experiment was used for model validation, with fourteen different case studies involving a range of dispersion coefficients as well as particle attachment and detachment rates. The following physical parameter values were adopted: column length $L = 0.1m$, Darcy velocity $v = 8 \times 10^{-5} msec^{-1}$ and bulk density $\rho_b = 1.5 \times 10^{-6} gm^{-3}$. Figure 2.1 illustrates the experimental setting of the hypothetical column experiment.

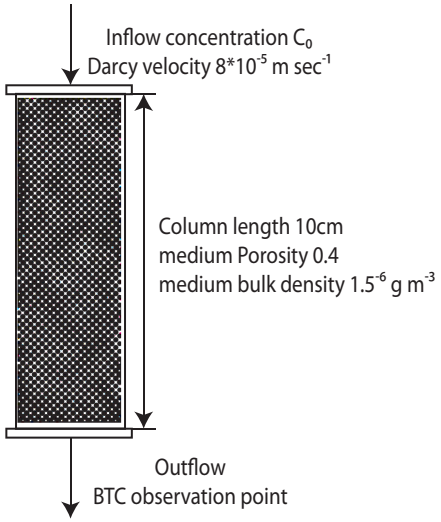

Figure 2.1: Illustration the experimental settings of the hypothetical column experiment. The effluent concentration is observed at the column's outflow point.

Numerical modeling parameters, including the spatial and temporal discretization, were chosen to be consistent across all numerical runs. In particular, the time step $\Delta t = 2sec$ and discretized distance $\Delta x = 10^{-3}m$ were used. For the hypothetical experiment, the total simulated experimental time was 6,000 seconds and included 2 stages. The first stage started with a stepwise particle solution injection period at a constant concentration c_0 at $x = 0m$ (the column inlet) for 3,600 seconds. This was followed by a "flushing period" for 2,400 seconds − the second stage − whereby $c = 0$ at $x = 0m$.

Table 2.1 reports the transport parameters and normalized errors for a set of simulation runs with KCTM, STANMOD, and HYDRUS-1D that involved 5 case studies. The normalized errors were calculated according to the following equation:

$$R^2 = 1 - \frac{SSE}{SST} = 1 - \frac{\sum_{i=1}^{N}(c_i - c_i^*)^2}{\sum_{i=1}^{N}(c_i - \overline{c})^2} \tag{2.15}$$

where R^2 is the residual, SSE is the sum of squared errors of prediction, SST is the total sum of squares, N is the time step index, c_i is the breakthrough concentration at

the $i-th$ time step using KCTM, c_i^* is the breakthrough concentration at $i-th$ time step using STANMOD or HYDRUS-1D, and $\overline{c}$ is the mean value of the breakthrough concentration using KCTM.

Figures 2.2 and 2.3 showed the simulated, normalized breakthrough curves (BTCs) for the four case studies described in Table 2.1. For the results in Figure 2.2, the dispersion coefficient remains constant while the particle attachment and detachment rates vary between the two case studies (case 1 and case 2). For the results in Figure 2.3, the particle attachment and detachment rates remain constant, while the dispersion coefficient varies between the three case studies (cases 2, 3 and 4).

Referring to Figure 2.2; the higher particle detachment than attachment rate in case 1 resulted in a BTC with a sharp rising and falling limb, and a plateau value of unity. For case 2, where the particle attachment rate was greater than the particle detachment rate, the rising and falling limbs of he BTC are less steep than in case 1, and a plateau of unity is only reached at the end of the particle injection phase of the simulation. In both cases, the HYDRUS and KCTM predictions slightly over-predict particle concentrations during the rising limb of the BTC, and then under predict concentrations during the falling limb. Nonetheless, the agreement between the two numerical models and the analytical solutions are considered very good. In addition, the results of the KCTM developed for the research presented in this thesis agree with the results of the popular HYDRUS-1D model.

Referring to Figure 2.3; the changes in the value of the dispersion coefficient lead to very small differences in the simulated BTCs. Again, in general the HYDRUS and KCTM predictions slightly over-predict particle concentrations during the rising limb of the BTC, and then under predict concentrations during most of the falling limb. For case 4, which had the lowest vale of D, the HYDRUS and KCTM predictions slightly over-predict particle concentrations during start of the falling limb. The differences between the numerical simulations and the STANMOD analytical solutions increases as D increases. This is attributed to numerical dispersion errors. Again,

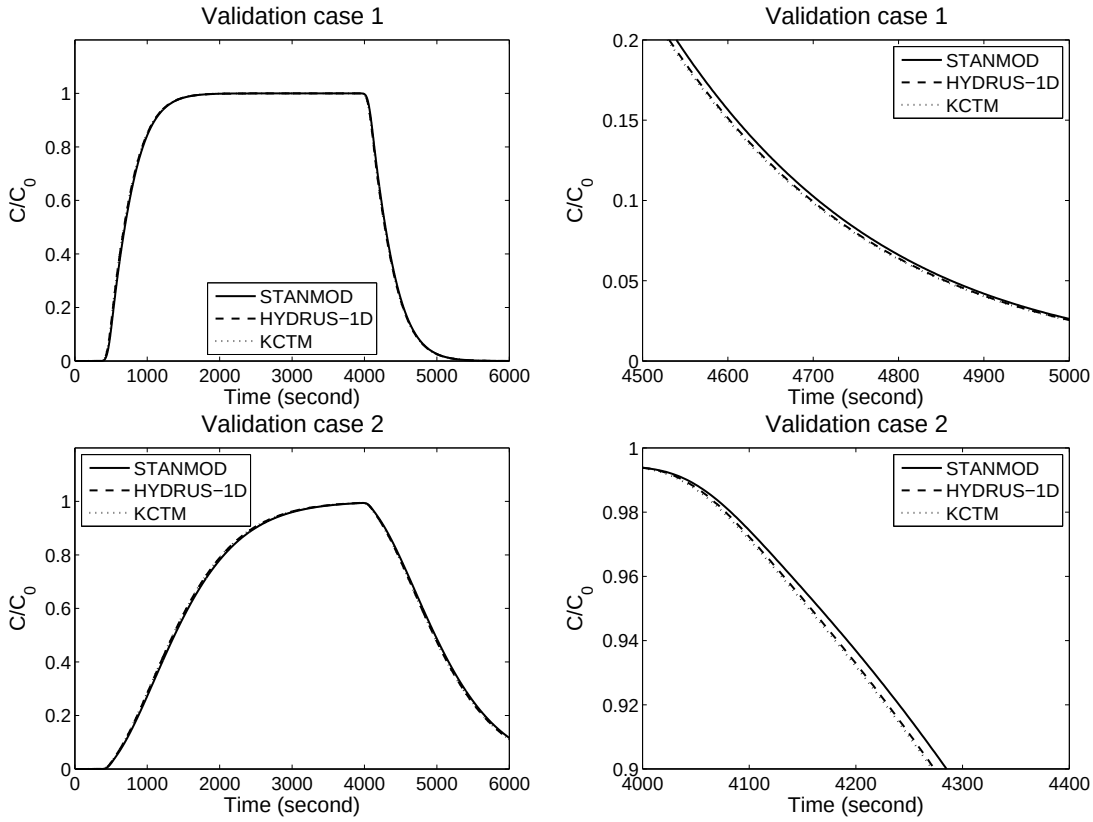

Figure 2.2: Simulated normalized, column breakthrough curves generated by STANMOD, HYDRUS-1D and KCTM for case 1 and case 2 (see Table 2.1 for simulation parameters). The right-hand figures show a zoom of the latter portion of the simulation.

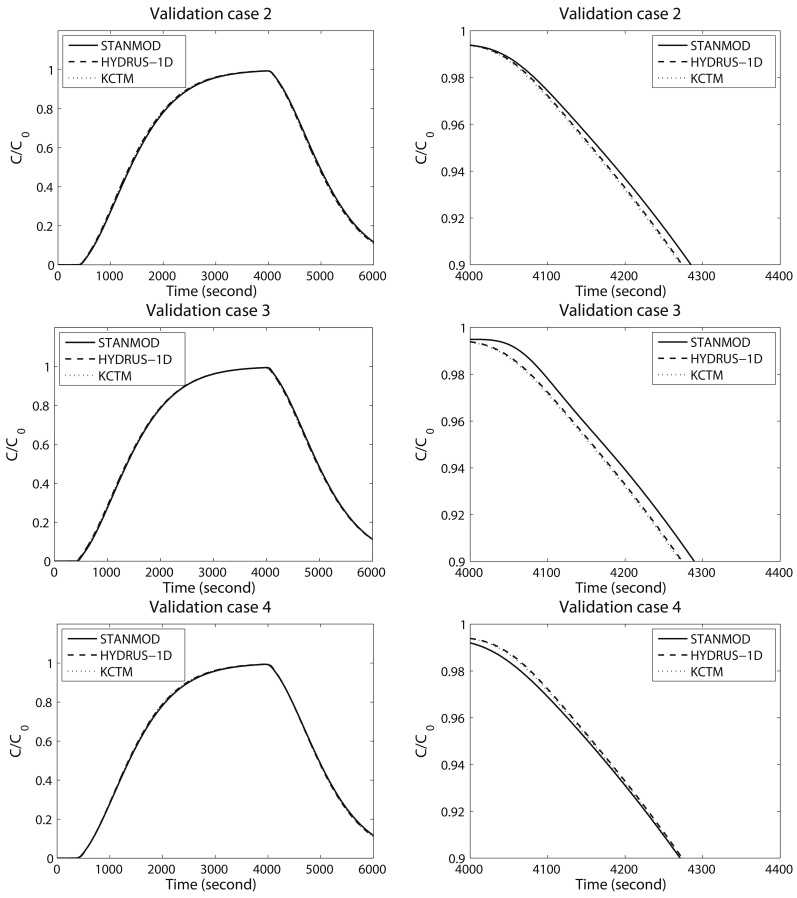

Figure 2.3: Simulated normalized, column breakthrough curves generated by STANMOD, HYDRUS-1D and KCTM for case 2, 3 and 4 (see Table 2.1 for simulation parameters). The right-hand figures show a zoom of the latter portion of the simulation.

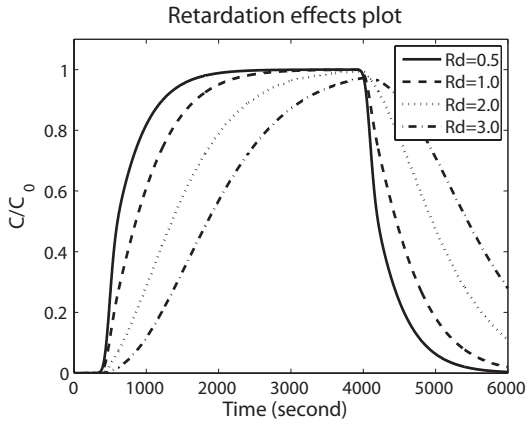

Figure 2.4: Simulated, normalized column breakthrough curves generated by KCTM for case 5, 6, 7 and 8 (see Table 2.2 for simulation parameters).

the agreement between the numerical simulations and the analytical simulations are considered very good, as is the agreement between KCTM and HYDRUS-1D results.

It worth to note the ratio of kinetic attachment and detachment rates, termed the retardation factor (R_d), represents the time delay caused by particle sorption activities during particle transport. Figure 2.4 shows a series of simulated, normalized BTCs using the KCTM for four case studies described in Table 2.2. For the results in Figure 2.4, the detachment rate remains constant, while the attachment rate increases. R_d varies from 0.5 to 3. As the R_d value increases, the rising and falling limbs of the BTCs change from sharp to mild slopes. The duration time during which the normalized concentration is unity and the peak concentration also reduce when R_d increases.

2.3.3 Two-site colloid transport comparison

Hydrus-1D was used for validation of the two-site kinetic model simulations. The "Two Site Kinetic Model" of HYDRUS-1D model was applied in order to do this. A total of 6 different sets of two-site kinetic coefficients were used to compare KCTM predictions with those of HYDRUS-ID, as listed in Table 2.3. The value of k_a/k_d

for both particle interaction sites (site 1 and site 2) increases from case 9 to case 14, while the value of k_{a1}/k_{a2} decreases. Table 2.3 also provides the R^2 values associated with each case study comparison. Note, the KCTM two-site kinetic is described by equations 2.1, 2.3 and 2.5.

Figures 2.5 and 2.6 show the two-site kinetic modeling BTCs generated by HYDRUS-1D and the KCTM. Figure 2.5 highlights the results of cases 9 to 11, while Figure 2.6 highlights the results of cases 12 to 14. As seen, the maximum value of the particle breakthrough concentration decreases as k_a/k_d increases from case 9 to case 14. In addition, the increase in BTC values over the time period from 500 to 4,000 seconds also decreases as k_a/k_d increases.

The two-site kinetic model was first constructed by *Schijven et al.* in order to solve the significant discrepancy between one-site kinetic modeling results and experiment BTCs at both the end of the of rising limb and the start of the falling limb of the BTC [Schijven *et al.*, 2002]. The shape of the falling limb of the predicted BTC, as well as the tail of the BTC, define some of the major differences between predictions obtained from a two-site versus a one-site kinetic modeling approach. The two-site approach provides two separate solid-phase concentration sites, each with different detachment rates. This, generates BTC falling limbs and tails that are not log-linear. *Schijven and Simunek* reported that the sum of the two-site kinetic attachment rates were close to a one-site kinetic attachment rate for all of their experiments [Schijven and Simnek, 2002]. This is because the BTC plateau concentration is governed by the total filtration efficiency of the system itself, which would represent the sum of the two-site kinetic attachment rates.

In general, the KCTM results are in very good agreement with the results of HYDRUS-1D. The R^2 values decreased slightly from case 9 to case 14. However, all values were basically close to 1.

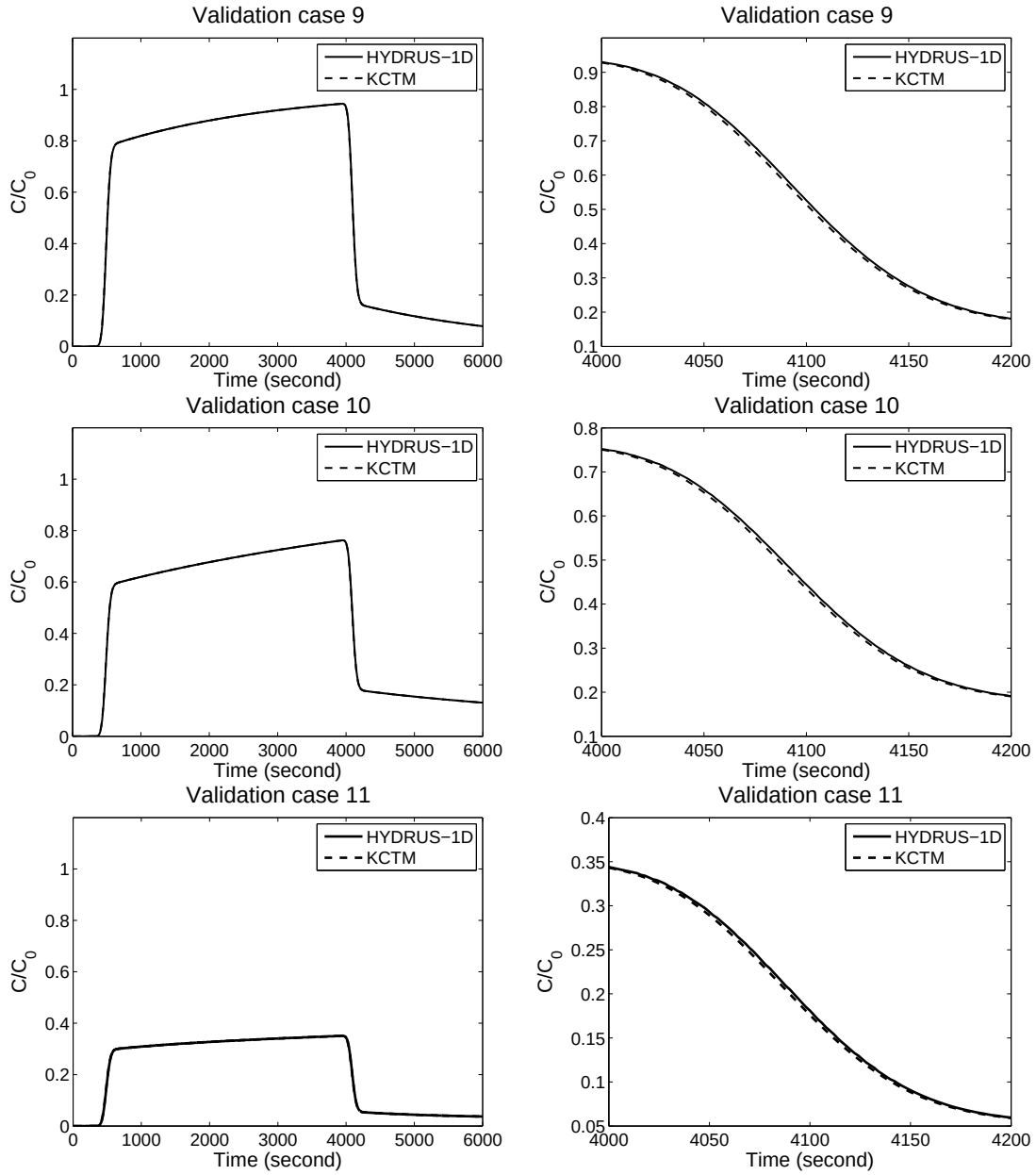

Figure 2.5: Simulated normalized, column breakthrough curves generated by, HYDRUS-1D and KCTM for case 9, 10 and 11 (see Table 2.3 for simulation parameters). The right-hand figures show a zoom in of the latter portion of the simulation.

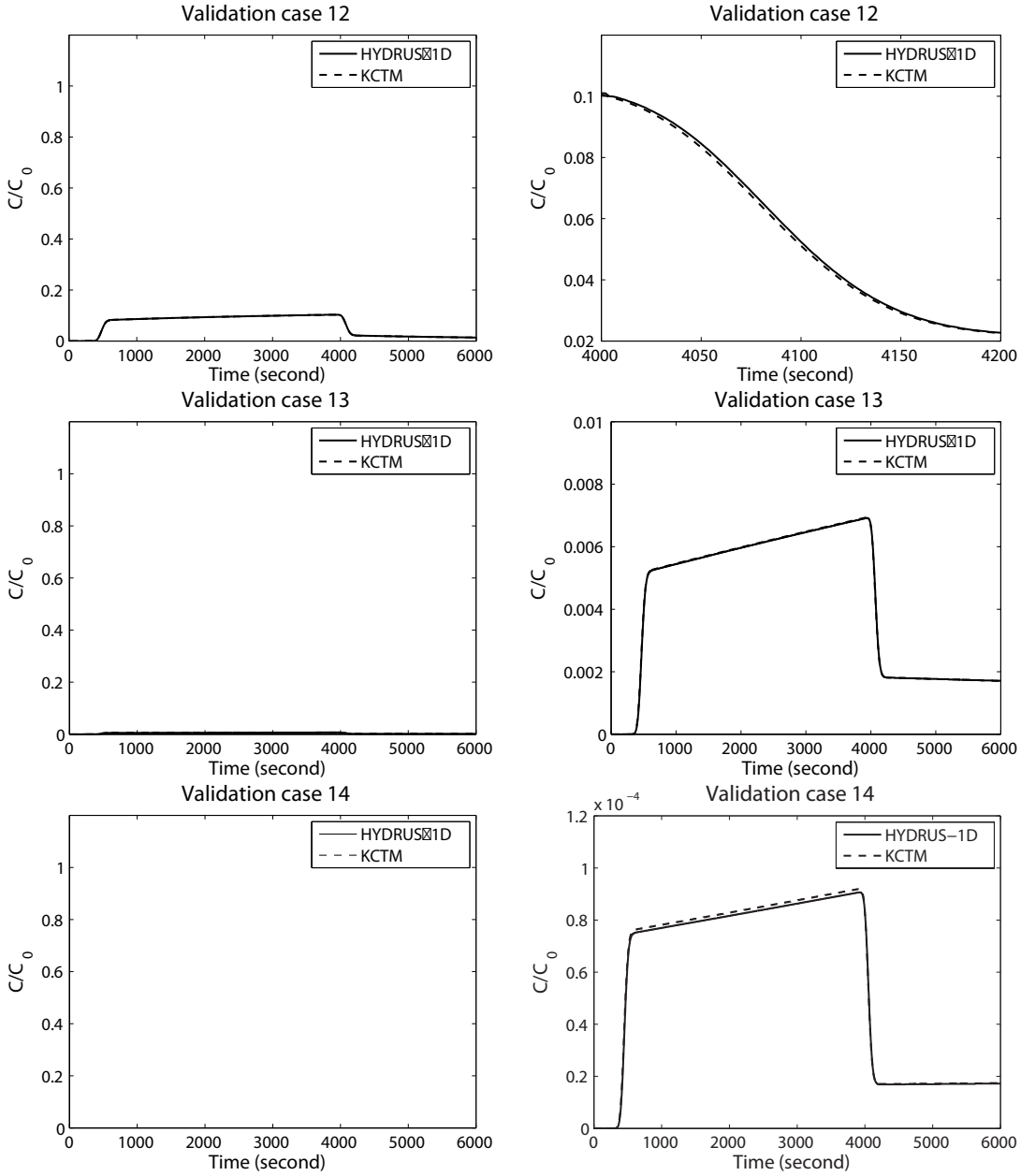

Figure 2.6: Simulated normalized, column breakthrough curves generated by HYDRUS-1D and KCTM for case 12, 13 and 14 (see Table 2.3 for simulation parameters). The right-hand figures show a zoom of the latter portion of the simulation for case 12, and the BTC for cases 13 and 14 with a scaled vertical axis.

2.4 Summary

This chapter presented the development and validation of a numerical model for colloid/ particle transport in saturated porous media, termed the KCMT, which is based on a finite-difference scheme implemented using Matlab. In addition to being able to simulate two-site particle attachment and detachment kinetics, the KCMT can also simulate dual-mode or two-population particle transport behavior, which cannot be simulated using current open software or commercial platforms. KCMT allows both forward prediction of particle transport problems as well as parameter fitting for a given set of observations. The KCMT was validated against analytical solutions generated by the STANMOD program and numerical simulations obtained using the popular software, HYDRUS-1D. Comparisons between KCMT, STANMOD and HYDRUS-1D were undertaken for one-site particle attachment and detachment kinetics, and between KCMT and HYDRUS-1D for two-site particle attachment and detachment kinetics. Good agreement between the results of KCMT, STANMOD and HYDRUS-1D were obtained over a range of modeling conditions. The following chapters of this thesis present the use of KCMT in the prediction and interpretation of complex particle transport behavior. In addition, Appendix A presents collaborative work that used the KCTM to analyze E.coli transport behavior in saturated sand columns of aquifer material obtained from a Bangladesh field site. The kinetic parameters obtained from the KCTM were further used in a modeling exercise to evaluate the impacts of anisotropic hydraulic conductivity on bacteria transport at an instrumented Bangladeshi field site.

2.5 Tables

Table 2.1: List of model parameters used for analytical solution predictions (STANMOD) and numerical modeling predictions (HYDRUS-1D and KCTM). The R^2 values represent the relative error between KCTM and STANMOD/ HYDRUS-1D.

Model	Parameter	Case 1	Case 2	Case 3	Case 4
KCTM,	D (m^2s^{-1})	1.00E-07	1.00E-07	2.00E-07	5.00E-08
STANMOD,	$k_a(s^{-1})$	4.00E-03	8.00E-03	8.00E-03	8.00E-03
HYDRUS	$k_d(s^{-1})$	8.00E-03	4.00E-03	4.00E-03	4.00E-03
	R (-)	1.50	3.00	3.00	3.00
STANMOD	β (-)	0.67	0.33	0.33	0.33
	ω (-)	2.00	4.00	4.00	4.00
HYDRUS	R^2	0.999990	0.999995	0.999995	0.999995
STANMOD	R^2	0.999682	0.999451	0.999765	0.999671

Table 2.2: List of the model parameters used for reversible model simulations. The R_d values represent the retardation factor (k_a/k_d).

Parameter	Case 5	Case 6	Case 7	Case 8
k_a (sec^{-1})	2.00E-3	4.00E-3	8.00E-3	1.2E-2
k_d (sec^{-1})	4.00E-3	4.00E-3	4.00E-3	4.00E-3
R_d	0.5	1.0	2.0	3.0

Table 2.3: List of model parameters used for two-site kinetic model predictions. The R^2 values represent the relative error between KCTM and Hydrus-1D.

Parameter		Case 9	Case 10	Case 11	Case 12	Case 13	Case 14
$D(m^2s^{-1})$		1.00E-07	1.00E-07	1.00E-07	1.00E-07	1.00E-07	1.00E-07
Site 1	$k_a(s^{-1})$	4.95E-04	1.04E-03	2.29E-03	4.46E-03	8.34E-03	1.29E-02
	$k_d(s^{-1})$	4.48E-04	2.00E-04	2.44E-05	2.50E-06	1.98E-07	1.95E-08
Site 2	$k_a(s^{-1})$	1.17E-05	4.35E-05	1.83E-04	6.69E-04	2.58E-03	7.22E-03
	$k_d(s^{-1})$	1.06E-03	1.00E-03	7.53E-04	3.49E-04	8.50E-05	1.88E-05
R^2		0.999968	0.999965	0.999963	0.999954	0.999908	0.999094

Chapter 3

Can Varying Velocity Conditions be One Possible Explanation for Differences between Laboratory and Field Observations of Bacterial Transport in Porous Media?

3.1 Abstract

Laboratory column experimental results are frequently used to estimate field-scale, fecal bacterial transport distances. However, it is not uncommon for fecal bacteria to be observed at greater distances than predicted by up-scaling laboratory results. Fluctuating or varying velocity conditions is one complex in-situ condition that might account for such inaccurate prediction, yet it is often neglected in laboratory column experiments. In this study, one-dimensional, laboratory column experiments were performed under both constant and varying velocity conditions using $2\mu m$ microspheres and $100\mu m$ glass beads to simulate bacterial transport in saturated porous media.

Particle breakthrough curves and particle concentrations retained in the column at the end of an experiment were obtained for five constant and three varying velocity conditions. The range of constant velocities investigated was between 3.17m/day and 27.65m/day. For varying velocity conditions, the velocity was steadily increased and/or decreased over the period of the experiment within the same range. Results from the constant velocity experiments were successfully modeled using first order, irreversible particle attachment kinetics. The irreversible attachment coefficients obtained from the constant velocity experiments were used to derive a power function relationship between a dimensionless irreversible attachment coefficient, K_i^* and velocity, v. This relationship was then used to model the varying velocity experiments, with limited success (NRMSE $> 10\%$ for all model fits). A comparison of K_i^* values obtained from direct fitting of the varying velocity tests, with the K_i^* values derived from the results of the constant velocity experiments, revealed a potential dependence of K_i^* on the rate of change of velocity. Observed particle breakthrough curves (BTCs) for the varying velocity experiments were also modeled using a constant value of K_i^* based on the average velocity of each experiment. The results of this modeling under-estimated observed maximum breakthrough concentrations for the column experiments where velocity increased, and especially under conditions where velocity increased then decreased. Overall, the results of this study point to the need for better understanding of how varying velocity conditions impact bacterial transport in the field.

3.2 Introduction

Diarrheal diseases cause illness and death globally, killing an estimated 1.8 million people every year [WHO, 2004]. Fecal bacteria, a major source of diarrheal disease [Prüss-Üstün *et al.*, 2008], are widespread in shallow aquifers and detected even when fate and transport predictions would indicate otherwise [Goss *et al.*, 1998; Schijven

and Hassanizadeh, 2000]. Laboratory column tests and field scale investigations are the two main experimental approaches for investigating subsurface bacterial fate and transport and advancing predictive theory.

Bacteria are micron-sized particles, often classified as colloid particles, whose attachment and detachment to the solid phase of a porous medium are controlled by physical, chemical, and biological interactions between a particle and the grains of the medium. Over the past several decades, a large number of laboratory column experiments have been used to investigate the effects of flow velocity magnitude, flow direction, particle size, grain size, grain surface roughness, liquid temperature, liquid pH, liquid ionic strength (IS), and bacterial characteristics on particle column breakthrough concentrations and retained concentration profiles [Kanti Sen and Khilar, 2006]. For example, *Hendry et al.* investigated *Klebsiella oxytoca* and *Burkholderia cepacia* transport in laboratory columns at four different, constant flow velocities and observed that the peak breakthrough concentrations of bacteria increased as the velocity increased [Hendry *et al.*, 1999]. Through modeling, they also demonstrated that particle attachment and detachment behavior are bacteria specific and related to surface chemistry. Based on their results, these researchers recommended that the relationship between velocity and particle behavior be determined before using column results to predict field behavior. *Keller et al.,* conducted laboratory column experiments under constant velocity conditions with bacteriophage MS2 and two different size microspheres to quantify the effect of velocity magnitude and particle size on the early breakthrough of particles [Keller *et al.*, 2004]. They found that both particle size and velocity magnitude influence early breakthrough behavior, and thus, potentially, rapid transport phenomena in aquifer systems. *Vasiliadou and Chrysikopoulos* conducted laboratory column experiments with *Pseudomonas Putida* bacteria and kaolinite clay particles, both separately and together, in order to examine their cotransport effects on particle behavior [Vasiliadou and Chrysikopoulos, 2011]. For tests examining the individual transport characteristics of the bacterial and kaolinite, these

authors reported a decrease in mass recovery for both particle types with decreasing velocity. More recently, *Shang et al.* halted flow for different time intervals during laboratory column experiments in order to examine how dynamic groundwater conditions might impact the transport of engineered nano-porous particles in saturated porous media [Shang *et al.*, 2013]. Although *Shang et al.* found that nanoparticle detachment was influenced by the duration of the no-flow period, they were able to model observed particle transport using theory developed for constant flow conditions. Nonetheless, despite the fact that dynamic groundwater conditions are the norm in aquifer systems contaminated with fecal bacteria, very few column studies have systematically investigated how varying velocity conditions impact colloid transportation in saturated media.

Complementing column experiments, numerous field scale experiments have also been undertaken to study bacteria transport in shallow aquifers [Bales *et al.*, 1997; Kersting *et al.*, 1999; Cvetkovic *et al.*, 2004; Knappett *et al.*, 2012]. Compared with laboratory testing, field scale experiments occur in a more complex environment and are subject to many uncontrollable factors, including subsurface physical and chemical heterogeneity, as well as often ill-defined three dimensional flow conditions. Previous research reported that up-scaling column experiment results to predict bacterial transport at the field scale always fall short of observed transport distances in the field [Dong *et al.*, 2006; Foppen and Schijven, 2006; Pang, 2008]. *Knappett et al.* speculated that one reason for this at their Bangladeshi experimental field site, might be the rapidly increasing and decreasing advective transport velocities observed during the monsoon season, which are not accounted for in laboratory experiments conducted at constant flow velocity [Knappett *et al.*, 2014]. *Anders and Chrysikopoulos* conducted field tests with bacterial viruses in order to specifically examine recharge source effects [Anders and Chrysikopoulos, 2005]. Their results showed time-dependence of particle collision efficiencies, which they concluded was mainly due to fluctuations of the interstitial fluid velocity.

This study investigated the effects of varying velocity on particle transport in saturated porous media by modifying traditional column test protocols to enable simulation of increasing and decreasing flow velocities during an experiment. Results from varying velocity experiments were compared with results from experiments conducted under constant velocity conditions. In addition, models derived from the constant velocity experiments were used to predict the varying velocity experiments, in order to explore whether relationships derived under constant conditions could predict transport in transient systems.

3.3 Material and methods

3.3.1 Particles

Spherical, mono-dispersed, fluorescent, carboxylate-modified, polystyrene latex microspheres were used as the micron sized particles in the experiments (Molecular Probes, Inc., Eugene, OR). The microsphere diameter was $2\mu m$, and the excitation and emission wavelengths of the particles were $365nm$ and $415nm$, respectively. The solids concentration of the manufacturer-supplied stock solution was $0.02g/mL$. The experimental solutions were prepared by diluting the stock solution using artificial groundwater (AGW) at the desired ionic strength (IS) and pH value.

3.3.2 Porous media

Glass beads of $100\mu m$ diameter (USA Scientific, Inc., Ocala, FL) were used to simulate sediment in the experiments. The glass beads were washed with deionized water and dried in an oven at 60^oC prior to the preparation of each column experiment.

3.3.3 Solution chemistry

The AGW was made with KCl at an IS of $100mM$. The solution pH value was adjusted to 6.8 ± 0.05 by using $0.1M$ NaOH and 3% HCl solution. Column inlet solutions contained the $2\mu m$ diameter microspheres at a concentration of $2.67\times10^{-3}mg/L$, referred to as C_0. Inlet solutions were stirred throughout each experiment to help ensure a uniform particle inlet concentration.

3.3.4 Experimental set-up and protocol

In order to simulate both constant and fluctuating velocity conditions, the experimental protocol designed of *Feighery et al.* was modified (Figure 3.1) [Feighery *et al.*, 2013]. Eight flex columns (Kimble Chase Life Science and Research Products LLC, Rockwood, TN) of 2.5cm inner diameter and 8cm length were used in the experimental series. The columns were equipped with stainless steel screens on both the top and bottom to retain the glass beads. The glass beads were wet-packed into the columns at an average porosity of 0.33. Columns were alphabetically labeled from A to H, with each letter referring to a different velocity condition. Prior to an experiment, each column was attached to a ring stand and each column inlet was leveled to the same elevation. Before particle injection, clean AGW was upwardly injected for 10 pore volumes at the base of each column to saturate the glass beads and flush out impurities.

To simulate different velocity conditions, eight velocity protocols were designed. A multi-channel peristaltic pump (Minipuls 3, Gilson, Inc., Middleton, WI) was used to introduce test solutions directly into the columns or the Varying Velocity Simulator (VVS), which comprised of a 2.54cm inner diameter and 100cm length PVC pipe (Schedule 40, Georg Fisher Harvel LLC, Easton, PA). Columns A to E involved experiments with constant advective velocities of 3.17, 3.54, 11.8, 21.28, and 27.65m/day, respectively. For column F to H, the VVS was used to imitate transient velocity scenarios that included increasing (F), decreasing (G), and increasing then decreasing

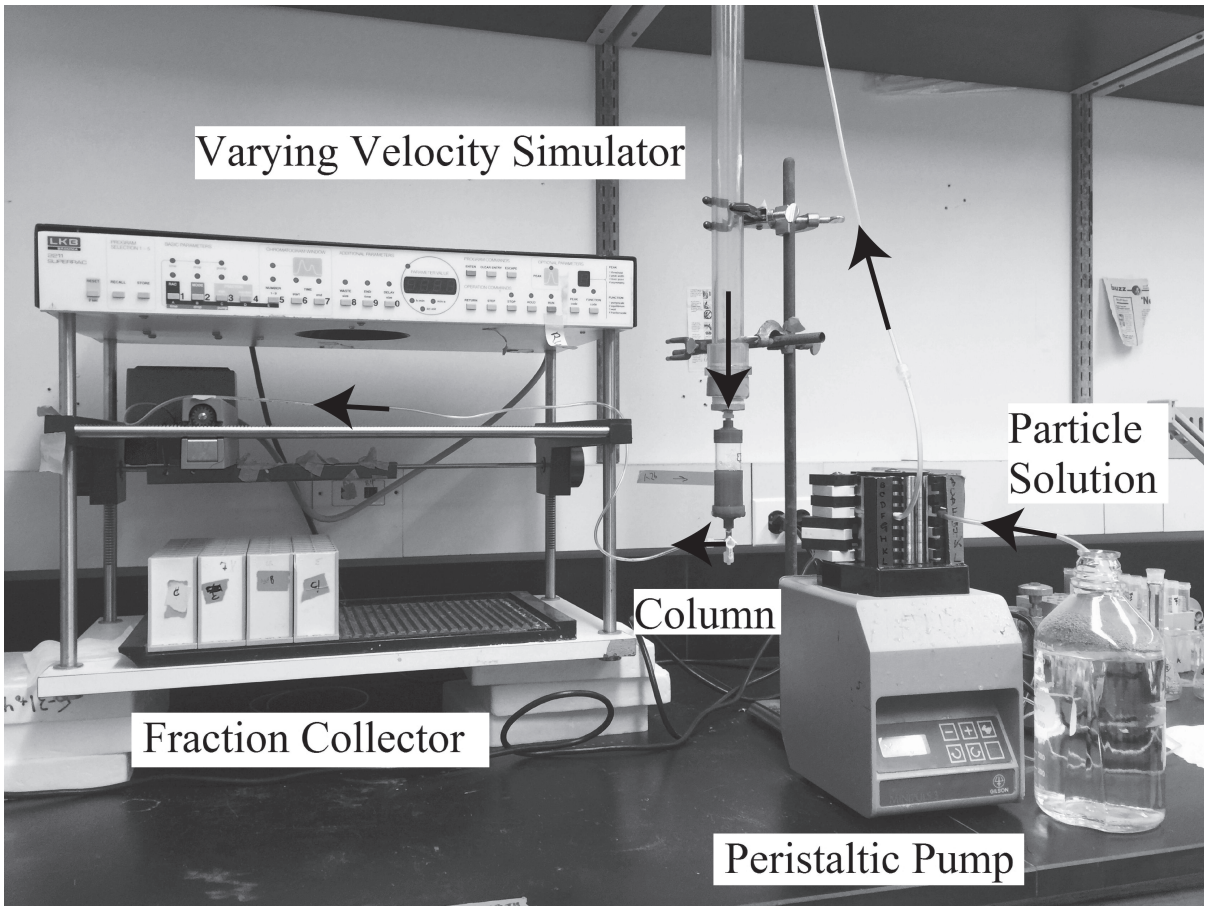

Figure 3.1: Set-up of column experiments for varying velocity conditions. The particle solution was introduced into the Varying Velocity Simulator (VVS) via a peristaltic pump. The flow velocity into the top of the column at any one point in time was determined by the height of the particle solution in the VVS, which changed over the course of each experiment. The solution exiting the base of the column was collected in aliquots using a fraction collector. For the constant velocity experiments, the Varying Velocity Simulator was removed and the peristaltic pump introduced the particle solution into the top of the column at a constant, predetermined rate.

(H) flow velocities over ranges that had been observed at a fecal contaminated, field site in Bangladesh [Knappett *et al.*, 2011b]. Column F was connected to an empty VVS, which was then pumped full of AGW, causing the packed glass bead column to experience increasing velocity conditions. Column G was connected to a VVS that began full of solution and was then drained, causing the column to experience decreasing velocity conditions. With column H, the VVS started empty, was pumped full of AGW, and was then left to drain. Thus, column H experienced increasing and then decreasing velocity conditions.

Column effluent samples were collected every $100sec$ in $15ml$ polypropylene tubes (Thermo Fisher Scientific, Inc., Pittsburgh, PA) using a fraction collector (LKB Bromma 2211, SuperRac, Sweden). All collected samples were weighed to support velocity calculations. The florescent intensity of each sample was determined using an excitation wavelength of 365nm and monitored at 415nm using a fluorimeter (PC1 Photon Counting Spectrofluorimeter, ISS, Inc., Champaign, IL). The intensity of fluorescence in each sample was used to estimate the concentration, C, of particles in the sample. The ratio of this concentration to the column inlet concentration yielded C/C_0 values for each fraction.

At the end of each experiment, the columns were dissected into five equal sections of length to measure the retained particle concentration profile. The glass beads from each section were deposited into 50ml polypropylene tubes (Thermo Fisher Scientific, Inc., Pittsburgh, PA). Twenty ml of deionized water was added to each tube to detach the microspheres from the glass beads. After 2 hours of shaking on an incubator shaker (New Brunswick Classic C25KC, Eppendorf AG, Hamburg, Germany), the supernatants were extracted and their fluorescence intensity was measured by the aforementioned fluorimeter. This measurement was used to estimate the retained particle concentration in each column section.

The normalized mass recovery of microspheres for each experiment was obtained by summing the measured light intensities of the effluent samples and the retained

particle samples, and dividing by the total light intensity of introduced microspheres.

3.3.5 Modeling constant velocity experiments

The advection-dispersion equation, which is commonly used to describe the particle concentrations associated with the liquid phase and solid phases of a saturated porous medium during transport was adopted for modeling [Johnson *et al.*, 2007b]:

$$\frac{\partial c}{\partial t} + \frac{\rho_b}{\theta}\frac{\partial s}{\partial t} = D\frac{\partial^2 c}{\partial x^2} - v\frac{\partial c}{\partial x} \tag{3.1}$$

where c is the particle concentration in the pore fluid $[M/L^3]$, s is the attached particle concentration associated with solid phase $[M/M]$, x is the distance from the particle inlet boundary $[L]$, t is the time $[T]$, D is the hydrodynamic dispersion coefficient $[L^2/T]$, v is the average steady state pore fluid velocity $[L/T]$, ρ_b is the bulk density of the solid phase $[M/L^3]$, and θ is the porous medium porosity $[-]$. Note, Particle growth and decay were neglected in this study because of the use of latex microspheres.

Particle attachment/detachment processes, which govern particle fluxes between the liquid and solid phases of a porous medium, are usually described by a first order kinetic expression. In this study, only irreversible attachment was considered because of the high IS conditions of the experiments and the fact that experiments did not involve a particle flushing stage, which might have led to particle detachment. The first-order irreversible kinetic expression used was:

$$\frac{\rho_b}{\theta}\frac{\partial s}{\partial t} = k_i c \tag{3.2}$$

where k_i is the first-order particle irreversible attachment coefficient $[T^{-1}]$.

To enable the numerical solution of Equations 3.1 and 3.2, a MATLAB program based on a finite difference scheme was developed. The program discretized the time derivative using a *Crank-Nicolson* approximation and the space derivative using a central difference approximation. To simulate the column experiments, a *Dirichlet*

boundary condition and *Neumann* boundary condition were applied at the column inlet and outlet points of the modeled domain, respectively. For the experimental conditions of the study, the appropriate initial and boundary conditions were:

$$c_i(0, x) = 0 \tag{3.3}$$

$$c(t, 0) = \begin{cases} 0, t < t_p \\ c_0, t \geq t_p \end{cases} \tag{3.4}$$

$$\frac{\partial c(t, L)}{\partial x} = 0 \tag{3.5}$$

where $t_p[T]$ is the particle injection start time, which was equal to 0 in this study, $c_i[M/L^3]$ is the initial particle concentration in the liquid phase, also equal to 0 in this study, and $L[L]$ is the column length. Note, the *Dirichlet* boundary condition equation 3.4 implies that the inlet particle concentration is constant over time, while the *Neumann* boundary condition equation 3.5 preserves particle concentration continuity at the outlet of the column. The discretized grid size and time step were automatically checked against numerical stability criteria and adjusted accordingly.

To obtain a relationship between k_i and v, Equations 3.1 and 3.2 were fitted to the observed data taking $\rho_b = 1.675 g/cm^3$ (the bulk density of the glass beads), $\theta = 0.33$ (the porosity of the columns) and $D = \alpha_L \times v$ [Yoon *et al.*, 2006], where the longitudinal dispersivity, α_L, of the packed columns was taken as $200 \mu m$ (twice the diameter of the glass beads). To estimate k_i for each of the constant velocity experiments, an iterative process of fitting observed data, using k_i as the only fitting parameter, was used. Specifically, for each experiment k_i was obtained by minimizing the sum of squared residuals (i.e., the difference between the measured and modeled concentrations) at the column outlet location and within the column for the retained concentration profile at the end of an experiment. For minimizing the residuals, the numerical model used a modified version of the MATLAB fminsearch function, which is based on the Nelder-Mead simplex algorithm. Residuals were computed in

log space to avoid biasing the model fit to the highest concentration portions of the breakthrough curve.

3.3.6 Modeling varying velocity experiments

In order to predict microsphere breakthrough under the varying velocity conditions, it was necessary to estimate first-order kinetic irreversible attachment rates as a function of velocity. First a dimensionless attachment coefficient was defined [Keller *et al.*, 2004], namely:

$$K_i^* = \frac{Lk_i}{v} \tag{3.6}$$

where K_i^* is dimensionless irreversible attachment coefficient and L is a characteristic length of the system under consideration $[L]$ (e.g., column length).

Next, a regression was performed between the response variable, v, and the predictor variable K_i^*. The regression yielded an empirical formula to estimate K_i^* from v, from which k_i was obtained for each time-step in the numerical solution of Equations 3.1 and 3.2. Note, for the varying velocity experiments the value of $v(t)$ needed at each time step in Equation 3.1 was calculated from measurements of the weight of fluid exiting the column, which were taken over two-minute intervals. Because the modeling time step was less than two-minutes, a linear interpolation was used to provide a continuous function of v versus t.

3.4 Results

3.4.1 Constant velocity experiments

Five columns were tested with different constant velocity conditions (Table 3.1 and Figure 3.2). Column A and B had the two lowest velocities at 3.17 and 3.54m/day, respectively, with averaged, normalized plateau concentrations for the breakthrough curves (BTC) of 0.0018 and 0.002, respectively. Column C had medium velocity at

11.8m/day with an average, normalized BTC plateau concentration of 0.019. Column D and E had the highest velocities at 21.28 and 27.65m/day, respectively. The averaged, normalized BTC plateau concentration for Column D was 0.12, while for Column E it was 0.11. The mass recovery was 79% for Column A, 88% for B, and was lower for Columns C to E (74%, 76% and 66%, respectively). All particle retention profiles (RPs) exhibited a peak concentration in the column section closest to the inlet, which decreased in a log linear fashion toward the column outlet.

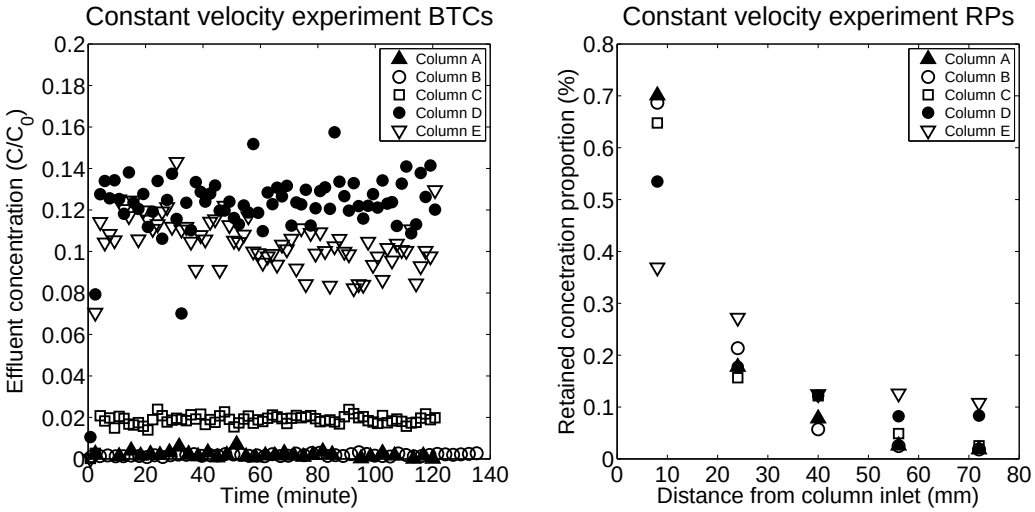

Figure 3.2: Constant velocity experimental results: (a) breakthrough concentrations and (b) retention profiles

3.4.2 Varying velocity experiments

Three columns were tested with varying velocity conditions (Table 3.1 and Figure 3.3). In Column F, velocities increased in a log-linear fashion from 10.38 to 27.78m/day, mimicking velocity increases observed at a Bangladeshi field site during monsoonal rains [Knappett *et al.*, 2014]. The normalized breakthrough concentrations for this test followed a similar trend to the velocity increase, rising rapidly to 0.08 at 17.5 minutes following particle injection, then more slowly to 0.12 at 29.2 minutes. In

Column G velocities decreased in a log-linear fashion from 18.78 to 2.91m/day, mimicking velocity decreases observed at the aforementioned Bangladeshi site following monsoonal rains. Column G exhibited essentially no particle breakthrough during the test period, with an observed, averaged normalized breakthrough concentration of 0.011. In column H, the velocity increased log linearly from 8.24 to 17.04m/day, then decreased to 3.76m/day, mimicking rising, followed by falling, aquifer velocities. During the initial portion of this test, normalized breakthrough concentrations increased to 0.07 during the first 22.5 minutes of particle injection, then increased more slowly to 0.1 over the next 57 minutes. After switching to a decreasing velocity condition, the normalized concentrations decreased from 0.1 to 0.002 over about 20 minutes, then remained low with an average value of 0.001. All end-of-test particle retention profiles had a peak concentration in the top section of the column, which decreased in a log-linear manner from the column inlet to outlet. The particle mass recovery rates were 67%, 82%, 66% for column F, G, and H, respectively.

3.4.3 Model fits of constant velocity experiments

The kinetic irreversible attachment model (Equations 3.1 and 3.2) was sufficient to fit observations from all constant velocity experiments (Figure 3.4). As defined by the calculated RMSE values (Table 3.1), fits to the experimental BTCs were always superior to those for the retained particle concentrations. In general, RMSE values decreased with the column advective velocity. For the BTCs, Column A had an RMSE of 0.002, Column B an RMSE of 0.001, and Column C, D and E had RMSEs of 0.003, 0.013 and 0.018, respectively. For the retained profiles, RMSEs for columns A and B were 0.024, and for Columns C, D and E, 0.051, 0.071 and 0.034, respectively.

Values of k_i obtained from the fits were converted to dimensionless attachment coefficient values with Equation 3.6. Column A and B, which had the lowest advective velocities, had the highest K_i^* values of 33.9 and 33.1, respectively. Column C had a medium K_i^* of 18.5. Column D and E, which had the highest advective velocities,

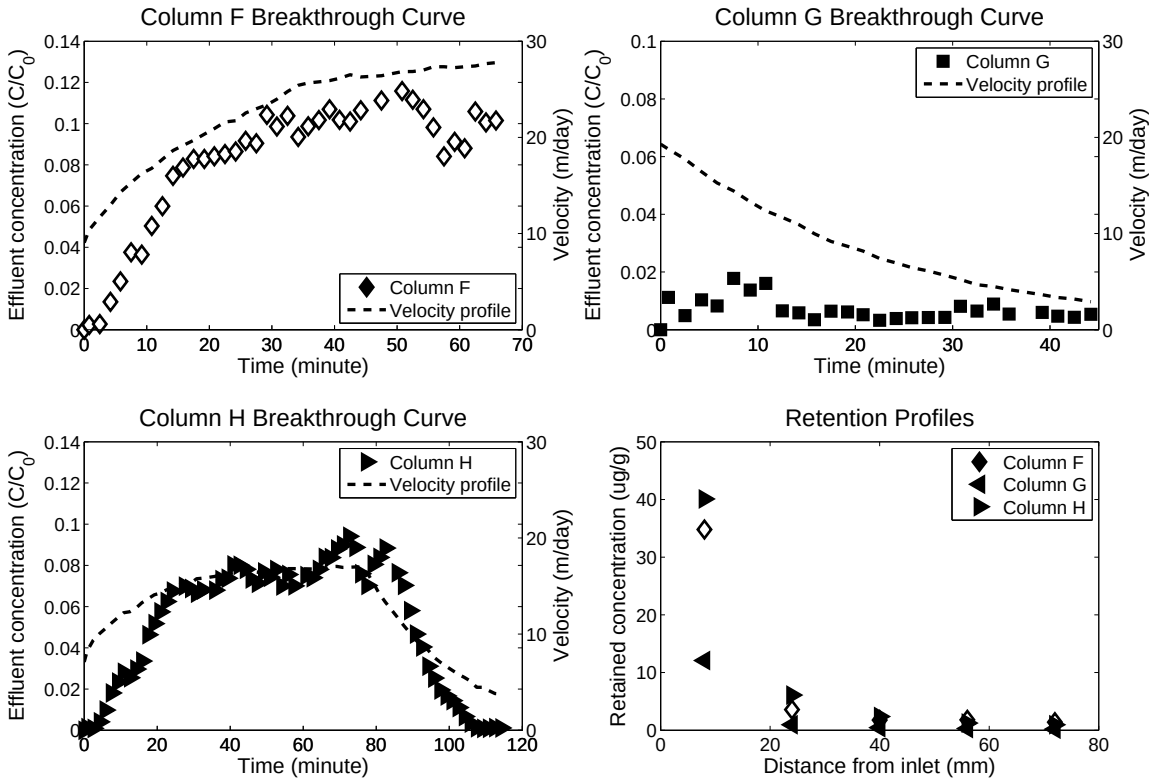

Figure 3.3: Varied velocity experimental results and corresponding measured velocity profiles (dash lines): (a) Column F increasing velocity breakthrough curve,(b) Column G decreasing velocity breakthrough curve, (c) Column H increasing then decreasing velocity breakthrough curve and (d) retention profiles for all tests.

had the lowest K_i^* values of 8.5 and 8.7, respectively.

3.4.4 Relationships between K_i^* and v

The K_i^* values obtained from the constant velocity experiments were plotted against velocity, and a regression using a power function distribution ($y = ax^b$) was performed with advective velocity, v, as the response variable and K_i^* as the predictor variable (Figure 3.5). The choice of a power-function regression was based on exploration of linear, exponential and power function regressions of K_i^* versus v for the results of the constant velocity experiments reported here as well as those reported in previous study [Yoon *et al.*, 2006]. Overall, a power function distribution provided the best fit for all sets of experimental data. For the constant velocity experiments reported here, the power function regression has coefficients $a = 68.34$ and $b = -0.595$. The corresponding SSE (sum of square error) and R^2 values of the regression were 16.13 and 0.97, respectively, while the *Akaike information criterion* (AIC) and *Bayesian information criterion* (BIC) were 23.66 and 22.49, respectively. Based on these values, the regression was considered statistically significant [Burnham, 2004; Kadane and Lazar, 2004; Cohen, 1988].

3.4.5 Model fits of varying velocity experiments

Prediction of the experimental results obtained for Columns F, G and H was undertaken using Equations 3.1 3.2 and 3.6, in conjunction with the power function regression between K_i^* and v shown in Figure 3.5, referred to as the regression power function. To enable comparison between the model fits of each varying velocity experiment, the Normalized Root-Mean-Square Error (NRMSE) was calculated for each fit (see Table 3.1).

For Column F, the modeling results under-estimated measured normalized particle concentrations in the BTC during the initial stages of the test, and over-estimated concentrations during the latter stages of the test (Figure 3.6a1). A similar trend was

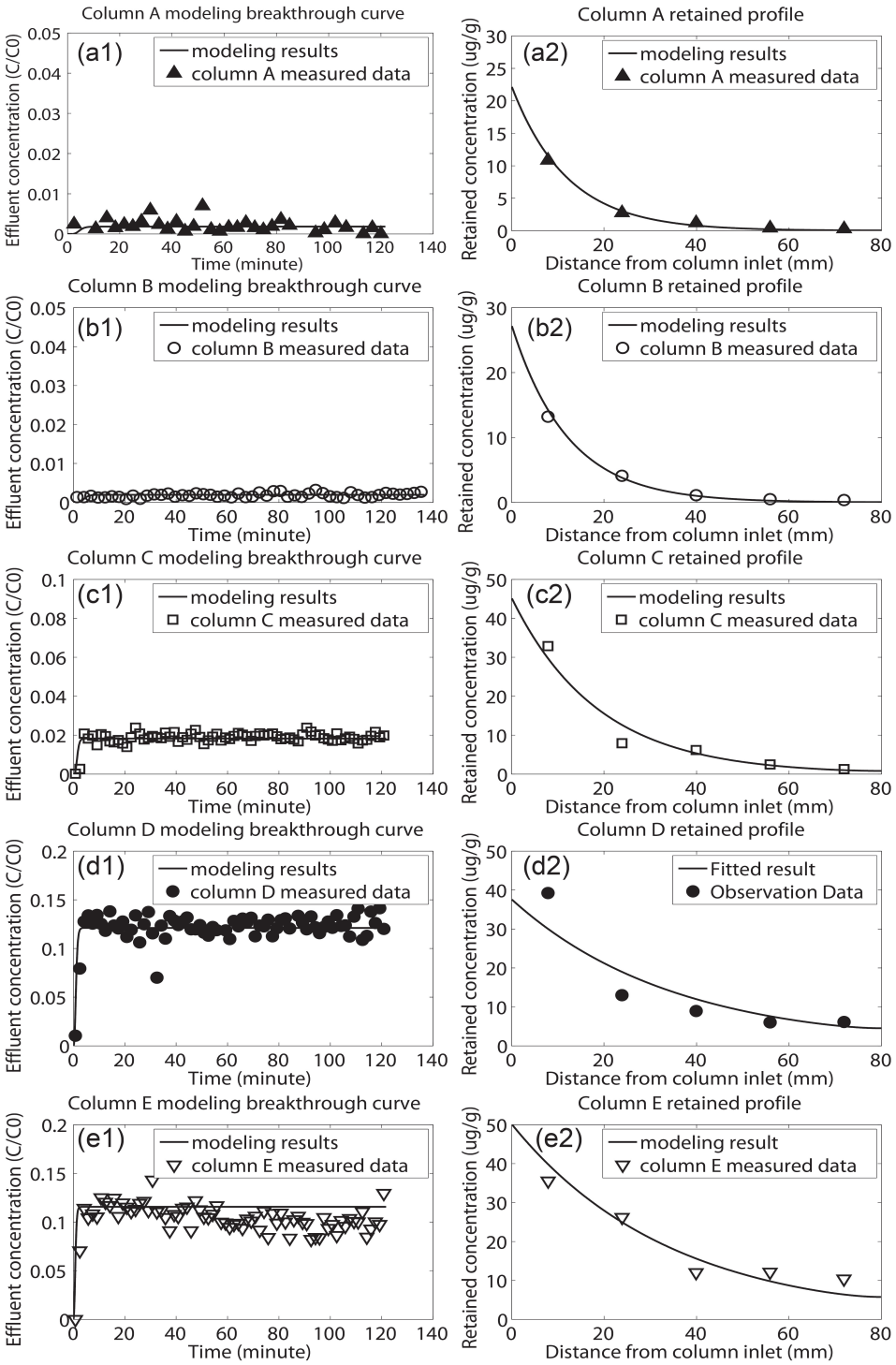

Figure 3.4: Comparison of model fits to experimental data using Eqs. (3.1) and (3.2) for Columns A to E. Left side (a1 to e1) BTCs. Right side (a2 to e2) retention profiles.

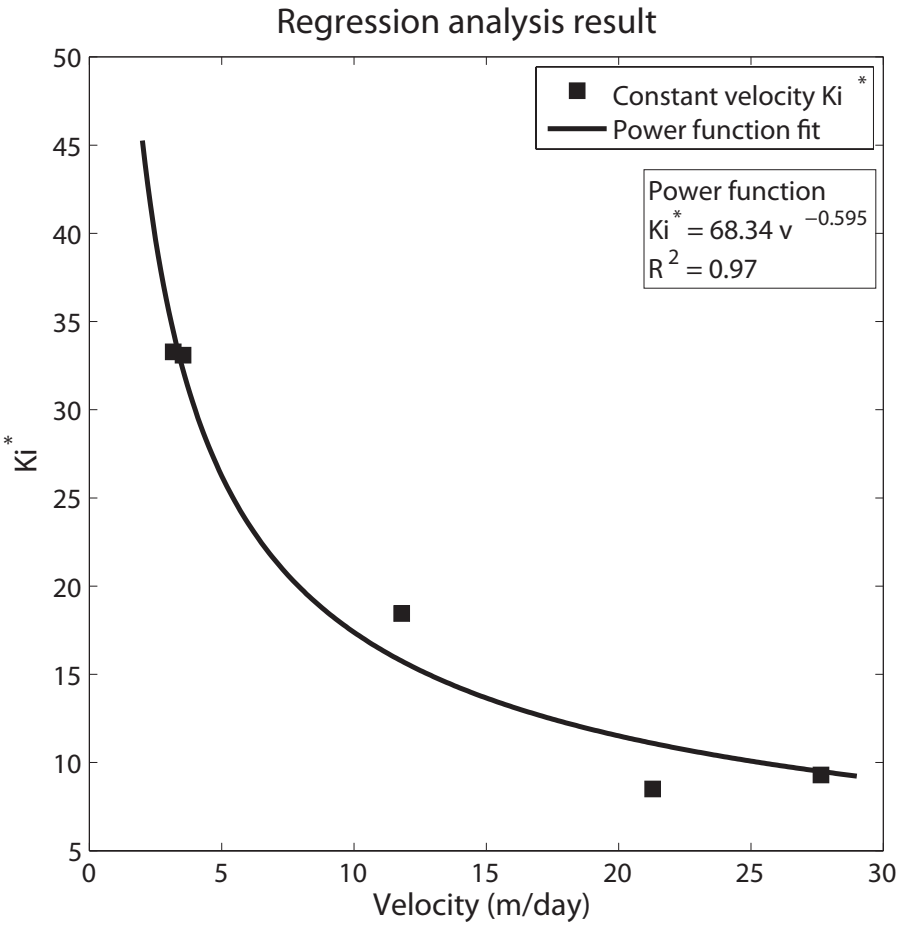

Figure 3.5: Regression analysis of the relationship between K_i^* and advective velocity based on K_i^* values obtained from the 5 constant velocity experiments and a power function relationship.

seen for the particle retention profile, with an under-estimation of particle concentrations in the initial portion of the column closest to the inlet, and an overestimation of particle concentrations in the latter portion of the column closest to the outlet (Figure 3.6a2). For Column F, the NRMSE values for the BTC and retention profile model fits were 0.11 and 0.25, respectively. For Column G, the modeling results over-estimated BTC concentrations over most of the experiment, but under-estimated concentrations toward the end of the experiment (Figure 3.6b1). As per Column F, retained particle concentrations were underestimated in the initial portion of the column and over-estimated in the latter potion of the column (Figure 3.6b2). The NRMSE values for the model fits of the Column G BTC and retained profile were 0.74 and 0.19, respectively. For Column H, the modeling results underestimated BTC concentrations over most of the experiment, excepting the initial 10 minutes (Figure 3.6c1), and once again retained particle concentrations were underestimated in the initial portion of the column and over-estimated in the latter potion (Figure 3.6c2). The NMRSE model fit values for the BTC and retention profile of Column H were both 0.19. According to *Jean et al.* an NRMSE of 10% or less represents an adequate model calibration [Jean *et al.*, 2013]. Using this criterion, none of the model predictions illustrated by Figure 3.6 performed adequately.

3.5 Discussion

3.5.1 Constant velocity experiments

There were significant differences in the magnitude of normalized breakthrough concentrations and retention profiles between the five constant velocity experiments (Figure 3.2a). Increasing velocity increased effluent concentrations and flattened particle retention profiles. For example, the approximate order-of-magnitude difference between advective velocities in column A ($v = 3.17m/day$) and column E ($v = 27.65m/day$) led to almost two orders of magnitude difference in the correspond-

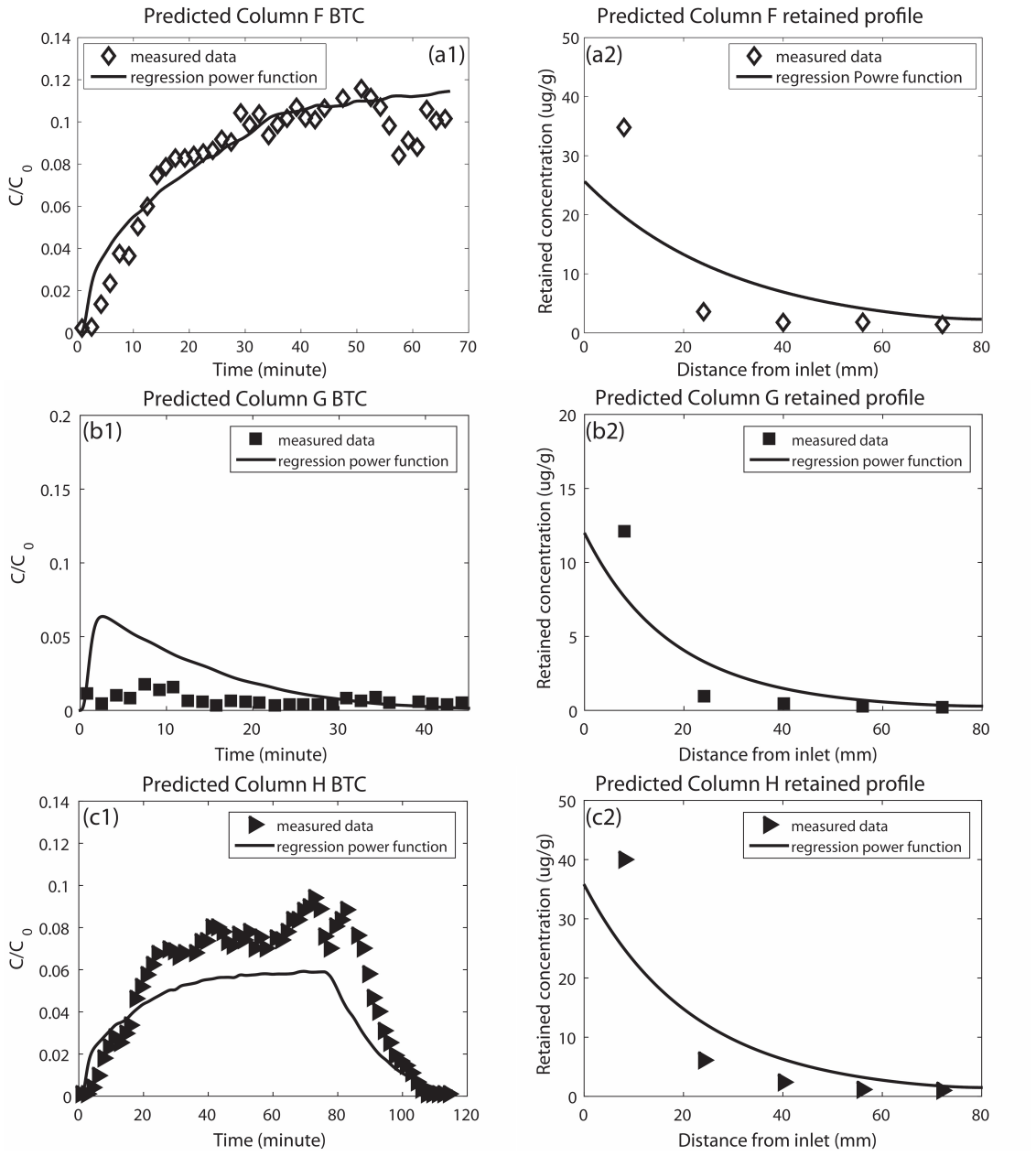

Figure 3.6: Comparison of observed and predicted data for the varied velocity tests using the power function regression shown on Figure 3.5 to describe the relationship between K_i^* and advective velocity. (a1) to (c1) show fits for BTCs for Columns F to G, respectively. (a2) to (c2) show fits for retained particle profiles for Columns F to G, respectively. Note, the BTC experimental data are presented as a three-point moving average to clarify trends

ing averaged BTC plateau concentration (A= 0.0018 and E= 0.11). Peak retention profile concentrations also decreased from 70% (A) to 37% (E) (Figure 3.2b), while the average retention concentration in the bottom three sections of the column increased from 0.04% (A) to 0.12% (E). Finally, estimated K_i^* values decreased from 33.9 to 8.7 (column A and E), demonstrating higher velocity reduces kinetic attachment rates and leads to longer transport distances. These findings are consistent with those reported from other experimental investigations exploring the role of advective velocity on particle transport behavior [Hendry *et al.*, 1999; Vasiliadou and Chrysikopoulos, 2011; Gannon *et al.*, 1991; Marlow *et al.*, 1991; Tan *et al.*, 1994; Chrysikopoulos and Sim, 1996; Camesano and Logan, 1998; Becker *et al.*, 2004; Tong and Johnson, 2006; Choi *et al.*, 2007].

Particle mass recovery rates decreased with increasing velocity (see Table 3.1), with recovery rates ranging from 88% ($v = 3.54m/day$) to 66% ($v = 27.65m/day$). At the low flows, recovery rates are similar to those reported by other researchers. For example, *Tong and Johnson* reported recovery rates ranging from 80.4% to 105.3% for column experiments examining microsphere transport in glass beads at a velocity of 4m/day [Tong and Johnson, 2006]. A reduction in mass recovery with increasing velocity was also reported by *Li et al.* during column experiments involving the transport of $36\mu m$ spheres in quartz sand, with recovery rates dropping from 96% to 67% when the column velocity increased from 86.4m/day to 216m/day [Li *et al.*, 2006]. As velocity increases so does the mass flux of particles, which led to an increase in retained particle mass with velocity for the Columns A to E (see Figure 3.4). It is speculated that detachment of microspheres from the glass beads using the protocol described in Section 3.3.4 becomes less efficient as the mass of attached particles increases, thus mass recovery rates drop as with increasing velocity. Similar issues were also reported by Kim et al. and Sinton et al., who conducted column experiments using bacteria, aquifer sand and gravel [Kim *et al.*, 2009; Sinton *et al.*, 2011]. Exploration of different detachment protocols might improve recovery rates in

future tests.

The model fit RMSE values for the two columns with the lowest velocities, A and B, were lower than for columns C, D and E. This might be related to the decrease in particle recovery rates with increasing velocity, as discussed above. Another possible explanation is that high velocities, while decreasing irreversible attachment rates, increase reversible attachment and detachment rates [Yoon *et al.*, 2006], which will influence the shape of the particle retention curve. Thus, model fits based only on irreversible attachment processes might be expected to increase in error as velocity increases. Nonetheless, all fits based on Equations (1) and (2) were considered acceptable for the constant velocity experiments.

3.5.2 Varying velocity experiments

Normalized BTCs for Column F and H had a similar pattern of increasing particle breakthrough with velocity. For Column H, breakthrough concentrations were also observed to decrease as the velocity decreased. For Column G the same trend was seen, although it was less apparent than for Column H as breakthrough concentrations were low throughout this experiment. Retained particle mass at the end of each column experiment were higher for Columns F and H, than Column G, with the mass recovery rates for Columns F and H being comparable to those for Columns D and E, and the mass recovery rate for Column G being comparable to those for Column A and B. As per the constant velocity experiments, the lower mass recovery rates for the experiments with higher retained particle mass is attributed to increased difficulty in recovering all attached microspheres in the column sections, with increased retained mass.

Although Equations 3.1 and 3.2 were considered sufficient to model the five constant velocity experiments, the NRMSE values reported in Table 3.1 for the model fits based on Equations 3.1 and 3.2 and the relationship between K_i^* and v derived from the constant velocity experiments (see Figure 3.5), all exceeded 10%. Thus, for the

conditions of the experiments reported here, it was not possible to accurately predict particle transport under a varying advective velocity using a relationship between particle attachment rate and velocity inferred from constant velocity conditions. It is conceivable that velocity changes induce more complex particle attachment behavior, including blocking, ripening, and reversible attachment and detachment [Nascimento *et al.*, 2006; Basha and Culligan, 2010], than is not accounted for in Equations 3.1 and 3.2. Another explanation is that velocity changes themselves influence the relationship between K_i^* and v, which is not something quantifiable via a series of constant velocity experiments.

To examine why the modeling results based on a relationship between K_i^* and v derived from the constant velocity experiments, did not capture the behavior of the varying velocity experiments, the varying velocity experiments were fit assuming a power function relationships between K_i^* and v ($K_i^* = a{*}v^b$) with a and b as the fitting parameters. As per the constant velocity experiments (see Section 3.3.5), fitting was carried out by minimizing the sum of squared residuals between the experimental and model data using a modified version of the MATLAB fminsearch function. In addition, residuals were computed in log space to avoid biasing the model fit to the highest concentration portions of the breakthrough curve. For Columns F and G, one power function relationship was used to fit the entire experimental data set (i.e., the BTC and retained profile data). for Column H, the experimental data were fit with two power function relationships; one for the increasing velocity portion of the experiment (0 to 79 minutes) and another for the decreasing velocity portion of the experiment (79 to 115 minutes). For fitting the increasing velocity partition, the entire experimental data set was used and residuals were minimized for the BTC data from 0 to 79 minutes. For fitting the decreasing velocity portion, the initial conditions of the liquid and solid phase particle concentrations were obtained from the increasing velocity simulation results at 79 minutes, and residuals were minimized for the BTC data from 79 to 115 minutes and the final retained profile. The results

of the fitting are reported in Table 3.1 under "Fitted Power Function", and in Figure 3.7. As seen, use of the fitted power function, versus the regression power function, reduced the NMRSE for all three BTCs, as well as the RP of Column G.

Figure 3.8a is a plot of K_i^* versus experimental time based on the regression and fitted power function relationships, respectively. As seen, there is a general trend for the regression power function to over-estimate K_i^* under increasing velocity conditions (Column F and the initial 79 minutes of Column H) and under-estimate K_i^* during decreasing velocity conditions (Column G and the latter 36 minutes of Column H). To examine this trend further, values of $(K^*_{iregression} - K^*_{ifitted})$ were plotted for seven different ranges of dv/dt, Figure 3.8b. Of note, is that the mean value of $(K^*_{iregression} - K^*_{ifitted})$ is lowest (0.09) when dv/dt is closest to zero; i.e. when velocity conditions are almost constant. Additionally, for negative values of dv/dt, the mean value of $(K^*_{iregression} - K^*_{ifitted})$ is always less than zero, while for positive values of dv/dt, it is always above zero. While there is scatter in the value of $(K^*_{iregression} - K^*_{ifitted})$ within each range of dv/dt, the results presented in Figure 3.8b point to the possibility that macroscopic pore fluid accelerations might influence particle filtration processes, with accelerating fluid conditions decreasing the filtration efficiency and decelerating conditions increasing it. Nonetheless, further experimentation over a wider ranges of conditions than investigated here is needed to confirm this trend.

3.5.3 Implications for field observations

To understand how varying velocity conditions might explain the observation of fecal bacteria at greater distances in the field than forecasted via up-scaling from laboratory column tests, the BTC data from Column F, G and H were compared with predictions generated using a constant K_i^* associated with the average velocity of each experiment. The K_i^* values were estimated using the regression power function. Although not reported here, trends based on K_i^* values obtained from the fitted power functions were found to be similar. The results are shown in Table 3.1 and Figure

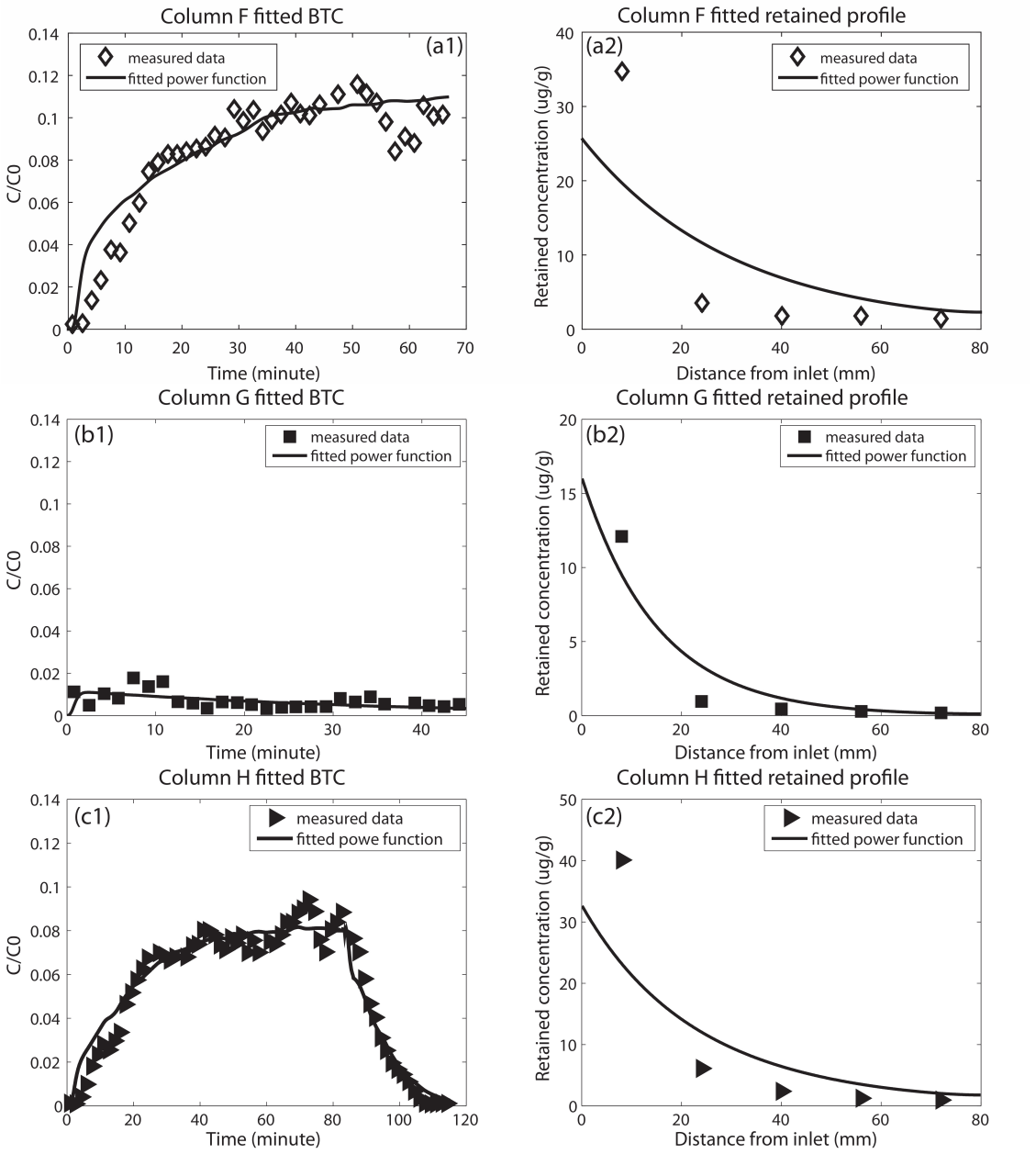

Figure 3.7: Comparison of observed and predicted data for the varied velocity tests using the fitted power function regressions provided in Table 3.1 to describe the relationship between K_i^* and advective velocity. (a1) to (c1) show fits for BTCs for Columns F to G, respectively. (a2) to (c2) show fits for retained particle profiles for Columns F to G, respectively. Note, the BTC experimental data are presented as a three-point moving average to clarify trends

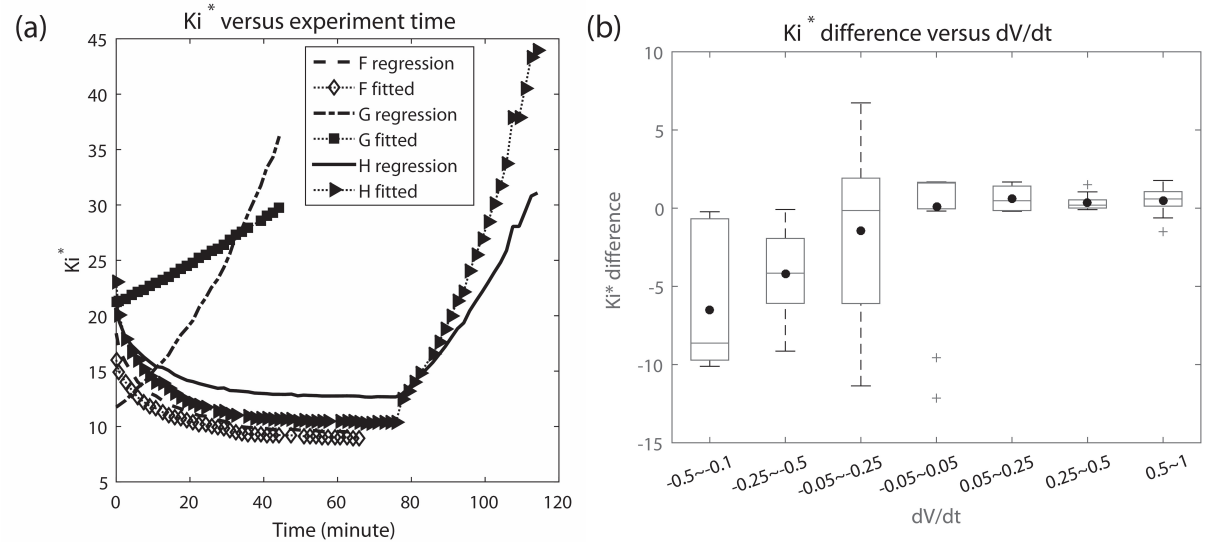

Figure 3.8: Comparison of K_i^* values obtained from regression and fitted power functions. (a) Variation of K_i^* values with experimental time for Columns F, G and H, (b) Boxplots of $(K^*_{iregression} - K^*_{ifitted}$ for seven different ranges of dv/dt; circles represent mean values.

3.9.

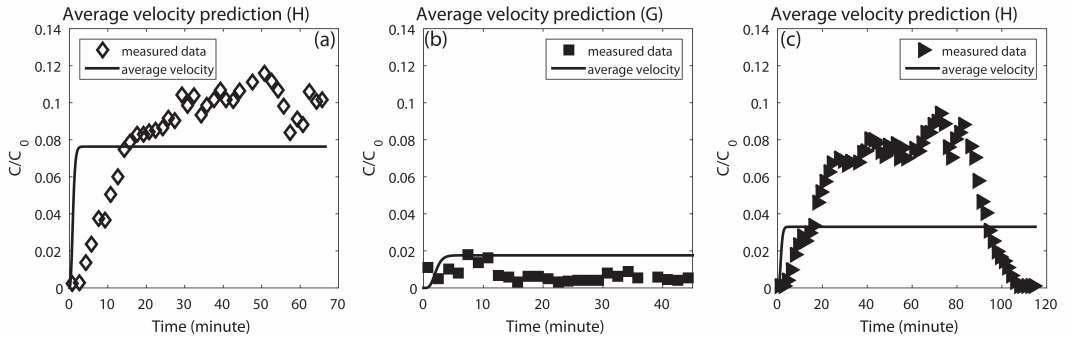

Figure 3.9: Comparison of observed and predicted data for the varied velocity tests using the constant average velocity of each test and the regression power function provided in Figure 3.5 to describe the relationship between K_i^* and advective velocity. Note, the BTC experimental data are presented as a three-point moving average to clarify trends.

Modeling results based on the average velocity, K_i^* led to under-prediction of the maximum particle breakthrough concentration for both of the experiments with increasing velocities (Figure 3.9a and 3.9c). This under-estimation was most pronounced for Column H, where predicted peak BTC concentrations were less than half of those observed. For Column G, the modeling results over-estimated observed BTC concentrations over most of the experiment (Figure 3.9b).

Comparing Figure 3.9 with Figure 3.6, the most notable under-estimation of maximum BTC concentrations occurred for Column H, with the greatest difference between model results and observed concentrations associated with use of the average velocity K_i^* (Table 3.1, NRMSE values). Nonetheless, the predictions based on the relationship between K_i^* and v derived from the constant velocity experiments still lead to underestimated of BTC concentrations. Thus, for the scenarios investigated in this study, conditions involving rising and falling velocities consistently lead to greater particle breakthrough than predicted using models derived from standard

laboratory column procedures. Rising and falling groundwater velocities occur naturally in the field under monsoonal rain conditions, for example. Such conditions are also commonly introduced via groundwater pumping for crop irrigation or drinking water supply. In many cases, the temporal velocity fluctuations are unknown, and therefore unaccounted for by modeling. Nonetheless, even if velocity fluctuations are known and accounted for, as per this work, the results of this study indicate that accurate predictions of particle transport distances might not be possible using model parameters derived from traditional laboratory column experiments. Furthermore, the work reveals a possible relationship between the rate of change of fluid velocity and particle filtration efficiencies, which is not accounted for in conventional modeling approaches.

3.6 Conclusion

One-dimensional, laboratory column experiments were performed under both constant and varying velocity conditions using 2μm microspheres and 100μm glass beads to simulate bacterial transport in saturated porous media. Particle breakthrough curves and particle concentrations retained in the column at the end of an experiment were obtained for five constant and three varying velocity conditions. The range of constant velocities investigated lay between 3.17m/day and 27.65m/day. For varying velocity conditions, the velocity was steadily increased and/or decreased over the period of the experiment within the same range.

Consistent with prior studies, increasing velocity increased particle effluent concentrations for the constant velocity experiments. Furthermore, results from the constant velocity experiments were successfully modeled using classical colloid filtration theory assuming a first order, irreversible particle attachment coefficient. The irreversible attachment coefficients obtained from the constant velocity experiments were used to derive a power function relationship between a dimensional irreversible

attachment coefficient, K_i^*, and velocity, v, which was then used to model particle transport in the three varying velocity experiments. These predictions over-estimated breakthrough concentrations for the experiment where velocity initially increased then decreased, and under-estimated breakthrough concentration for the experiment where velocity steadily decreased. For the experiment where velocity steadily increased, concentrations were initially over-estimated and then, generally, underestimated. The NRMSE values of the model fits for all three varying velocity experiments were above 10%, leading to the conclusion that relationships between K_i^* and velocity derived under constant velocity conditions might not be applicable for varying velocity conditions. To explore this further, the K_i^* values derived from the constant velocity experiments were compared with those obtained from directly fitting the results of the varying velocity experiments. Results of the comparison revealed that fitted K_i^* values were higher than those derived from the constant velocity experiments when velocities decrease, and lower than those derived from the constant velocity experiments when velocities increase, indicating a potential influence of fluid acceleration on particle attachment rates.

Breakthrough curve concentrations from the varying velocity experiments were also compared with predictions assuming a constant K_i^* based on the average velocity of each experiment. These predictions under-estimated peak breakthrough concentrations for the two experiments where velocity was increased, and in particular for the experiment where velocity was initially increased then decreased. For the column where velocity was decreased, the predictions generally over-estimated the observed break-though concentrations.

Overall, the results of this study point to the need for better understanding of how varying velocity conditions impact particle transport processes in saturated porous media. The work also provides some initial indication that rising then falling velocity conditions lead to greater particle breakthrough than predicted using models derived from traditional laboratory column testing protocols, even when changes in particle

attachment rate with velocity are accounted for. Given that sequences of rising and falling velocity conditions are not uncommon at many field sites, their occurrence might be one factor contributing to the observation of fecal bacteria at greater distances in the field than predicted by current up-scaling techniques. Finally, the work also highlights a need to further quantify how the rate of change of advective velocity influences particle filtration processes.

3.7 Acknowledgements

This study was supported by Grant W911NF-727 10-1-0123 from the Army Research Office. The authors are grateful for the comments provided by 2 anonymous reviewers, which significantly improved the work. Any opinions, findings, and conclusions expressed in this article are those of the authors and do not necessarily reflect the views of any supporting institution.

3.8 Tables

Table 3.1: Column tests conditions and fitted parameters. Columns A to E involved constant velocity tests. Columns F to H involved varying velocity tests. Mass recovery rates and the RMSE or NRMSE of each modeling result are also provided.

Column		A	B	C	D	E	F	G	H
Velocity [m/day]		3.17	3.54	11.8	21.28	27.65	increased from 10.38 to 27.78 (average 22.52)	decreased from 18.78 to 2.91 (average 8.89)	increased from 8.24 to 17.04 then decreased to 3.76 (average 12.67)
Ki*		33.9	33.1	18.5	8.5	8.7			
Recovery		79%	88%	74%	76%	66%	67%	82%	66%
BTC RMSE		0.002	0.001	0.003	0.013	0.018			
RP RMSE		0.024	0.024	0.051	0.071	0.034			
Ki* based on Regression power function	BTC NRMSE						0.11	0.74	0.19
	RP NRMSE						0.25	0.19	0.19
Ki* based on Fitted power function	Function						$K_i^* = 50.14v^{-0.52}$	$K_i^* = 36.03v^{-0.18}$	$K_i^* = 139.84v^{-0.92}$ $K_i^* = 136.71v^{-0.86}$
	BTC NRMSE						0.10	0.20	0.07
	RP NRMSE						0.25	0.14	0.2
Ki* based on Average velocity	BTC NRMSE						0.23	0.72	0.38
	RP NRMSE						0.25	0.18	0.18

Chapter 4

Particle Transport in Saturated Porous Media: Effects of Flow Direction on Uniform and Mixed Particle Populations for Two Different Particle Sizes

4.1 Abstract

A visualization technique was used to examine the effects of particle size and flow direction on particle transport in a saturated porous medium comprised of 500μm diameter glass beads. Packed column experiments with uniform (100% 1μm or 100% 6μm) and mixed (90% 1μm with 10% 6μm and 90% 6μm with 10% 1μm) polystyrene latex microspheres were performed in one-dimensional upward, horizontal and downward flow fields at a constant velocity of 1.7m/day. Particle concentrations were recorded over time in the interior of a column and at the column exit. Experimental results showed that upward flow conditions generally gave rise to higher retained par-

ticle concentrations and lower particle breakthrough concentrations than horizontal and downward flow conditions, indicating that gravitational settling decreases particle transport distances and enhances particle deposition mechanisms. Consistent with prior studies, results also showed increasing particle retention with increasing particle size. The 1μm particle tests results were successfully modeled using a first order, irreversible particle attachment model, indicating little filtration of this particle size within the glass bead columns during transport. Modeling of the 6μm particle tests required a two-site kinetic modeling approach that accounted for particle interactions with the surfaces of the glass beads as well as straining of particles at bead-bead contact points. The presence of a second particle population had little impact on the transport of the 1μm particles. For the 6μm particles, the presence of the second particle population increased particle attachment rates, with the greatest impact observed during downward flow conditions. Overall, the results of this study confirm that particle size and flow direction impact particle transport processes. The study also reveals that particle size heterogeneity could also impact particle transport under certain conditions. Both of these findings have implications for field-scale modeling of particle transport.

4.2 Introduction

Advancing understanding of the mechanisms influencing the fate and transport of colloid particles in saturated porous media is important to many environmental applications, including the operation of deep-bed filtration systems for water and wastewater treatment, the quantification of transport distances for pathogens and non-biological pollutants in groundwater, and the design of engineered nano-particle solutions for aquifer remediation [Torkzaban *et al.*, 2007; Molnar *et al.*, 2015].

Over the past several decades, numerous research groups have performed column studies using latex microspheres to investigate particle fate and transport in satu-

rated media. These studies, coupled with complimentary numerical investigations, have revealed multiple factors effecting particle behavior including; particle size [Ma *et al.*, 2009; James and Chrysikopoulos, 2011; Nelson and Ginn, 2011; Syngouna and Chrysikopoulos, 2011], grain/ collector size [Bolster *et al.*, 2001; Pazmino *et al.*, 2011; Syngouna and Chrysikopoulos, 2011], matrix porosity [Ma and Johnson, 2010], collector surface roughness [Tong and Johnson, 2006; Yoon *et al.*, 2006; Shen *et al.*, 2012], flow velocity [Marlow *et al.*, 1991; Camesano and Logan, 1998; Becker *et al.*, 2004; Tong and Johnson, 2006; Choi *et al.*, 2007], and water chemistry [Ryan and Gschwend, 1994; Grolimund and Borkovec, 2006; Tong *et al.*, 2008; Kim *et al.*, 2009; Tosco *et al.*, 2009; Bradford *et al.*, 2012]. Less studied is the influence of flow direction on particle fate and transport, despite variability in flow direction across a number of natural and engineered systems. Nonetheless, several studies have demonstrated that flow direction can influence particle deposition rates. For example, in column tests performed using a polydisperse population of microspheres ranging from 1 to 26μm in diameter, *Yoon et al.,* and *Basha and Culligan* reported greater overall particle retention for upward versus downward flow conditions[Yoon *et al.*, 2006; Basha and Culligan, 2010]. In addition, in parallel plate chamber tests undertaken using microspheres of 0.5, 1.1, and 1.8μm in diameter, *Chen et al.,* found greater particle deposition on the bottom, than the top, chamber surface for particles larger than 1μm in diameter [Chen *et al.*, 2010]. Finally, in column tests performed using micron-sized sized clay particles, *Chrysikopoulos and Syngouna* reported greater particle retention during upward than downward flow tests, as well as greater particle retention during diagonal, than horizontal, flow [Chrysikopoulos and Syngouna, 2014]. In all cases, the researchers conducting these studies concluded that gravity had a significant impact on observed particle behavior during their tests.

The primary objective of this study was to shed further light on the influence of flow direction on particle fate and transport, by examining the behavior of 1 μm and 6 μm diameter latex micro-spheres in saturated columns of glass beads under vertical,

horizontal and upward flow conditions. Because it is not uncommon for particle transport problems to involve particle populations of different sizes, a secondary objective was to understand if the presence of a small fraction (10%) of 6 μm microspheres influenced the behavior of the 1 μm particles, and vice-versa. The experimental component of the study made use of a visualization technique that allowed for real-time observations of particle concentrations within the interior of the glass bead pack, as well as observations of particle concentrations at the column outlet. In the sections that follow, the materials and methods used in the investigation are described, the experimental and modeling work are presented and discussed, and the conclusions that can be drawn from the work are presented.

4.3 Material and methods

4.3.1 Particles

Spherical, mono-dispersed, fluorescent, carboxylate-modified, polystyrene latex microspheres were used as the micron sized particles in the experiments (Bangs Laboratories, Inc., Fishers, IN). The microspheres diameters were 1μm and 6μm (flow cytometry results confirmed that the microsphere population was uniform), while the excitation and emission wavelengths were 480/520nm for 1μm particles and 660/690nm for 6μm particles. The solids concentration of the manufacturer-supplied stock solution was 10 mg/mL. The experimental solutions were prepared by diluting the stock solution using artificial groundwater (AGW) at the desired ionic strength (IS) and pH value.

4.3.2 Porous media

Glass beads of 500μm diameter (USA Scientific, Inc., Ocala, FL) were used to simulate sediment in the experiments. The glass beads were washed with deionized water,

ultra-sonicated and dried in an oven at 60^{o}C prior the preparation of each column experiment. Microscope images of the glass beads indicated that approximately 20% of a bead surface was covered with microscopic asperities that had a roughness height of about of about 0.65μm.

4.3.3 Solution chemistry

The AGW was made with KCl at an IS of 3.5 mM. The solution pH value was adjusted to 7.5±0.05 by using 0.1M NaOH and 3% HCl solution. The inlet particle solution contained 1μm or 6μm carboxylate polystyrene beads at a final concentration of 22mg/L, referred to as C_0, in uniform particle size transport tests. For the mixed particle transport experiments, the inlet solutions were made by combining 10% 6μm particles and 90% 1μm particles for the mixed 1μm particle solution, or 10% 1μm particles and 90% 6μm particles for the mixed 6μm solution. In both cases, the mixed solutions had a concentration of 22mg/L. All inlet solutions were stirred throughout each experiment to help ensure a uniform particle inlet concentration.

4.3.4 Visualization technique, experiment set-up and protocol

The visualization technique developed by *Yoon et al.,* and modified by *Pei et al.,* was adopted for this study with some enhancements that were necessary for the experimental protocol [Yoon *et al.*, 2006; Pei *et al.*, 2008]. The visualization technique makes use of two sub-systems: (1) the particle transport system, and (2) the optical system.

In the particle transport system (Figure 4.1), pretreated glass beads were wet packed into a rectangular column at a porosity of 0.39 to form the porous media. Two custom-designed and manufactured rectangular columns (Columbia University Carleton Laboratory, New York, NY) with interior dimensions 15(h)× 3.5(w) × 1(d)

cm (vertical column) and 3.5(h) × 14(w) × 1(d) cm (horizontal column) were used in the study. Void spaces created at the top and bottom of the vertical column, and at the left and right hand sides of the horizontal column, provided areas for monitoring particle inlet and outlet concentrations during experiments. In order to reduce light scattering effects from the fluorescent particles, separated scan-lines for measurement (Figure 4.2) were made by using black masking tape (ThorLab, Inc., Newtown, NJ) to cover the areas of the columns between the scan lines. The scan-lines themselves were 1 cm high by 3 cm wide and spaced 1cm apart from each other. Throughout each experiment, the distribution of fluorescent particles at the different distances from the column inlet was monitored by the optical system.

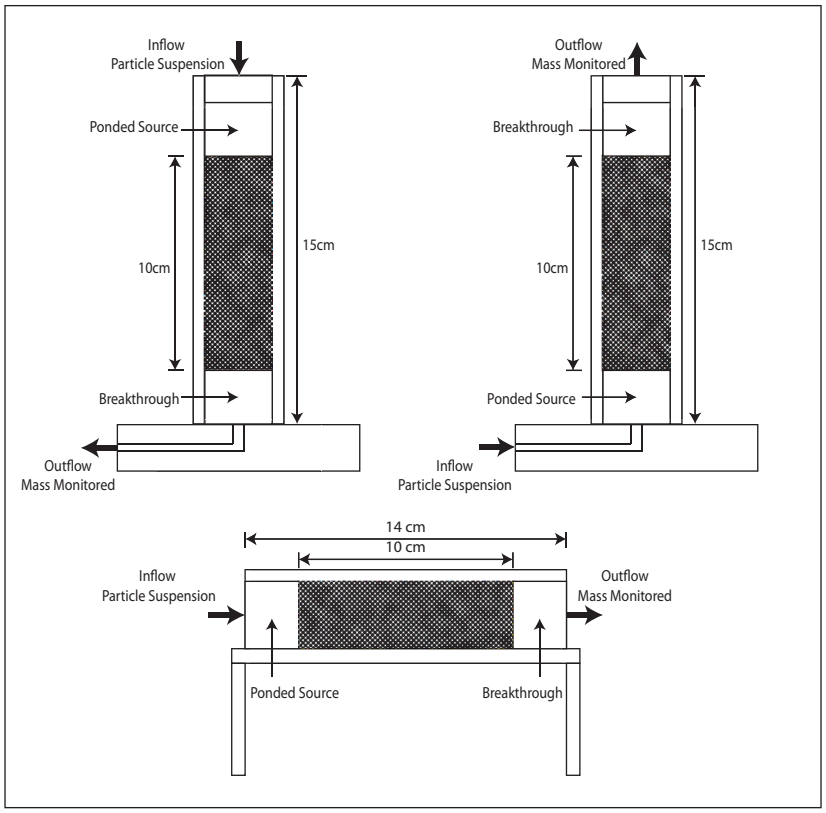

Figure 4.1: Schematic diagram of set-up for column experiments.

In the optical system (Figure 4.3), a 300W/12V halogen light bulb was installed

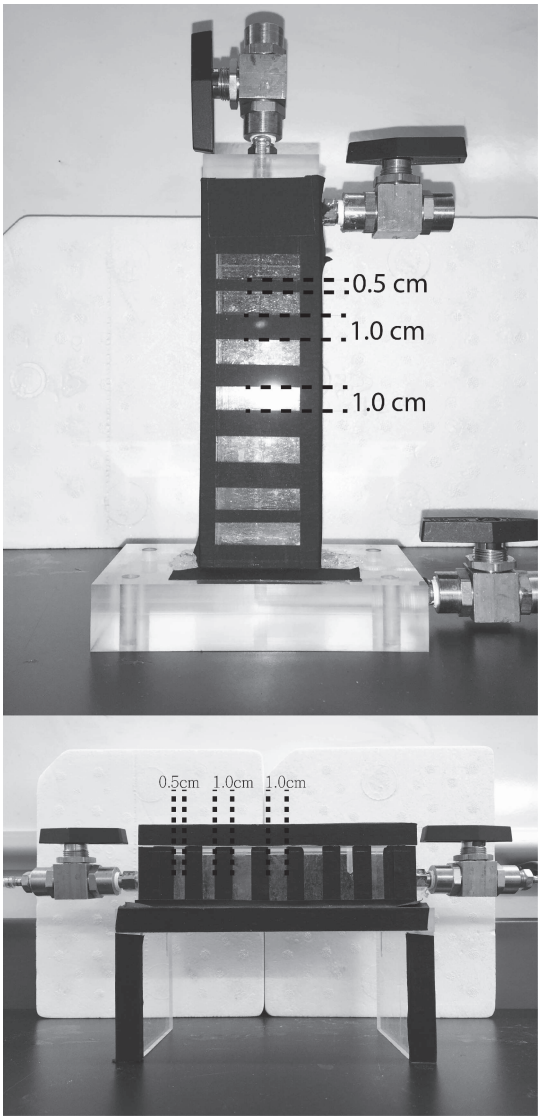

Figure 4.2: Both vertical (up) and horizontal (down) columns included separated scan lines in order to avoid light scattering effects.

in a Kodak 750H Carousel slide projector coupled with a specific bandpass filter (ThorLabs, Inc., Newton, NJ) corresponding to the relevant particle's excitation wavelength. The light source and coupled filter were used to excite the fluorescent particles within the scan lines. Images were captured at set time points using the MagnaFire digital camera (OPTRONICS, Muskogee, OK) equipped with a specific bandpass filter (ThorLabs, Inc., Newtown, NJ). The bandpass filter enabled the camera to only capture the emitted wavelength of the particles. A blackout fabric (Black Rubberized Fabric, ThorLab, Inc., Newtown, NJ) covered both the particle transport system and the optical system during each experiment in order to reduce interference from other local light sources.

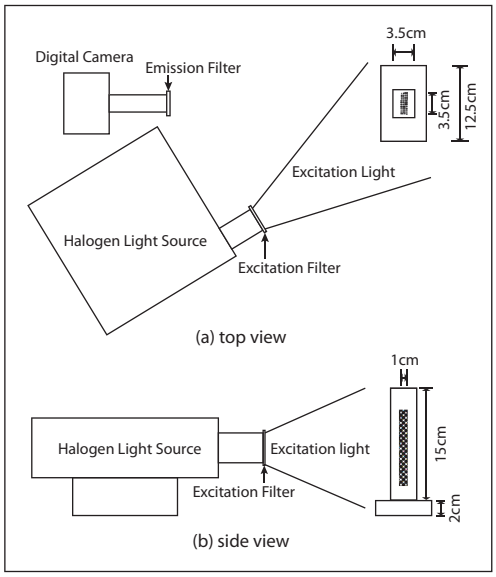

Figure 4.3: The optical system included a halogen light source and a digital camera. The digital camera was set up in front of the column and the light source was set up next to the digital camera with an angle. (a) top view and (b) side view

To prevent experimental error associated with the microscopic movement of any component of the above sub-systems, all components were set-up on an optically level breadboard (Thorlabs. Inc., Newton, NJ).

The combination of the two above systems enabled the fluorescent light intensity from all scan lines to be captured in one single image. For converting light intensity to particle concentration, a calibration curve was needed. Because the excitation light intensity from the halogen light varied for each of the scan-lines, due to differences in their positions relative to the halogen bulb, the calibration curve of each scan-line was constructed separately. The calibration curve was obtained by averaging the light intensity of each scan-line area for a series of different interior particle concentrations (Figure 4.4). Then, a linear regression was performed using particle concentration as the response variable and light intensity as the predictor variable.

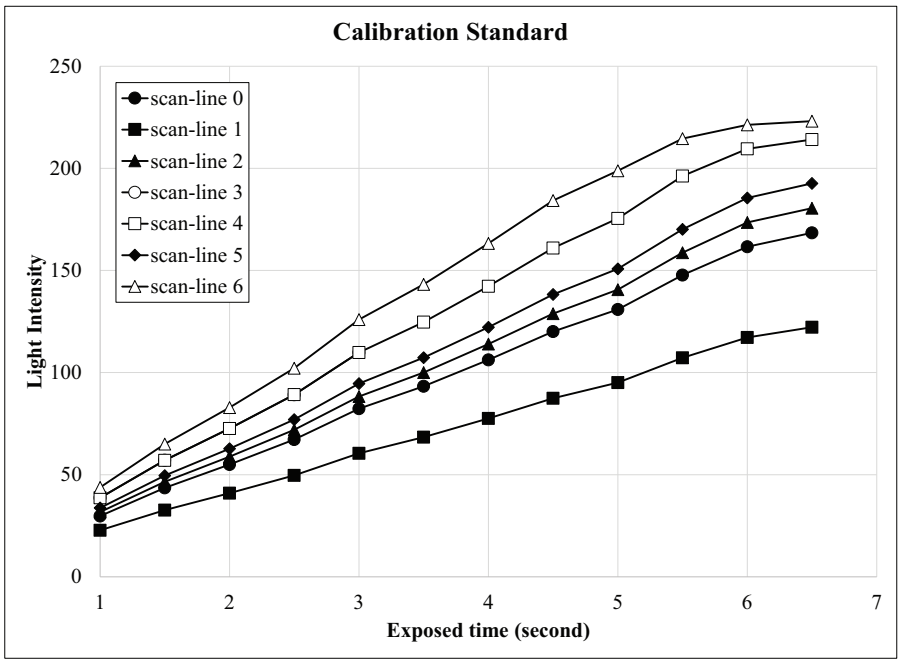

Figure 4.4: Example calibration curves (sample of uniform 1μm particle calibrations) were constructed via linear regression analysis of measured light intensities of different concentration solutions at a specific exposure time.

Prior to each experiment, the 500μm diameter glass beads were wet-packed into the appropriate column. For the vertical column, the washed glass beads were uniformly deposited in 2 cm high layers to a final height of approximately 10 cm. For the

horizontal column, the washed glass beads were uniformly deposited in 0.5 cm high layers to a final height of 3.5 cm. All column experiments involved one-dimensional, steady-state flow at velocity 1.7 m/day. This was achieved by using a multi-channel peristaltic pump (Gilson Minipuls 3) with 0.8 mm interior diameter inert tubes (Masterflex BioPharm platinuim-cured L/S 13, Fisher Scientific) to regulate column outlet flow. Column effluent samples were collected in 15 ml polypropylene tubes (Thero Fisher Scientific, Inc., Pittsburgh, PA) using a fraction collector (LKB Bromma 2211, SuperRac, Sweden).

Before the start of each experiment, columns were purged with 5 pore volumes (PVs) of particle-free AGW in order to eliminate air bubbles and clean out impurities. All column tests involved two stages. The first stage was the particle introduction stage, which involved the introduction of 10 PVs of specific particle solutions at the column inlet. The second stage was the particle flushing stage, which involved introducing 10PVs of particle-free (clean) AGW at the column inlet. Particle transport tests were conducted with 3 different flow directions (downward, upward, and horizontal flow) and 4 different types of particle solutions (uniform/mixed 1μm and 6μm particle solutions). For the mixed experiments, the optical system was set up to capture the concentration of the particles representing 90% of the population. All experimental settings are summarized in Table 4.1. A total of twenty experiments were conducted and can be categorized into the three different flow directions Uniform 1μm or 6μm particle solutions were applied to all three flow directions, while mixed 1μm or 6μm particle solutions were only applied to downward and upward flow conditions. The standard deviations of duplicate experiment results were used to generate error bands for the interior scan lines and the BTCs.

4.3.5 Modeling uniform particle transport

The advection-dispersion equation, which is commonly used to describe particle concentrations associated with the liquid and solid phases of a saturated porous medium

during transport [Johnson *et al.*, 2007b], was adopted for modeling:

$$\frac{\partial c}{\partial t} + \frac{\rho_b}{\theta}\frac{\partial s}{\partial t} = D\frac{\partial^2 c}{\partial x^2} - v\frac{\partial c}{\partial x} \tag{4.1}$$

where c is the particle concentration in the pore fluid $[M/L^3]$, s is the attached particle concentration associated with solid phase $[M/M]$, x is the distance from the particle inlet boundary $[L]$, t is the time $[T]$, D is the hydrodynamic dispersion coefficient $[L^2/T]$, v is the average steady state pore fluid velocity $[L/T]$, ρ_b is the bulk density of the solid phase $[M/L^3]$, and θ is the porous medium's porosity [-].

Particle attachment/detachment processes, which govern particle fluxes between the liquid and solid phases of a porous medium, are usually described by a first order kinetic expression. Based on different assumptions of particle attachment dynamics, there are three common models for particle attachment/detachment that can be expressed by different combinations of the following equations:

$$\rho_b\frac{\partial s}{\partial t} = k_i\theta c \tag{4.2}$$

$$\rho_b\frac{\partial s}{\partial t} = k_a\theta c - k_d\rho_b s \tag{4.3}$$

$$\rho_b\frac{\partial s}{\partial t} = k_i c + k_a\theta c - k_d\rho_b s \tag{4.4}$$

where k_i is the first-order particle irreversible attachment coefficient $[T^{-1}]$, and k_a and k_d are the first-order particle reversible attachment and detachment coefficients $[T^{-1}]$, respectively.

The first common model is the irreversible attachment model, which assumes that attached particles cannot detach from the solid phase of the porous medium once they are attached. The model can be mathematically expressed by equations 4.1 and 4.2. The second model is the reversible attachment model, which assumes that attached particles can always detach from a medium's solid phase. The corresponding mathematical expression for this model is a combination of equations 4.1 and 4.3. The

third type of model is the two-site model, which assumes that both irreversible and reversible attachment mechanisms exist for particles as a result of the particle properties themselves and/ or properties of the attachment surface. The corresponding mathematical expression for this model combines equations 4.1, 4.2, and 4.3.

For the column experiments conducted with the 6μm particles, the ratio of the particle diameter to the collector diameter (d_p/d_c) is 0.012, which is within the range where particle straining at grain-grain contact points is considered to be an important contributor to overall particle attachment/ detachment processes (Bradford et. al., 2003). Following the distance dependent straining model proposed by Bradford et al., (2003), the following equation was adopted to simulate particle straining for the 6μm particles:

$$\rho_b \frac{\partial s}{\partial t} = \theta k_{a,str} \Psi_a c - \rho_b k_{d,str} \Psi_d s \tag{4.5}$$

where $k_{a,str}$ and $k_{d,str}$ are the reversible attachment and detachment coefficients [T^{-1}], respectively, and Ψ_a and Ψ_d are depth-dependent power functions defined as:

$$\begin{cases} \Psi_a = \frac{(L+x)^{-\alpha})}{L} \\ \Psi_b = \frac{(L+x)^{-\beta})}{L} \end{cases} \tag{4.6}$$

where L is the column length [L], x is the distance from the column inlet [L], α and β are dimensionless fitting parameters that control the shape of the kinetic coefficients as a function of transport distance.

To enable the numerical solution of the different particle transport models, a MATLAB program based on a finite difference scheme was developed. The program discretized the time derivative using a Crank-Nicolson approximation and the space derivative using a central difference approximation. To simulate the column experiments, a Dirichlet boundary condition and Neumann boundary condition were applied at the column inlet and the outlet points of the modeled domain, respectively. The discretized grid size and time step were automatically checked against numerical stability criteria and adjusted accordingly.

To estimate the first-order attachment and detachment coefficients for each column experiment, for both single site and two-site modeling approaches, each model was fit to the observed data taking $\rho_b = 1.525$ g/cm^3 (the bulk density of the glass beads), $\theta = 0.39$ (the porosity of the columns) and $D = \alpha_L \times v$ [Yoon *et al.*, 2006], where the longitudinal dispersivity, α_L, of the packed columns was taken as 1,000μm (twice the diameter of the glass beads). To estimate k_i, k_a and k_d values for each experiment, an iterative process of fitting observed data was used. Specifically, the kinetic coefficients were obtained by minimizing the sum of the squared residual R (i.e., the difference between the measured and modeled normalized concentrations) over the duration of an experiment at the column outlet and interior locations for both the liquid and solid phase concentrations. The squared residual was calculated using the following equations [Simunek *et al.*, 2012]:

$$\begin{cases} R = \sum_j w_j (f^*(x,t) - f(x,t))^2 \\ w_j = \frac{1}{m_j \sigma_j^2} \end{cases} \tag{4.7}$$

where f^* and f were measured data and model estimated values, respectively, while the weighting coefficient w_j minimizes differences in weighting between different data types, which is necessary because of the different absolute values and data points involved in some cases, e.g., breakthrough concentration data values versus retained particle concentration data. The weight coefficient is normalized by the measured data variance σ^2, and number of data m. For the fitting conducted for this research, the breakthrough concentration data were actually not used in fitting exercises, due to the fact that scan line measurements were considered more accurate because of the sensitivity of the measurement system.

For minimizing the residuals, the numerical model used a modified version of the MATLAB fminsearch function, which is based on the Nelder-Mead simplex algorithm.

4.4 Results

A summary of all experiments conducted during the course of this research was provided in Table 4.1. Note, that all experimental conditions were investigated in duplicate. In the following sections, the results for each experimental condition are the averaged results of the duplicate experiments.

4.4.1 1μm particle experiment

Uniform 1μm particle solution tests with three different flow directions (Downward, Upward and Horizontal) and mixed 1μm particle solution tests with two different flow directions (Downward and Upward) were conducted. Averaged scan-line concentrations and breakthrough curves (BTCs) are presented in Figures 4.5 and 4.6. Note, the vertical axis of each graph is sum of the particle solid phase concentration and liquid phase concentration, $(C + S)$ normalized by the inlet concentration C_0

For all 1μm particle tests, the column interior concentrations exhibited a rapid increase in particle concentration soon after particle injection, followed by a stable plateau that was close to unity, indicating little particle attachment within the medium during transport. During particle flushing a rapid decrease in particle concentration was observed, which ended in a very low to zero residual. . Generally, the normalized scan-line concentration decreased from the upstream scan-line 1 (centered 1 cm from the column inlet), to the downstream scan-line 5 (centered 9cm from column inlet). For example, the uniform 1μm downward test had averaged plateau concentrations of 1.05, 1.04, 1.02, 1, and $0.98(C + S)/C_0$ for scan-lines 1 to 5, respectively. Comparing the different flow directions: The upward tests had the highest interior plateau concentrations and the downward tests had the lowest interior plateau concentrations. The BTC of the downward tests had similar features to those of the scan lines. For the horizontal and upward tests, the rising limb of the BTC was less steep than that of the scan lines, especially for the upward test with a

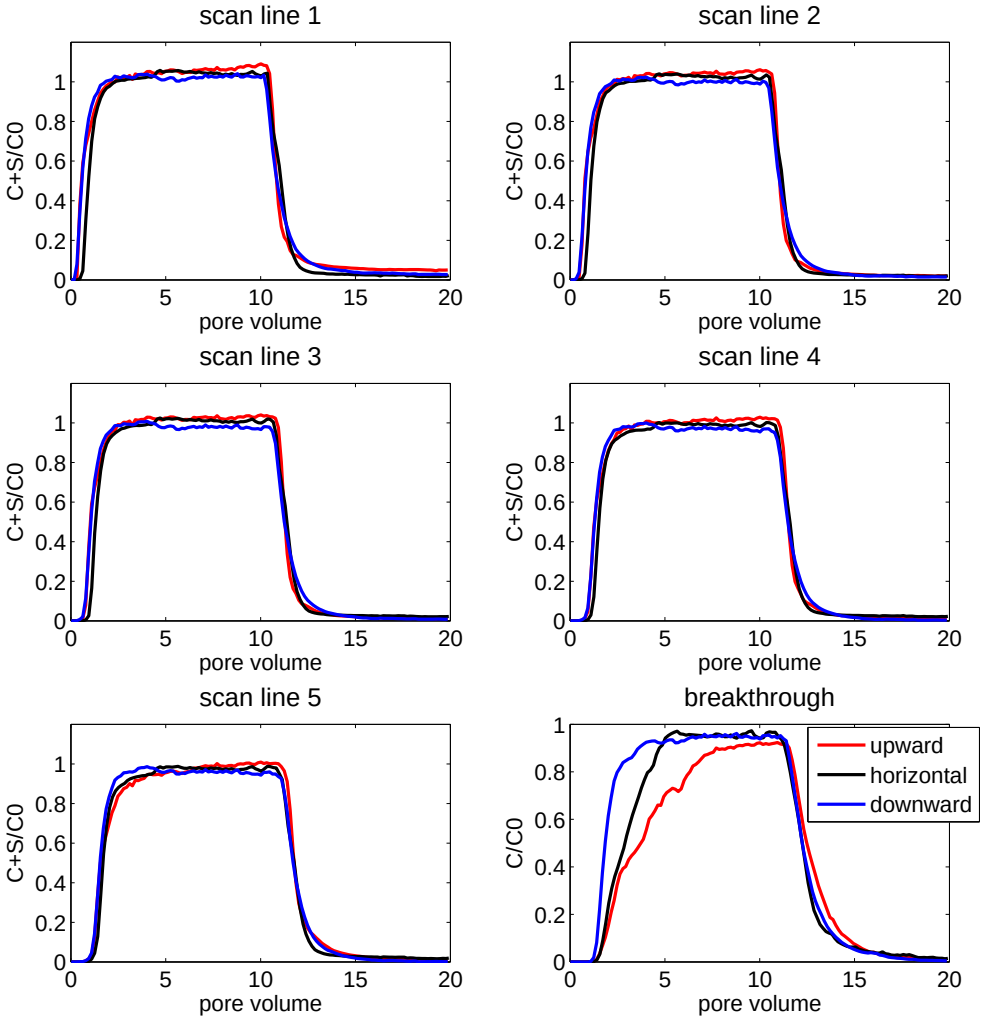

Figure 4.5: Uniform 1μm particle transport experiment results under upward, horizontal and downward flow directions.

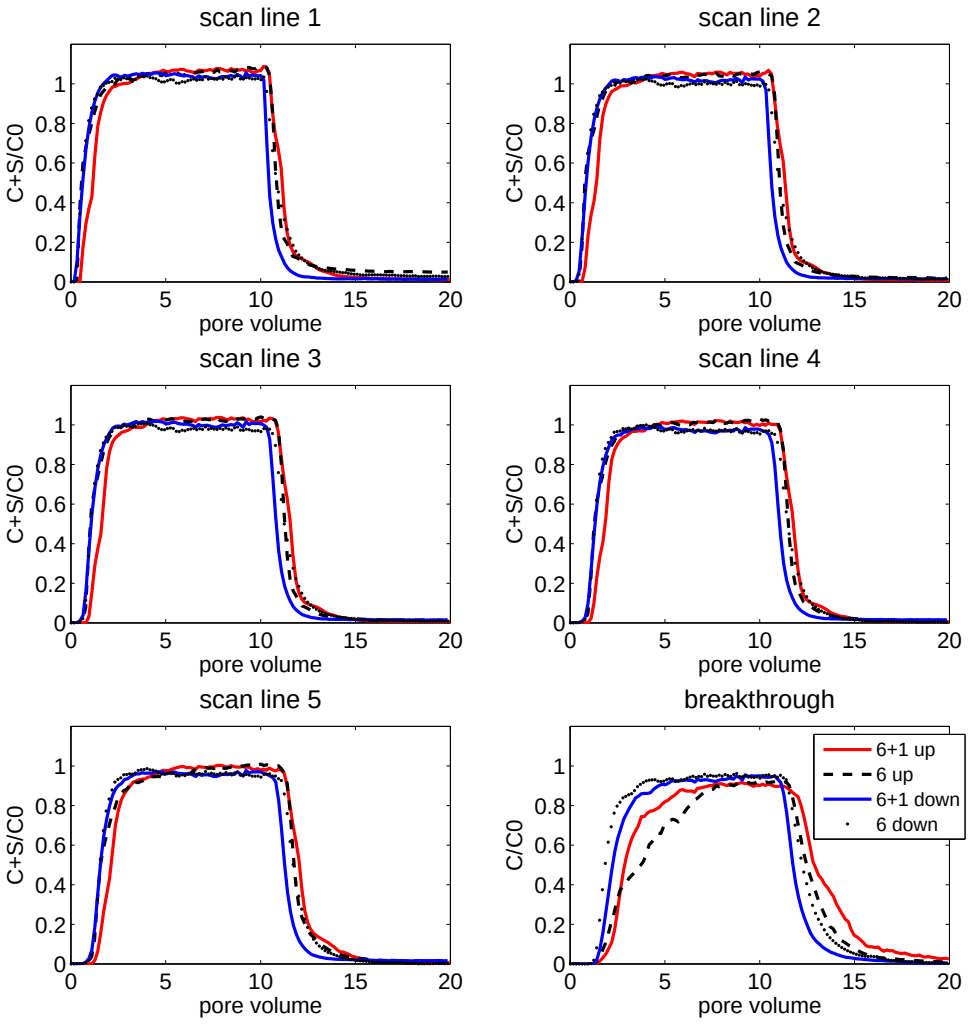

Figure 4.6: Mixed 1μm particle transport experiment results under upward and downward flow directions. Black dash and dotted lines represent uniform 1μm particle experimental results.

uniform particle solution. Overall, there was very little observable difference between the results of the uniform and mixed particle tests. .

4.4.2 6μm particle experiment

Uniform 6μm particle solution tests with three different flow directions (Downward, Upward and Horizontal) and mixed 6μm particle solution tests with two different flow directions (Downward and Upward) were also conducted. Averaged normalized scan-lines concentrations and BTCs are presented in Figures 4.7 and 4.8. Both uniform and mixed 6μm particle tests exhibited interior concentrations profiles similar to those reported by *Yoon et al.,* for experiments involving a poly-disperse particle population (Figure 4.9) [Yoon *et al.*, 2006]. During the particle introduction stage, the interior concentration first increased nonlinearly due to the increase in local liquid phase particle concentrations (phase A). Once the liquid phase concentration reached steady state, the scan-line concentration increased continuously in a linear fashion due to particle attachment processes (phase B). During the particle flushing stage, the local particle concentration in the liquid phase decreased and reversibly attached particles re-entrained into the moving liquid, leading to a rapid decrease in scan-line concentration (phase C). During the final phase (phase D), the liquid phase concentration was negligible. Thus, concentrations remained constant as a result of irreversible attachment to the medium's solid phase.

Peak interior concentrations decreased from upstream to downstream for all experiments. For example, the uniform 6μm particle experiment under upward flow conditions had peak concentrations of 8.4, 5, 3.4, 2.6 and 1.9$(C+S)/C_0$ for scan-lines 1 to 5, respectively. Comparing results for the different flow directions, the highest and lowest peak concentrations were observed in upward and downward flow tests, respectively. The upward flow tests also exhibited higher retained concentrations at the end of each test than the horizontal and downward flow tests. For the BTCs, the downward experiment's peak concentration occurred after a sharp rise in concentra-

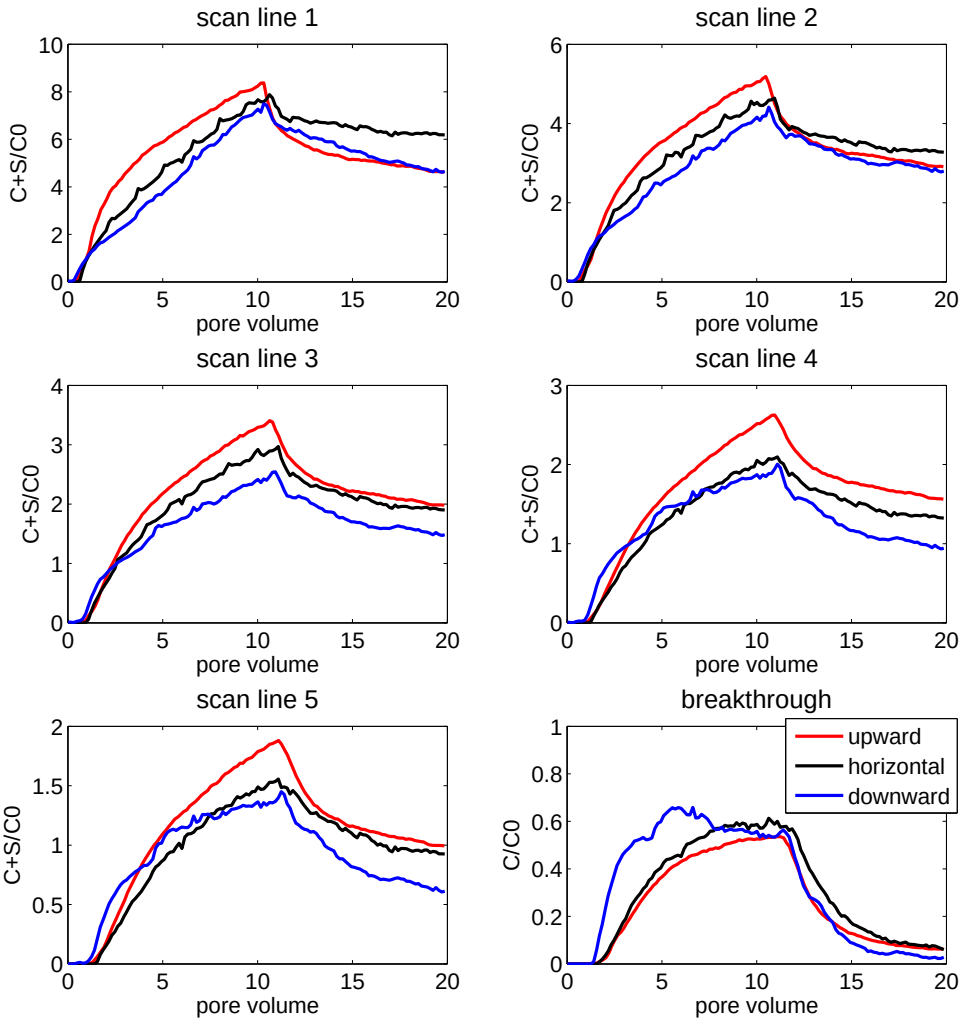

Figure 4.7: Mixed 6μm particle transport experiment results under upward, horizontal and downward flow directions.

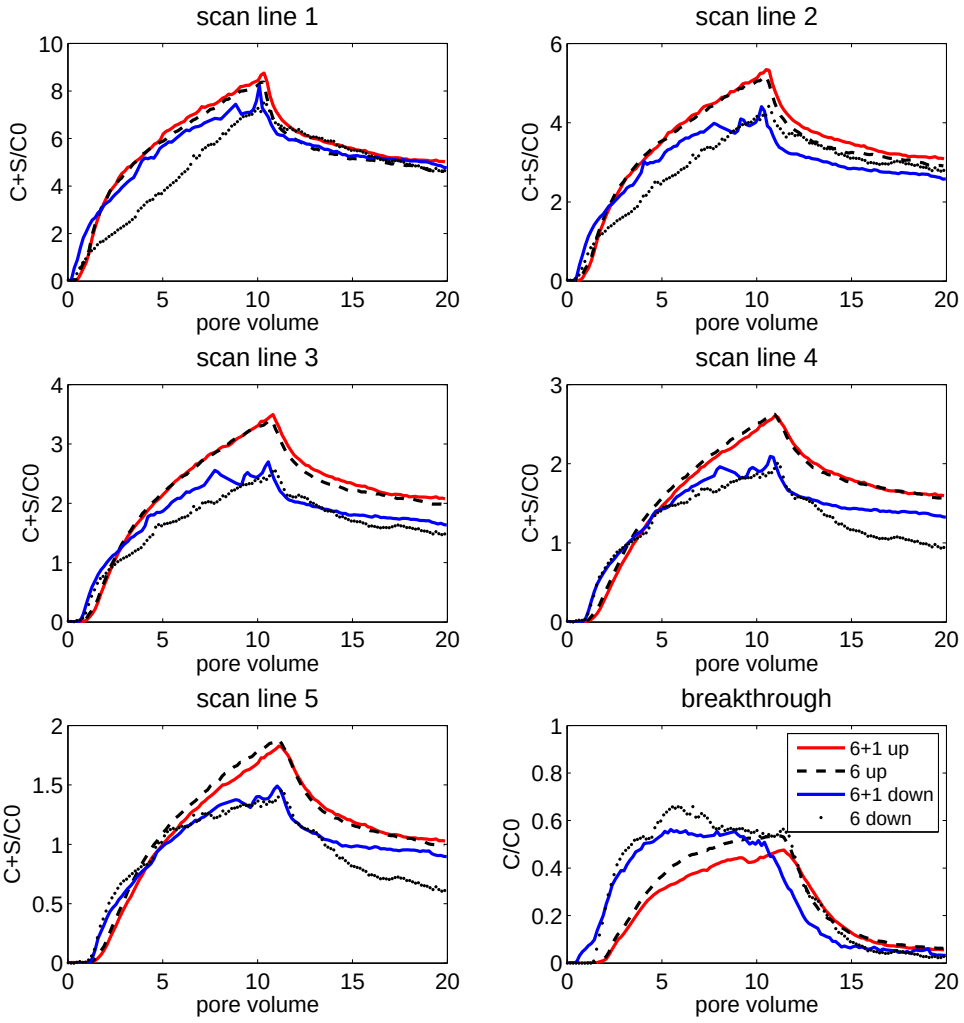

Figure 4.8: Mixed 6μm particle transport experiment results under upward and downward flow directions. Black dash and dotted lines represent uniform 1μm experimental results.

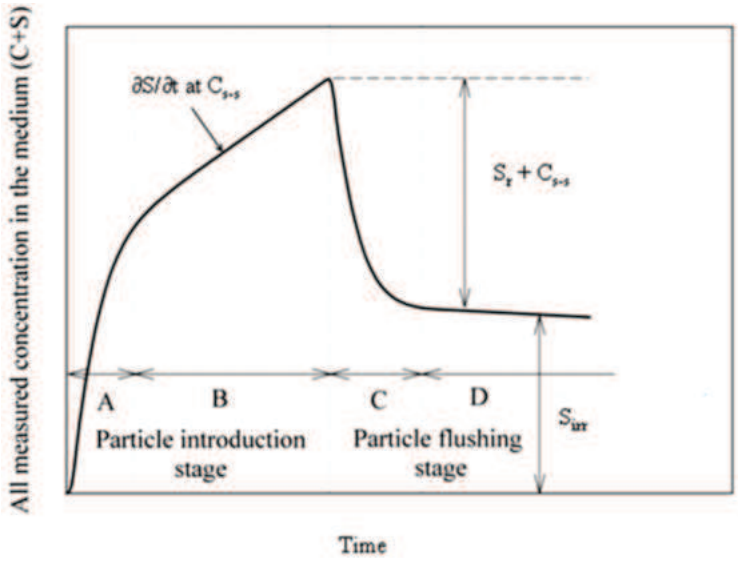

Figure 4.9: Typical interior concentration profile [*Yoon et al., 2006*].

tion around 6 PV, while the upward and horizontal experiments' peak concentrations occurred after a slow rise in concentration around 12 PV. During the flushing process, all BTC concentrations decreased rapidly until 15 PV, after which a slower decline in concentration was observed until the end of each experiment. The presence of the mixed particle population influenced observed behavior for both the downward and upward flow conditions, with a greater influence observable for the downward flow conditions.

4.4.3 Model fits of column experiments

4.4.3.1 1μm Model fitting results

The irreversible kinetic model (equation 4.1 and 4.2) was used to fit the uniform 1μm experimental observations because these observations indicated that the 1μm particles barely attached or detached from the glass beads comprising the porous medium. The estimated kinetic parameters and calculated squared residuals are listed in Table 4.2. Graphical results are presented in Figures 4.10 to 4.14, with the error band

representing the standard deviation of the two duplicated experimental observations (see Table 4.1). The fitting results demonstrate that an irreversible attachment model is sufficient to fit the experimental scan-lines, and also provides a reasonable fit for the BTCs, even though these data were not used in the fitting exercise.

4.4.3.2 6μm Model fitting results

A kinetic model that adopted equation 4.4 to model particle interactions with the surfaces of the glass beads and equation 4.5 to model particle straining at bead-bead contact points was used to fit the 6μm experimental observations. The estimated kinetic parameters and calculated squared residuals are listed in Table 4.3. Graphical results are presented in Figures 4.15 to 4.19, with the error band representing the standard deviation of the two duplicated experimental observations (see Table 4.1).

The kinetic model was sufficient to capture, broadly, the observed scan-line concentrations of both the uniform and mixed 6μm experiments. However, some features of both the rising and falling limbs of the scan-line concentration profiles were not well modeled, including the slope of the falling limb during the particle flushing stage of the experiments. In addition, the observed BTC data, which were not used in the fitting exercises, were overestimated by the modeling results for all 6μm tests. One possible reason for this overestimation was observation system error. In order to measure the higher retained particle concentrations obtained during the 6μm experiments without exceeding the maximum digital range of the measurement system, a reduction in the measurement exposure time was necessary. This reduction caused a reduction in the sensitivity of the system within the data range of the BTC measurements, where normalized particle concentrations were below unity. It is thus possible that the BTC particle concentrations estimated from the light intensity data are not an accurate representation of actual particle concentrations at the column outlet.

Figure 4.20 compares observed and predicted profiles of irreversible and reversible attached particle concentrations at the end of each experiment. In general, the com-

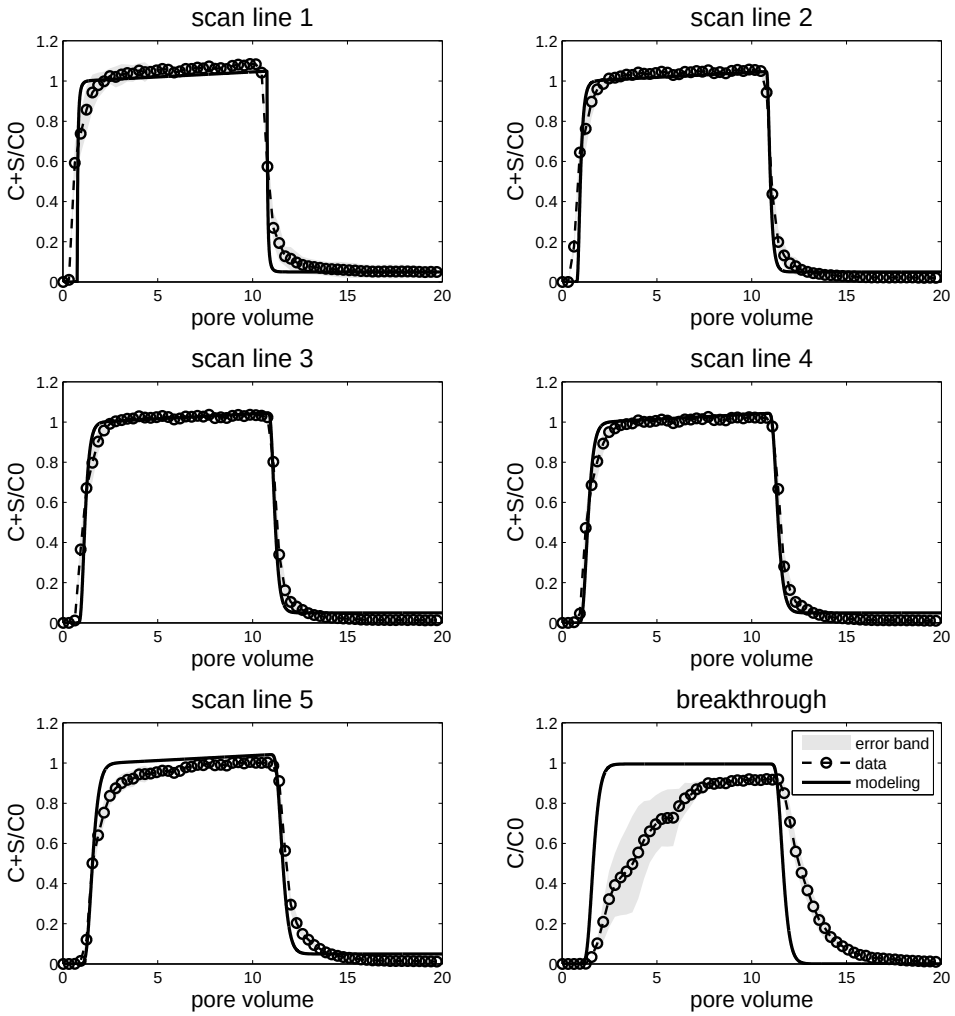

Figure 4.10: Modeling results for uniform 1μm particle experiments under upward flow conditions.

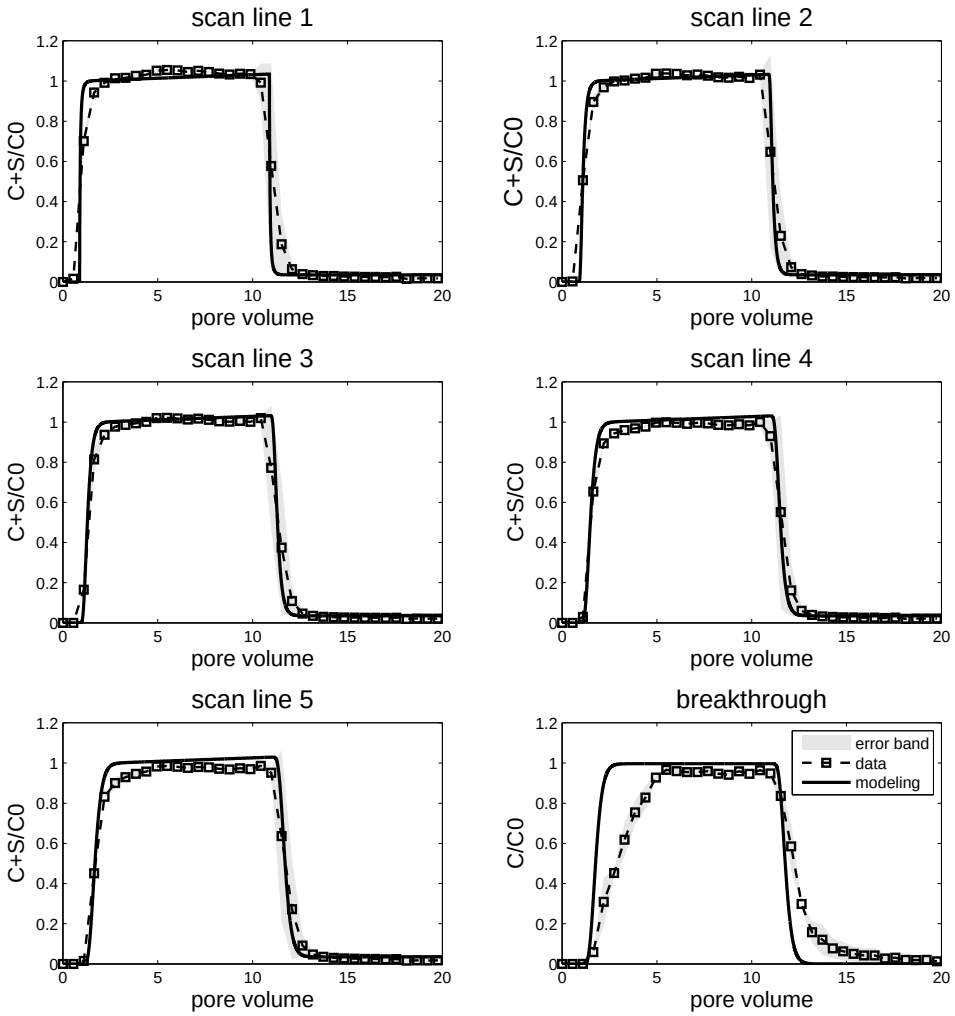

Figure 4.11: Modeling results for uniform 1μm particle experiment under horizontal flow conditions.

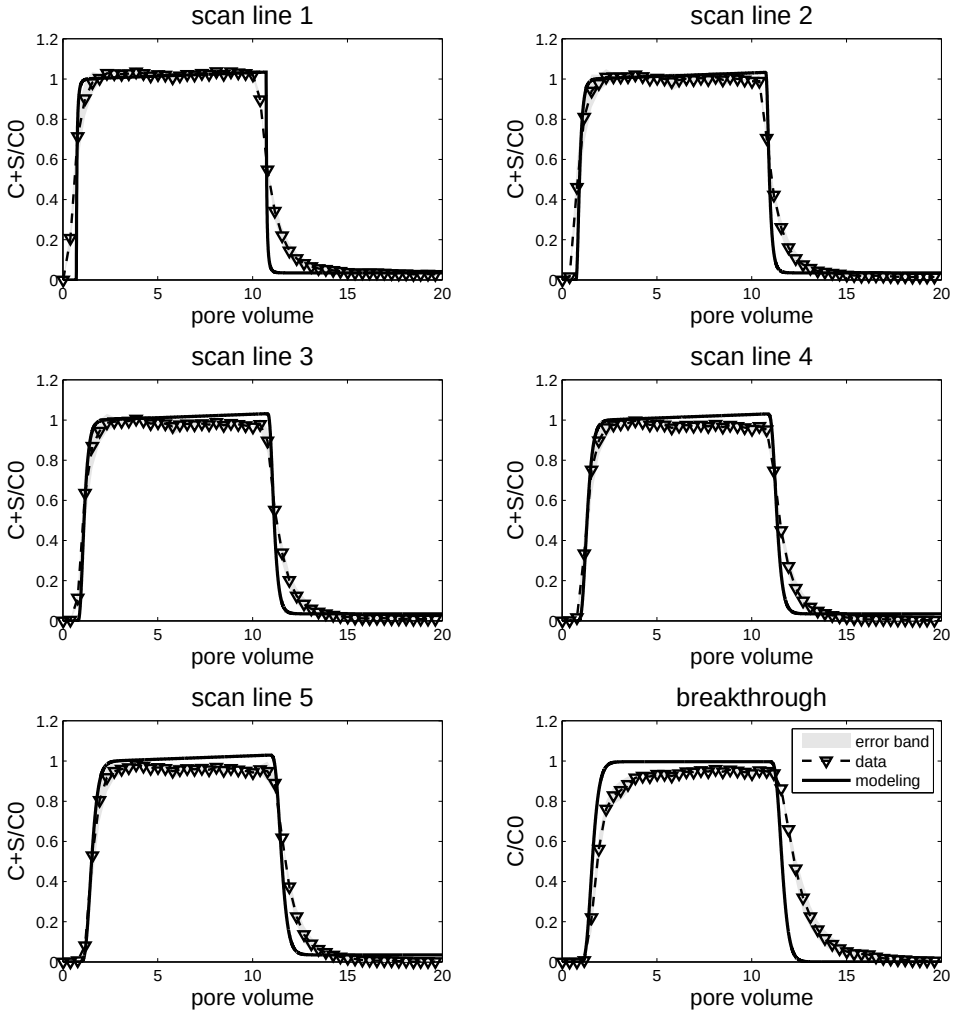

Figure 4.12: Modeling results of uniform 1μm particle experiment under downward flow conditions.

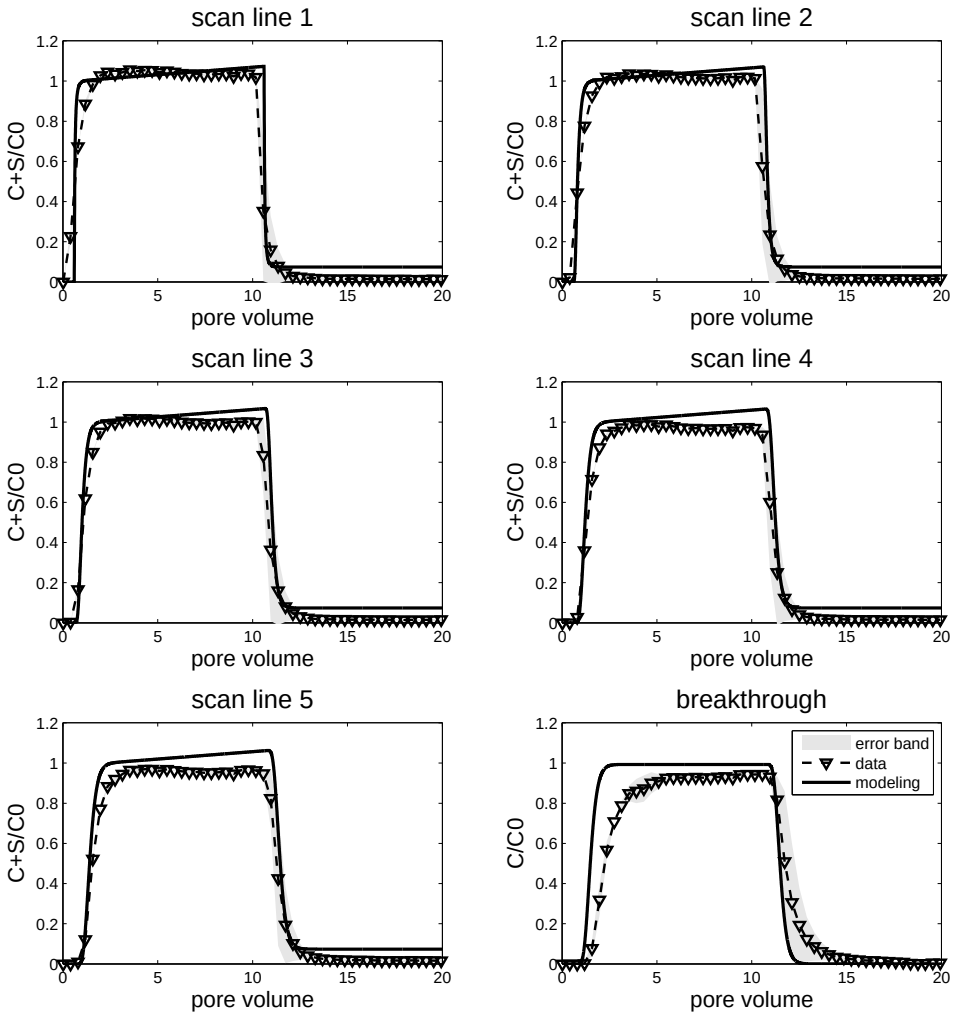

Figure 4.13: Modeling results of mixed 1μm particle experiment under upward flow conditions.

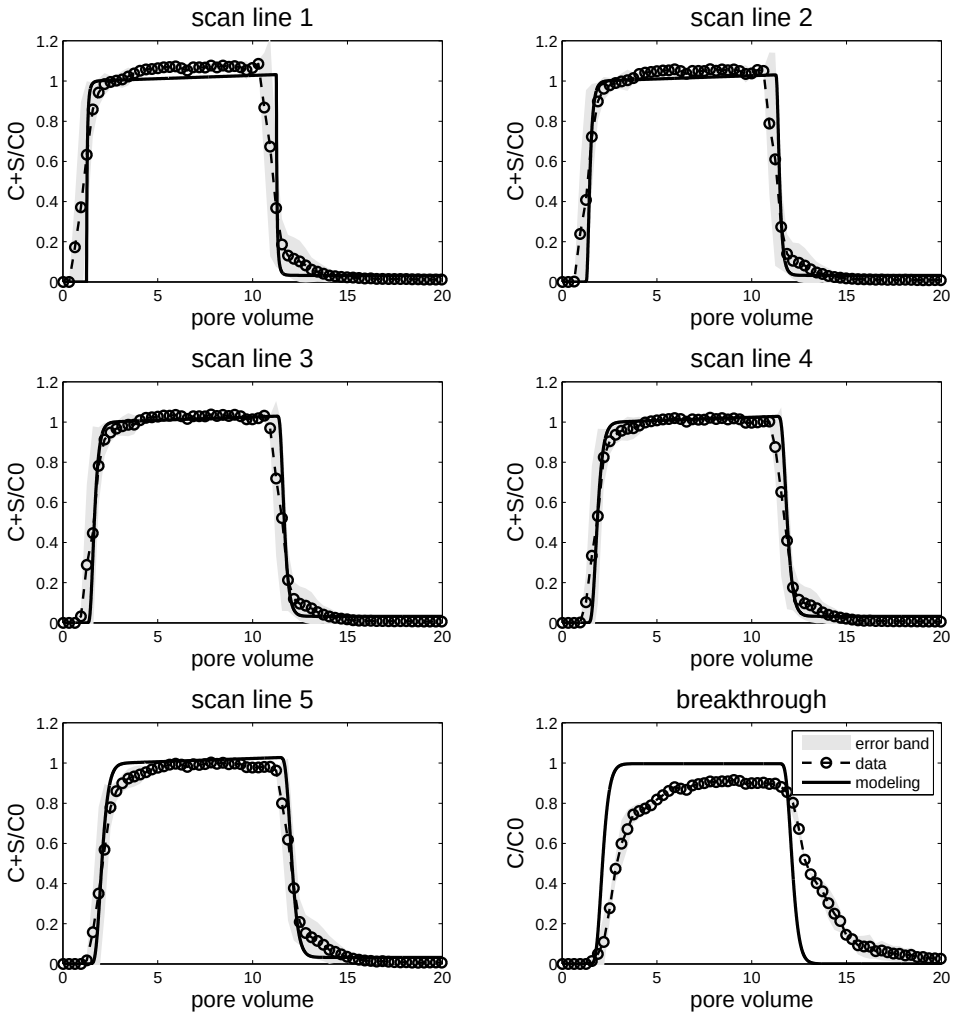

Figure 4.14: Modeling results of mixed 1μm particle experiment under downward flow conditions.

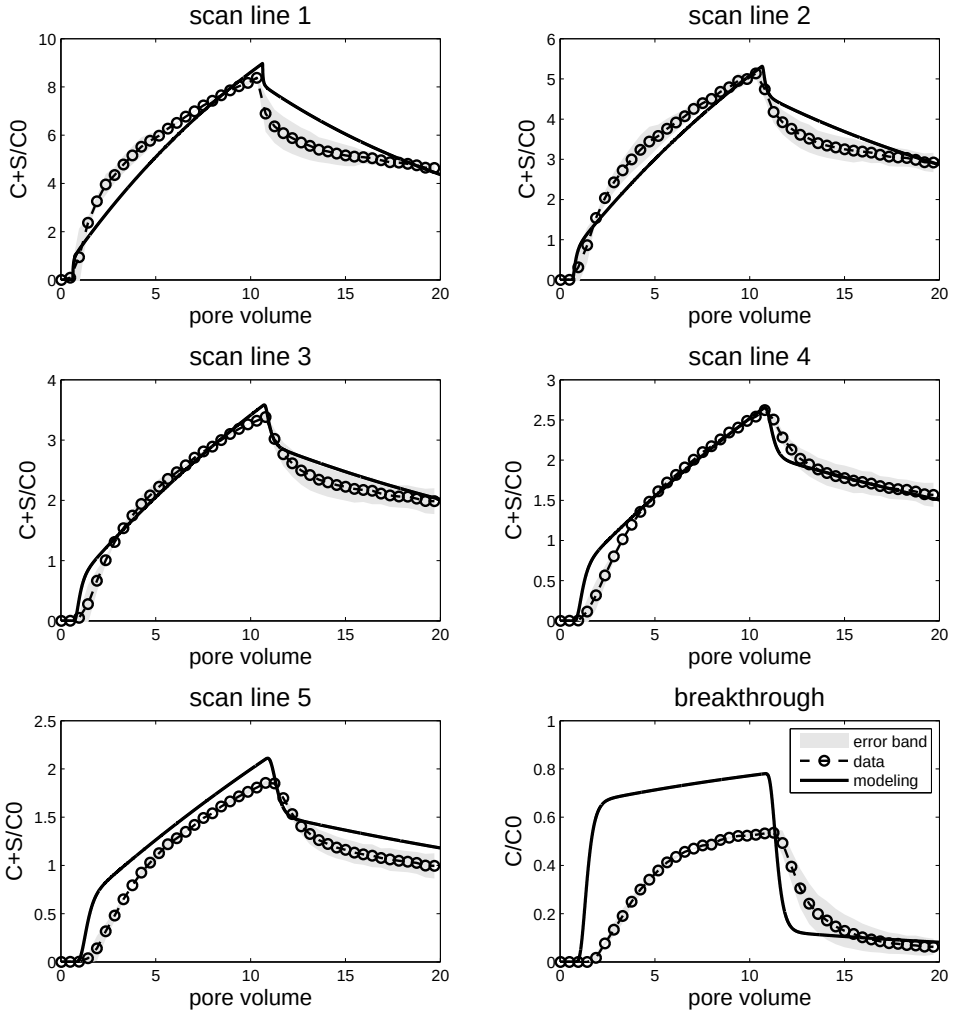

Figure 4.15: Modeling result of uniform 6μm particle test under upward flow condition.

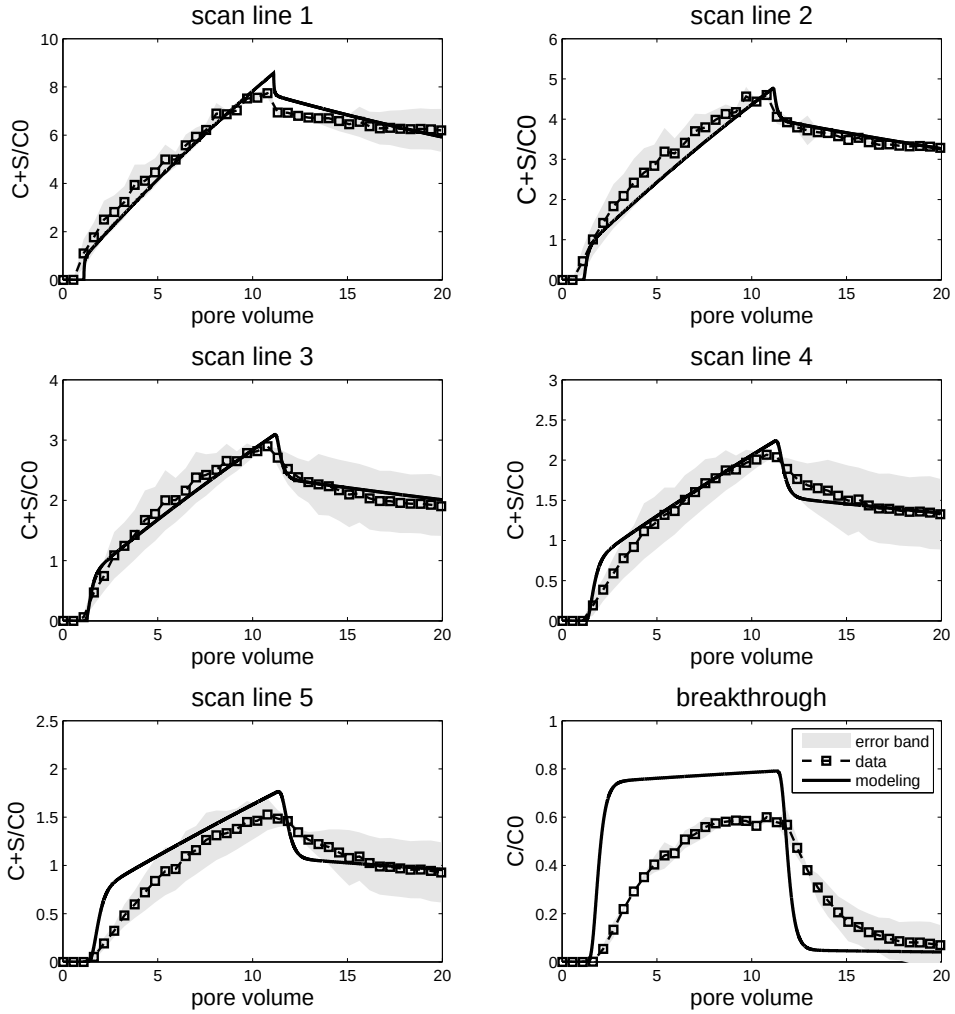

Figure 4.16: Modeling result of uniform 6μm particle test under horizontal flow condition.

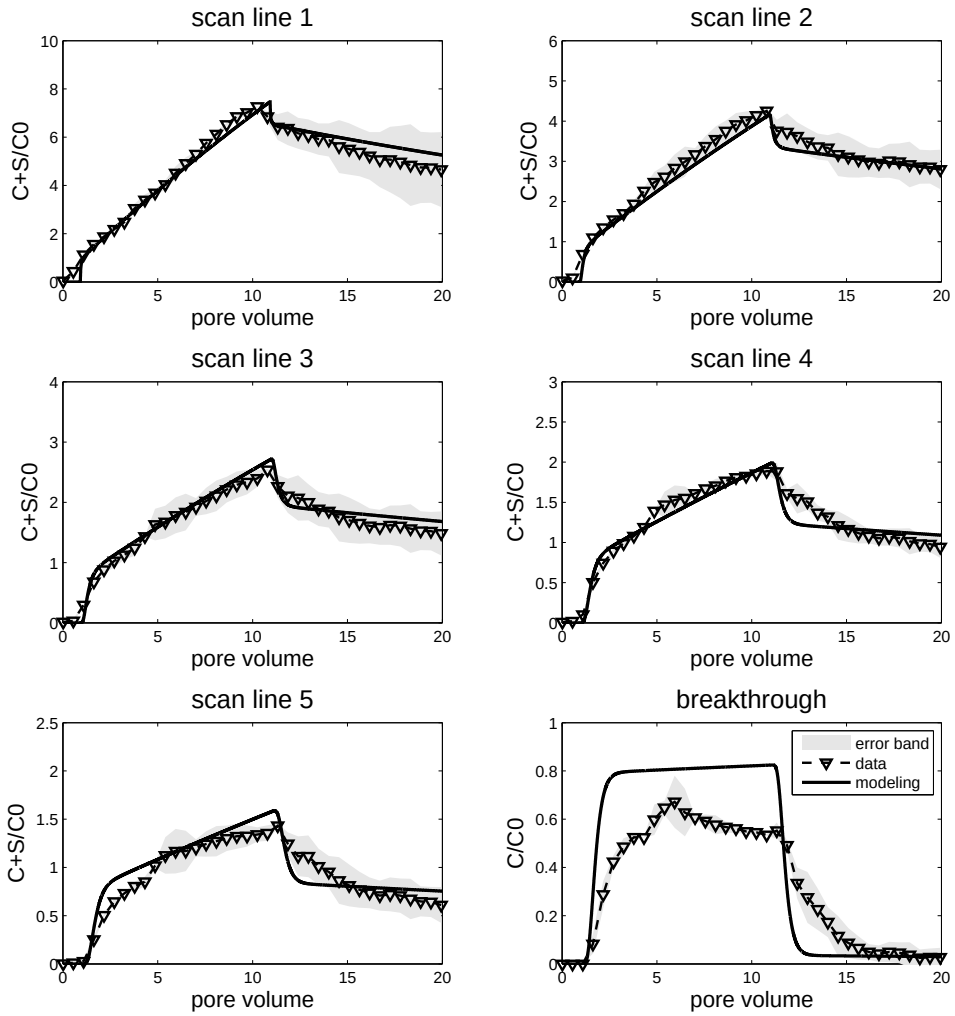

Figure 4.17: Modeling result of uniform 6μm particle test under downward flow condition.

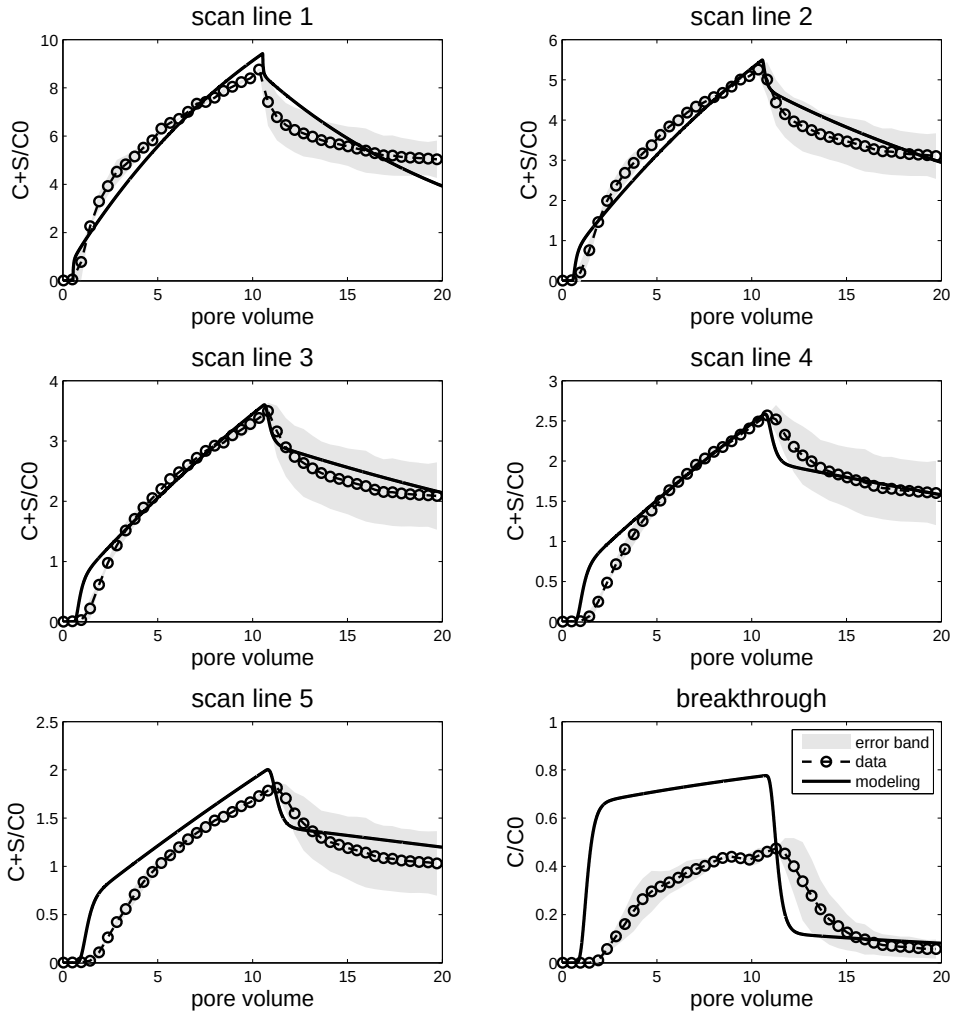

Figure 4.18: Model prediction of mixed 6μm particle test under upward flow condition

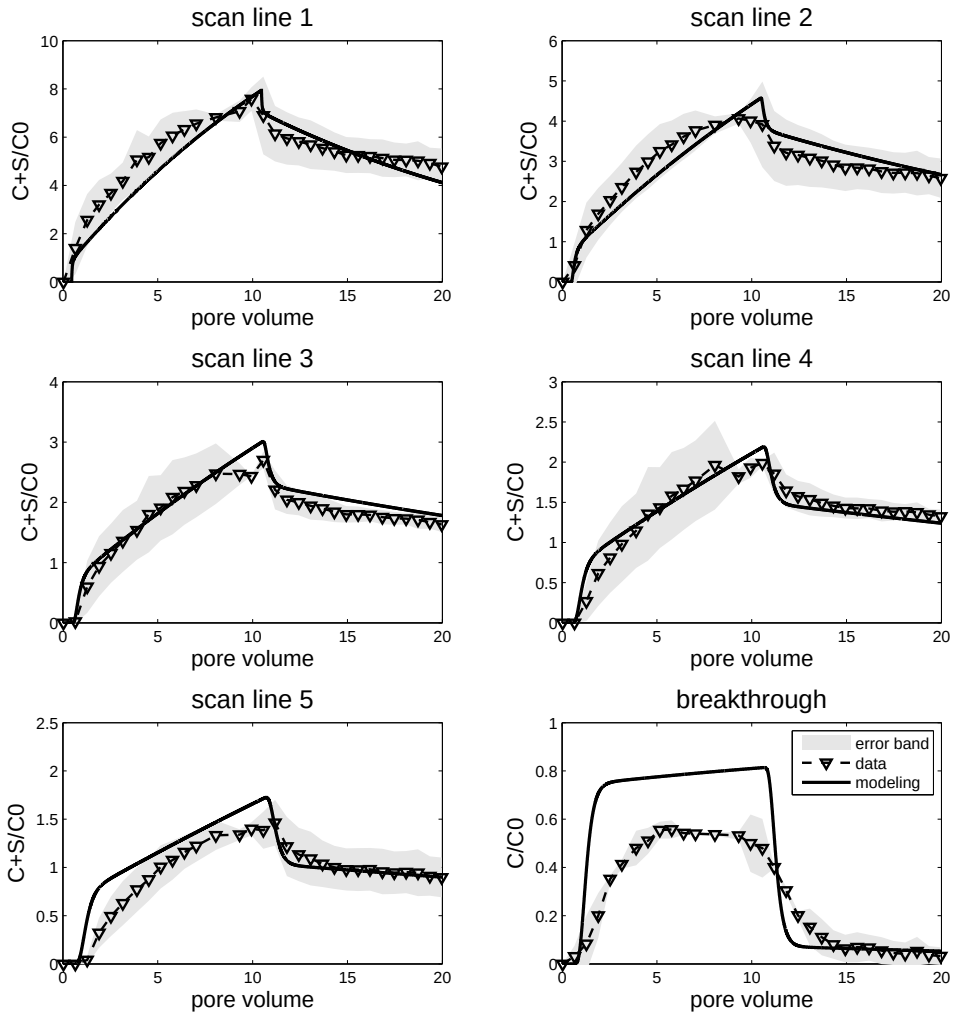

Figure 4.19: Model prediction of mixed 1μm particle test under downward flow condition

bined surface and straining model does capture well the retained particle concentration profiles. Nonetheless, with the exception of the downward test results for the uniform particle population, the reversible attached particle concentrations are generally over-estimated at the column inlet, while the irreversible particle populations are slightly under-estimated.

4.5 Discussion

4.5.1 Effect of Gravity

Previous studies have reported that Gravity could affect particle transport in saturated porous media, and have stated that such effects can be attributed to the following reasons: particle size, particle density, and flow direction. The influence of particle density was not covered in this study since the density of 1μm and 6μm particles used were all around 1.06 (Bangs Laboratories, Inc., Fishers, IN). Comparing the different results from the experiments conducted with different particle sizes (Figure 4.5 and Figure 4.7), the interior concentration profiles changed from profiles exhibiting a stable plateau with low retained particle concentrations, to profiles exhibiting no plateau and high-retained particle concentrations when the particle size increased from 1μm to 6μm. In tandem, the breakthrough curve concentrations reduced from $0.98C/C_0$ to $0.6C/C_0$. In addition, all 1μm experimental results were well fitted using a model assuming a very low irreversible attachment rates - of around $10^{-6}sec^{-1}$. Conversely, the 6μm experimental results required fitting using a model that involved different kinetic parameters for surface particle interactions and particle straining at grain-grain contact points. Both the experimental and numerical modeling results agree with previous studies that reported that an increase in particle size enhances particle deposition activities, and thus particle filtration within a porous medium.

Flow direction is another mechanism via which gravitation effects can influence particle transport in a saturated porous medium. The results of this study demon-

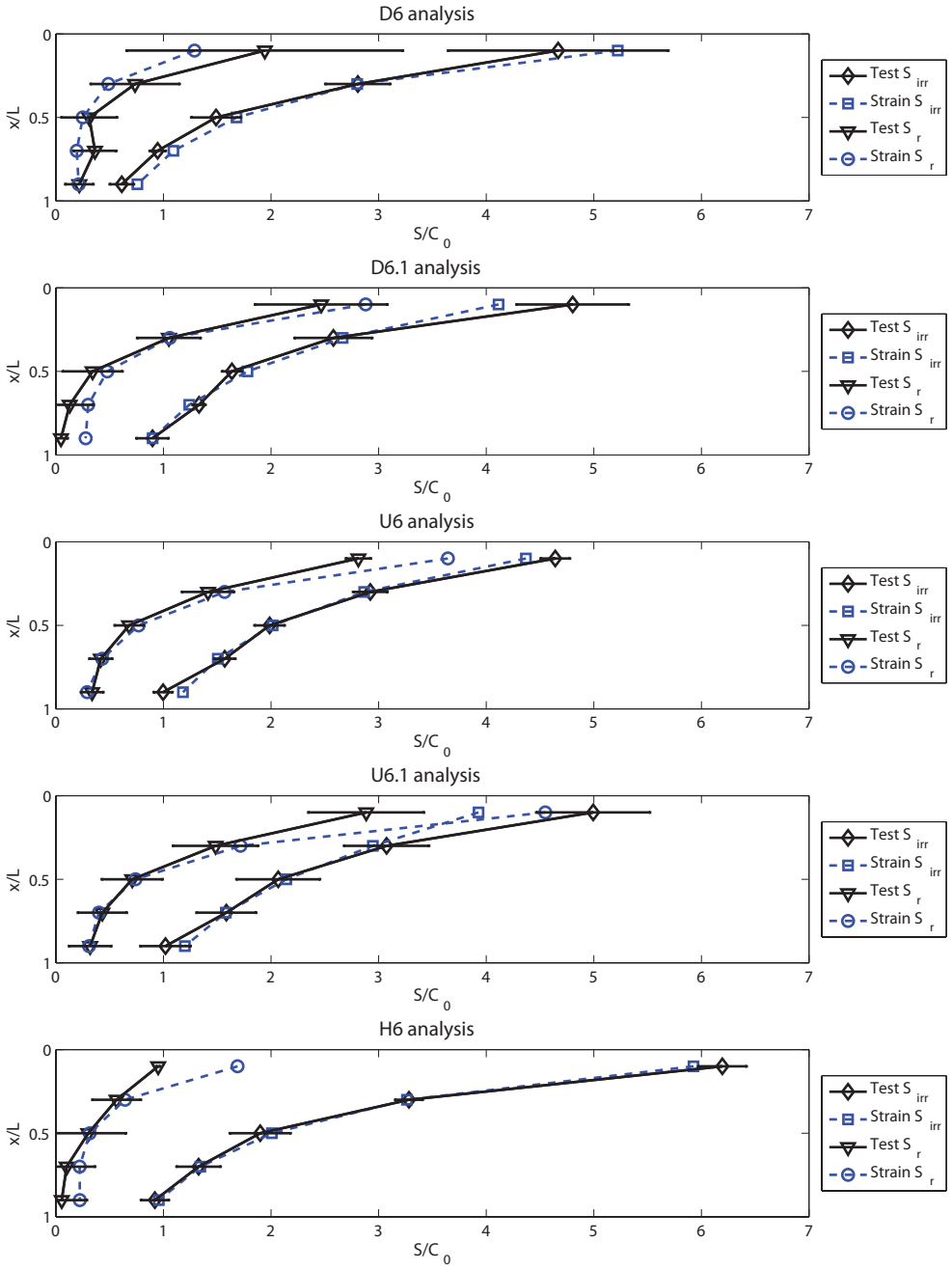

Figure 4.20: Observed and modeled values of S_{irr} and S_r profiles at the end of each experiment.

strated the greatest particle attachment rate for upward flow and the least particle attachment rate for downward flow, for both the 1μm and 6μm experimental and modeling results. Given the highly unfavorable electrostatic conditions present in all experiments as a result of both the particles and glass beads carrying negative surface charges, which will have prevented particle attachment to solid surfaces via attractive van der Waals forces, it is hypothesized that all particle interactions with the medium's solid phase were the result of physical processes, including particles being held temporarily or more permanently by asperities on the surfaces of the glass beads, as proposed by *Yoon et al.,* particles being physically immobilized at bead-bead contact points, and particles being immobilized in the low flow regions generated in the downstream wake of a glass bead, Figure 4.21 [Yoon *et al.*, 2006]. As seen in Figure 4.21, gravitational forces will act to favor the surface attachment of particles in the downstream wake of a glass bead for upward flow, but not for downward flow. For the straining mechanism, gravity will favor forcing particles through narrow channels between beads for downward flow but not upward flow. In both cases, horizontal flow conditions lie between the downward and upward flow conditions. The conditions illustrated conceptually in Figure 4.21 do explain the trends in the experimental observations with respect to flow direction.

4.5.2 Effect of particle interactions

Column tests with mixed 1μm and 6μm particle solutions were conducted in order to study the effects of interactions between different particle sizes (Figure 4.6 and Figure 4.8). For the mixed 1μm particle experiments, the interior scan-line profiles showed similar trends to the experimental results for the uniform particle population, and the fitted particle attachment rates were also very similar (Table 4.2). Thus, it would appear that the presence of a small fraction of 6μm particle did not influence, in any measurable way, the transport behavior of the 1μm particles. This is likely because the 1μm particles basically transported through the saturated packed columns having

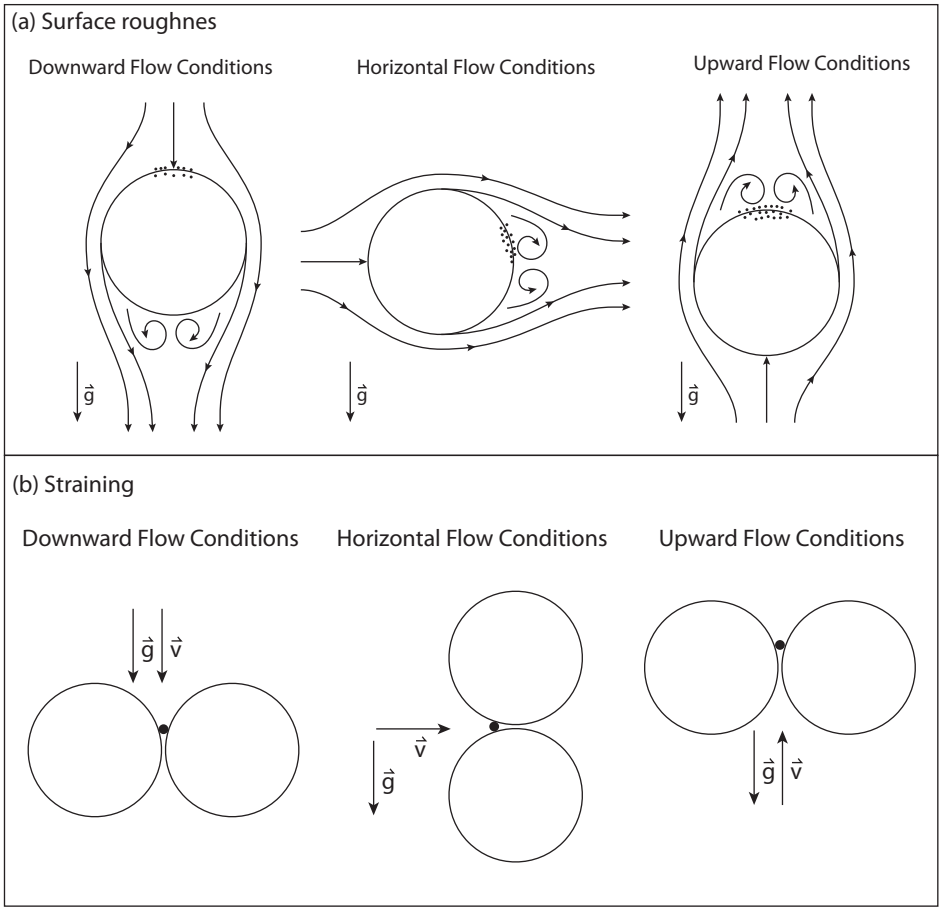

Figure 4.21: (a) Surface roughness and microscopic flow conditions retain particles on bead surfaces - illustration of capture zones for different flow directions (b) Straining mechanisms retain particles at grain-grain contact points

little interaction with the medium's solid phase, and the presence of the 6μm particles did not impact any liquid phase transport.

For the 6μm particle experiments, the presence of the 1μm particles increased both the irreversible and reversible attachment rates of the 6μm particles, as well as the detachment rate of the 6μm particles at the straining sites (Table 4.3). This phenomenon was observed to be greater during downward flow conditions than upward flow conditions. It is hypothesized that the 1μm particles act as facilitators for 6μm particle attachment, by interacting with attached 6μm particles in ways that retard their detachment from surface sites or straining sites. 1μm particles approaching some straining sites might also perturb flow fields in ways that enhance particle detachment at the straining sites.

4.6 Conclusion

One-dimensional, laboratory column experiments were performed under upward, downward, and horizontal flow directions using 1μm and 6μm microspheres and 500μm glass beads to simulate particle transport in saturated porous media. Via use of a novel visualization system, particle interior scan-lines and breakthrough curves were obtained for both uniform and mixed particle transport tests. Both the uniform and mixed particle concentrations were conducted at a particle injection concentration of 22mg/L: the difference between experimental protocols was that the mixed particle solutions were a combination of 90% of the major particle size and 10% of the minor particle size.

Consistent with prior studies, gravitational effects introduced by particle size and flow direction conditions influenced particle transport behavior. Increasing particle size decreased particle effluent concentrations and increased interior retained particle concentrations for all experiments. Changing flow direction from downward to horizontal then upward also increased interior retained concentrations and de-

creased effluent concentrations. For all experimental conditions, the 1μm particles basically transported through the saturated bead columns with little interaction with the medium's solid phase. In contrast, the 6μm particles attached on bead surfaces and at bead-bead contact points. The presence of 6μm particles had little impact on the transport behavior of the 1μm particles, while the presence of 1μm particles increased attachment rates for the 6μm particles.

Overall, the results of this study confirm that gravity, particle size and flow direction impact particle transport processes. The study also reveals that particle size heterogeneity could also impact particle transport under certain conditions. Both of these findings have implications for field-scale modeling of particle transport.

4.7 Acknowledgements

This study was supported by Grant W911NF-727 10-1-0123 from the Army Research Office. Any opinions, findings, and conclusions expressed in this article are those of the authors and do not necessarily reflect the views of any supporting institution.

4.8 Tables

Table 4.1: List of column experiment conditions including particle solution composition and flow direction

Column	Particle Solution Composition	Flow direction	Column	Particle Solution Composition	Flow direction
D1-1	100% 1μm	Downward	D6-1	100% 6μm	Downward
D1-2	100% 1μm	Downward	D6-2	100% 6μm	Downward
D1.1-1	90% 1μm; 10% 6μm	Downward	D6.1-1	90% 6μm; 10% 1μm	Downward
D1.1-2	90% 1μm; 10% 6μm	Downward	D6.1-2	90% 6μm; 10% 1μm	Downward
U1-1	100% 1μm	Upward	U6-1	100% 6μm	Upward
U1-2	100% 1μm	Upward	U6-2	100% 6μm	Upward
U1.1-1	90% 1μm; 10% 6μm	Upward	U6.1-1	90% 6μm; 10% 1μm	Upward
U1.1-2	90% 1μm; 10% 6μm	Upward	U6.1-2	90% 6μm; 10% 1μm	Upward
H1-1	100% 1μm	Horizontal	H6-1	100% 6μm	Horizaontal
H1-2	100% 1μm	Horizontal	H6-2	100% 6μm	Horizaontal

Table 4.2: Irreversible kinetic model fitting results of 1μm column experiments

Column	Solution type	Flow direction	Kir (sec-1)	Residual
D1	100% 1μm	Downward	1.80E-06	0.12
D1.1	90% 1μm; 10% 6μm	Downward	2.09E-06	0.08
U1	100% 1μm	Upward	2.55E-06	0.09
U1.1	90% 1μm; 10% 6μm	Upward	1.83E-06	0.33
H1	100% 1μm	Horizontal	2.49E-06	0.56

Table 4.3: Fitting results of 6μm column experiments involving kinetic modeling of both surface (Equation 4.4) and straining (Str) (Equation 4.5) processes.

Column	Solution type	Flow direction	K_a (sec^{-1})	K_d (sec^{-1})	K_i (sec^{-1})	$K_{a,str}$ (sec^{-1})	α	$K_{d,str}$ (sec^{-1})	β
D6	100% 6μm	Downward	1.63E-06	4.03E-06	1.22E-06	4.53E-04	3.51E+00	1.31E-05	6.01E-01
H6	100% 6μm	Horizontal	2.65E-06	3.68E-06	3.90E-06	5.43E-04	3.37E+00	1.59E-05	5.34E-01
U6	100% 6μm	Upward	2.98E-06	3.38E-06	1.27E-05	6.67E-04	2.99E+00	3.78E-05	4.19E-01
D6.1	90% 6μm; 10% 1mum	Downward	2.53E-06	3.51E-06	1.23E-05	5.88E-04	3.75E+00	3.17E-05	6.79E-01
U6.1	90% 6μm; 10% 1mum	Upward	6.60E-06	3.65E-06	1.28E-05	7.11E-04	3.28E+00	3.96E-05	3.49E-01

Chapter 5

Contributions and Recommendations for Future Work

The prevention of health risks and environmental hazards related to groundwater contaminated with harmful particulates requires accurate prediction of particle transport mechanisms. In order to increase the accuracy and suitability of particle transport modeling for real world applications, increased understanding the fundamental mechanisms governing particle transport is needed. The research contained in Chapters 2 to 4 of this dissertation aimed to fill certain knowledge gaps in current particle transport research, which led to several novel contributions. Among these contributions was the development of a numerical modeling program, termed the Kinetic Colloid Transport Model (KCTM), that can be used for predicting particle transport, or for back-fitting the results of laboratory column experiments in order to shed light on particle attachment and detachment behaviors under different transport conditions. The research also identified impacts of velocity effects on particle behavior, which to date have been ignored in conceptual models for particle transport. In addition, explorations into the impacts of particle size, mixed particle populations and flow direction on particle transport revealed the significance of flow direction for larger sized (6 micron) particles, as well the importance of depth, or path-length, depen-

dent straining in explaining particle behaviors observed during laboratory column experiments. A summary of the contributions of this work is provided below.

5.1 Chapter 2: Particle Transport Modeling

Currently, there is no publicly or commercially available particle transport models that provide dual mode kinetic sub-models, or depth-dependent kinetic sub-models, for predicting particle transport through saturated porous media, or for analyzing laboratory or field scale experiment data. Yet, several researchers have employed such kinetic sub-models to explore observed discrepancies between current predictive methods for particle transport and experimental results. The development of the Kinetic Colloid Transport Model (KCTM) presented in Chapter 2 responds to the need for a customizable particle transport model capable of employing different kinetic sub-models and analyzing data obtained from different experiment protocols.

Introduced in section 2.2, the KCTM was derived from the one-dimensional advection-dispersion-sorption equation. The KCTM incorporates not only common one-site and two-site kinetic sub-models for particle interactions with the solid phase of a porous medium, it also includes dual mode kinetic modeling capacity and a depth-dependent straining model. In section 2.3, the KCTM was validated against analytical solutions generated by the STANMOD program and numerical simulations obtained using the popular open software, HYDRUS-1D. For all case studies considered in the validation process, the KCTM results were in very good agreement with the results of STANMOD and HYDRUS-1D.

The most beneficial feature of the new KCTM is that it is capable of not only directly simulating particle transport in a saturated porous medium, it can also inversely solve for various kinetic particle attachment and detachment parameters using different data types/ sources. For example, the different column experiment protocols described in Chapter 3 and 4 of this thesis generated a range of particle concentration

measurements, all of which were successfully analyzed using the KCTM. In addition, the collaborative work described in Appendix A successfully applied the KCTM to analyze *E.coli* transport behaviors in sand filled columns of aquifer material obtained from a field site in Bangladesh.

5.2 Chapter 3: Can varying velocity conditions be one possible explanation for differences between laboratory and field observations of bacterial transport in porous media?

Chapter 3 offers a significant contribution that uncovers the impact of varying velocity conditions on particle transport in a saturated porous medium. Most prior research into particle transport behaviors has either neglected, or regarded as insignificant, the potential of varying velocity effects. The ability of varying velocity to affect particle transport therefore has not been well investigated.

Introduced in section 3.3, a new modified column experiment protocol was developed to simulate natural groundwater flow velocity variations due to hydraulic head changes. Three different velocity variations can be simulated with this new protocol, including increasing, decreasing, and increasing followed by decreasing, velocity conditions.

Introduced in section 3.4, an empirical power function relationship between velocity and a dimensionless kinetic particle attachment coefficient was derived from the results of a series of constant velocity column experiments. The empirical formula was incorporated into the KCTM to predict the results of varying velocity experiments, with very limited success. This outcome indicated that, even when predictions account for how particle attachment rates change with velocity, varying velocity conditions cannot be well modeled.

Introduced in section 3.5, a relationship between particle attachment rates and velocity obtained for directly fitting the varying velocity experiments, and that obtained from the constant velocity experiments, indicates that fluid acceleration might influence particle filtration processes. This finding is new, and potentially significant to the field of particle transport modeling.

5.3 Chapter 4: Particle transport in saturated porous media: effects of flow direction on uniform and mixed particle populations for two different particle sizes

Particle transport in saturated porous media has been confirmed to be affected by multiple physical factors. Chapter 4 provides research that was undertaken to explore the individual and/or combined effects of the flow direction, particle size, and particle-particle interaction on particle transport processes. For this research, a novel visualization technique was used to obtain particle concentrations in the interior of column experiments whose porous medium comprised saturated packs of glass beads.

Introduced in section 3.3, an irreversible attachment model was sufficient to reproduce observed 1μm particle transport behavior, however, only a two-site kinetic model coupled with a path-length dependent straining model could fit the observed 6μm particle transport behavior with tolerant residuals.

Introduced in section 4.1, differences between estimated kinetic parameters for the same sized particle tests transporting under downward, horizontal or upward conditions implied that different flow fields might trigger and/or amplify certain particle attachment or detachment activities. Conceptual models for particle attachment behaviors on glass bead surfaces, as a result of surface roughness and slow moving microscopic flow regions, and at grain-grain contact points, as a result of particle

straining, were introduced and successfully used to explained the different observed behaviors. However, the results and models raise questions about commonly observed non-log-linear attachment/detachment profiles in porous media, and whether current understanding of reversible particle attachment kinetics is sufficient. Such questions point out the need for increased micro-scale knowledge on particle behavior in the interior of a porous medium.

Introduced in section 4.2, a small fraction of 6μm particles transporting in the presence of 1μm particles was shown to have limited impact on the transport behavior of the 1μm particles. However, a small fraction of 1μm particles transporting in the presence of 6μm particles enhanced both irreversible and reversible attachment rates of the 6μm particles. This phenomenon was observed to be greater during downward flow conditions than upward flow conditions. The actual mechanisms of different sizes particle-particle interaction are still unclear. It was hypothesized that the 1μm particles act as facilitators for 6μm particle attachment, by interacting with attached 6μm particles in ways that retard their detachment from surface sites or straining sites.

5.4 Appendix A (collaborative research)

The ultimate goal of particle transport research is accurately predicting particle transport for real world applications, including field scale applications. However, many uncertain factors related to particle transport often restrict up-scaling predictions obtained from laboratory column tests to field scale applications. Appendix A combines multi-scale experiments and modeling work in order to identify several key factors that might improve up-scaling techniques. Specifically, the work combined observations and modeling of *E.coli* transport in laboratory column experiments with observations an modeling at an instrumented field site.

Introduced in section A.4.1 and A.4.2, both one-dimensional and two-dimensional

modeling results showed the RMSEs obtained when modeling the laboratory column experiments dramatically decreased while the sub-model describing particle attachment/ detachment mechanisms with the medium's solid phase changed from irreversible to reversible, two-site, and dual mode kinetics. This indicates that applying the proper particle attachment/ detachment model is crucial to either analyzing laboratory column experiments or to up-scaling predictions from laboratory column results to field scale problems. The kinetic model sensitivity analysis for the investigated field scale conditions was also conducted by applying two sets of dual mode kinetic parameters in a two-dimensional model of the field site. The noticeable differences between estimated *E.coli* transportation distances and observed transport distances highlighted the scaling problem between laboratory scale and field scale.

Introduced in section A.5.1, the *E.coli* transport distance was shown to be effected by anisotropy in subsurface hydraulic conductivity due to the relative proportion of horizontal to vertical groundwater flow velocity. However, anisotropy in hydraulic conductivity is not always a property that is measured during field transport studies. The sensitivity analysis showed that *E.coli* could transport deeper when hydraulic anisotropy slightly increases. This finding points out that groundwater flow fields should also be considered in up-scaling predictions.

5.5 Recommendations for future work

The research presented in this dissertation utilized a new numerical model, modified column experimental protocols, and visualization techniques, to successfully identify important physical factors that influence particle transport behavior. Nonetheless, the findings of the work presented in this thesis raise further questions with respect to understanding particle transport in saturated porous medium. The following sections outline some potential research topics for future research that could help meet the goal of accurately predicting particle transport processes.

5.5.1 Micro-scale experiments, modeling and non-log-linear reversible attachment mechanisms

Current studies generally agree that particle transport in saturated porous media are governed by advection-dispersion-sorption equations. Further, most assume that particle attachment/ detachment behaviors follow first order kinetics with respect to interactions with a collector (i.e., the solid phase of a porous medium). However, the results presented in Chapter 4 illustrated differences between observations and model predictions for the column experiments conducted using the 6 um particles , particularly during the particle flushing stage of an experiment. These differences indicate that the first order kinetic model assumptions of particle transport might be fundamentally different than certain, actual particle behaviors. Previous studies related to direct observations of particle transport in the interior of a porous medium, including those presented by *Yoon et al.,* have already reported unpredictable particle deposition behaviors, such as particles stacking on the top of collectors due to flow circulation fields, and particles falling from collector surface tops after stacks reach a certain height, and then depositing on upstream collectors [Yoon *et al.*, 2006]. Ignoring observation results such as these, and further expanding kinetic models with more and more assumptions, such as multiple populations of particles, and dual permeabilities of porous media, which might increase the reproduction capability of the kinetic models, but not truly model the fundamental particle transport behavior. itself Developing non-log-linear reversible attachment models based on micro-scale experiments and micro-scale modeling is the key to accurately predicting particle transport in the future.

5.5.2 Applications of the visualization technique

Results presented in Chapter 3 illustrated the use of column experiment protocol that only provides limited particle transport information, such as the BTC and retain par-

ticle concentration profile at the end of an experiment. Lack of information on particle concentrations within the interior of a porous medium might lead to over-simplified experiment observations for analyzing particle transport mechanisms. Results presented in Chapter 4 proved that particle transport behavior can be monitored in real time by applying novel visualization techniques. The modeling results also demonstrate that over-simplified one-site/two-site models cannot always accurately reproduce observations of particle behavior in the interior of a porous medium. Thus, to generate sufficient knowledge of some particle transport processes, the application of visualization techniques can be necessary. For example, in Chapter 3, the influence of fluid acceleration on particle attachment rates was identified via observations made at the outlet of a column experiment and a profile of retained particle concentrations at the , end of the experiment. Combing the experiment protocol in Chapter 3 with the visualization technique in Chapter 4, could help further clarify any relationship between fluid acceleration and particle attachment mechanisms, and might help uncover approaches to modeling this phenomenon. Moreover, as noted in the above section, detailed understanding of the micro-mechanisms responsible for particle attachment/ detachment on collector surfaces remains uncertain. Visualization techniques can be used to observe the particle-collector reactions directly, providing the foundation for building accurate micro-models of particle transport in porous media.

5.5.3 Mixed particle sizes experiment

Numerous studies have reported that particle size distribution was the main cause of observed high variance in particle deposition behaviors. Also, co-transport of different particle types, particles and chemical solutes, and particles and microbial entities were found to increase general transport distances. In Chapter 4, tried to uncover the effects of mixed particle sizes on particle transport mechanisms via column experiments conducted using uniform 1μm and 6μm particle populations, as well as mixed 1μm and 6μm particle populations. The presence of the 6μm particles did not

appear to influence the transport of the 1μm particles. However, the 6μm particle transport behavior was changed by the presence of the 1μm particles. Further work in this area should conduct experiments with particles of three or more different sizes, in order to continue to investigate the influence of different particle sizes on particle transport behavior. In addition, extension of the reported visualization technique to enable the simultaneous visualization of two or more particle populations during transport would also help advance understanding in this area.

Bibliography

[Abu-Lail and Camesano, 2003] Nehal I. Abu-Lail and Terri A. Camesano. Role of lipopolysaccharides in the adhesion, retention, and transport of Escherichia coli JM109. *Environmental Science and Technology*, 37(10):2173–2183, 2003.

[Abudalo *et al.*, 2005] R a Abudalo, Y G Bogatsu, J N Ryan, R W Harvey, D W Metge, and M Elimelech. Effect of ferric oxyhydroxide grain coatings on the transport of bacteriophage PRD1 and Cryptosporidium parvum oocysts in saturated porous media. *Environmental science & technology*, 39(17):6412–9, sep 2005.

[Adamczyk *et al.*, 2013] Zbigniew Adamczyk, Małgorzata Nattich-Rak, Marta Sadowska, Aneta Michna, and Katarzyna Szczepaniak. Mechanisms of nanoparticle and bioparticle deposition Kinetic aspects. *Colloids and Surfaces A: Physicochemical and Engineering Aspects*, 439:3–22, dec 2013.

[Anders and Chrysikopoulos, 2005] Robert Anders and C. V. Chrysikopoulos. Virus fate and transport during artificial recharge with recycled water. *Water Resources Research*, 41(10):1–14, 2005.

[Auset and Keller, 2004] Maria Auset and Arturo A. Keller. Pore-scale processes that control dispersion of colloids in saturated porous media. *Water Resources Research*, 40(3):n/a–n/a, mar 2004.

[Bales *et al.*, 1997] Roger C Bales, Shimin Li, T.-C. Jim Yeh, Melissa E. Lenczewski, and Charles P. Gerba. Bacteriophage and microsphere transport in saturated porous media: Forced-gradient experiment at Borden, Ontario, apr 1997.

[Basha and Culligan, 2010] H. A. Basha and P. J. Culligan. Modeling particle transport in downward and upward flows. *Water Resources Research*, 46(7), jul 2010.

[Baygents *et al.*, 1998] J. C. Baygents, J. R. Glynn, O. Albinger, B. K. Biesemeyer, K. L. Ogden, and R. G. Arnold. Variation of Surface Charge Density in Monoclonal Bacterial Populations: Implications for Transport through Porous Media. *Environmental Science & Technology*, 32(11):1596–1603, 1998.

[Becker *et al.*, 2004] Matthew W. Becker, Samantha A. Collins, David W. Metge, Ronald W. Harvey, and Allen M. Shapiro. Effect of cell physicochemical characteristics and motility on bacterial transport in groundwater. *Journal of Contaminant Hydrology*, 69(3-4):195–213, apr 2004.

[Bhattacharjee *et al.*, 2000] Subir Bhattacharjee, Jeffrey Y. Chen, and Menachem Elimelech. DLVO interaction energy between spheroidal particles and a flat surface. *Colloids and Surfaces A: Physicochemical and Engineering Aspects*, 165(1-3):143–156, may 2000.

[Bolster *et al.*, 2001] C H Bolster, a L Mills, G M Hornberger, and J S Herman. Effect of surface coatings, grain size, and ionic strength on the maximum attainable coverage of bacteria on sand surfaces. *Journal of contaminant hydrology*, 50(3-4):287–305, aug 2001.

[Bradford and Bettahar, 2006] Scott a Bradford and Mehdi Bettahar. Concentration dependent transport of colloids in saturated porous media. *Journal of Contaminant Hydrology*, 82(1-2):99–117, jan 2006.

[Bradford *et al.*, 2003a] Scott A. Bradford, Jirka Simunek, Mehdi Bettahar, Martinus Th Van Genuchten, and Scott R. Yates. Modeling colloid attachment, strain-

ing, and exclusion in saturated porous media. *Environmental science & technology*, 37(10):2242–50, may 2003.

[Bradford *et al.*, 2003b] Scott A. Bradford, Jirka Simunek, Mehdi Bettahar, Martinus Th Van Genuchten, and Scott R. Yates. Modeling colloid attachment, straining, and exclusion in saturated porous media. *Environmental Science and Technology*, 37(10):2242–2250, 2003.

[Bradford *et al.*, 2006a] S. a. Bradford, J. Simunek, M. Bettahar, M. T. van Genuchten, and S. R. Yates. Significance of straining in colloid deposition: Evidence and implications. *Water Resources Research*, 42(12):n/a–n/a, dec 2006.

[Bradford *et al.*, 2006b] Scott a. Bradford, Jirka Simunek, and Sharon L. Walker. Transport and straining of E. coli O157:H7 in saturated porous media. *Water Resources Research*, 42(12):n/a–n/a, dec 2006.

[Bradford *et al.*, 2012] Scott a. Bradford, Saeed Torkzaban, Hyunjung Kim, and Jiri Simunek. Modeling colloid and microorganism transport and release with transients in solution ionic strength. *Water Resources Research*, 48(9):n/a–n/a, sep 2012.

[Brown and Jaffé, 2001] D G Brown and P R Jaffé. Effects of nonionic surfactants on bacterial transport through porous media. *Environmental science & technology*, 35(19):3877–83, oct 2001.

[Brush *et al.*, 1999] C F Brush, W C Ghiorse, L J Anguish, J Y Parlange, and H G Grimes. Transport of Cryptosporidium parvum oocysts through saturated columns. *Journal of Environmental Quality*, 28(3):809–815, 1999.

[Burnham, 2004] K. P. Burnham. Multimodel Inference: Understanding AIC and BIC in Model Selection, 2004.

[Camesano and Logan, 1998] Terri a. Camesano and Bruce E. Logan. Influence of Fluid Velocity and Cell Concentration on the Transport of Motile and Nonmotile

Bacteria in Porous Media. *Environmental Science & Technology*, 32(11):1699–1708, jun 1998.

[Camesano *et al.*, 1999] Terri a. Camesano, Kenneth M. Unice, and Bruce E. Logan. Blocking and ripening of colloids in porous media and their implications for bacterial transport. *Colloids and Surfaces A: Physicochemical and Engineering Aspects*, 160(3):291–307, 1999.

[Camper *et al.*, 1993] a. K. Camper, J. T. Hayes, P. J. Sturman, W. L. Jones, and a. B. Cunningham. Effects of motility and adsorption rate coefficient on transport of bacteria through saturated porous media. *Applied and Environmental Microbiology*, 59(10):3455–3462, 1993.

[Chalk *et al.*, 2012] P. Chalk, N. Gooding, S. Hutten, Z. You, and P. Bedrikovetsky. Pore size distribution from challenge coreflood testing by colloidal flow. *Chemical Engineering Research and Design*, 90(1):63–77, jan 2012.

[Chen *et al.*, 2010] Gexin Chen, Yongsuk Hong, and Sharon L Walker. Colloidal and Bacterial Deposition: Role of Gravity. *Langmuir*, 26(1):314–319, jan 2010.

[Choi *et al.*, 2007] Nag-Choul Choi, Dong-Ju Kim, and Song-Bae Kim. Quantification of bacterial mass recovery as a function of pore-water velocity and ionic strength. *Research in Microbiology*, 158(1):70–78, jan 2007.

[Chrysikopoulos and Sim, 1996] Constantinos V. Chrysikopoulos and Youn Sim. One-dimensional virus transport in homogeneous porous media with time- dependent distribution coefficient. *Journal of Hydrology*, 185:199–219, 1996.

[Chrysikopoulos and Syngouna, 2014] Constantinos V. Chrysikopoulos and Vasiliki I. Syngouna. Effect of Gravity on Colloid Transport through Water-Saturated Columns Packed with Glass Beads: Modeling and Experiments. *Environmental Science & Technology*, 48(12):6805–6813, jun 2014.

[Clement *et al.*, 1997] T.P. Clement, B.M. Peyton, R.S. Skeen, D.a. Jennings, and J.N. Petersen. Microbial growth and transport in porous media under denitrification conditions: experiments and simulations. *Journal of Contaminant Hydrology*, 24(3-4):269–285, jan 1997.

[Cohen, 1988] J Cohen. *Statistical power analysis for the behavioral sciences*, volume 2nd. 1988.

[Cvetkovic *et al.*, 2004] V. Cvetkovic, S. Painter, D. Turner, D. Pickett, and P. Bertetti. Parameter and model sensitivities for colloid-facilitated radionuclide transport on the field scale. *Water Resources Research*, 40(6), jun 2004.

[de Kerchove and Elimelech, 2008] Alexis J de Kerchove and Menachem Elimelech. Bacterial swimming motility enhances cell deposition and surface coverage. *Environmental science & technology*, 42(12):4371–7, jun 2008.

[Derjaguin and Landau, 1993] B Derjaguin and L Landau. Theory of the stability of strongly charged lyophobic sols and of the adhesion of strongly charged particles in solutions of electrolytes. *Progress in Surface Science*, 43(1-4):30–59, may 1993.

[Derx *et al.*, 2013] J. Derx, A.P. P Blaschke, A.H. H Farnleitner, L. Pang, G. Blöschl, and J.F. F Schijven. Effects of fluctuations in river water level on virus removal by bank filtration and aquifer passage–a scenario analysis. *Journal of contaminant hydrology*, 147:34–44, apr 2013.

[Dong *et al.*, 2002] Hailiang Dong, T C Onstott, Mary F Deflaun, Mark E Fuller, Timothy D Scheibe, Sheryl H Streger, Randi K Rothmel, and Brian J Mailloux. Relative dominance of physical versus chemical effects on the transport of adhesion-deficient bacteria in intact cores from South Oyster, Virginia. *Environmental science & technology*, 36(5):891–900, mar 2002.

[Dong *et al.*, 2006] Hailiang Dong, Timothy D Scheibe, William P Johnson, Crystal M Monkman, and Mark E Fuller. Change of collision efficiency with distance in bacterial transport experiments. *Ground water*, 44(3):415–29, 2006.

[Elimelech, 1991] M Elimelech. Effect of particle size on the kinetics of particle deposition under attractive double layer interactions. *Journal of colloid and interface science*, 146(2), 1991.

[Escamilla *et al.*, 2013] V. Escamilla, P. S. K. Knappett, M. Yunus, P. K. Streatfield, and M. Emch. Influence of Latrine Proximity and Type on Tubewell Water Quality and Diarrheal Disease in Bangladesh. *Annals of the Association of American Geographers*, 103(2):299–308, 2013.

[Feighery *et al.*, 2013] John Feighery, Brian J Mailloux, a S Ferguson, Kazi Matin Ahmed, Alexander van Geen, and Patricia J Culligan. Transport of E. coli in aquifer sediments of Bangladesh: Implications for widespread microbial contamination of groundwater. *Water Resources Research*, 49(7):3897–3911, jul 2013.

[Fetter, 2001] C.W. Fetter. *Applied Hydrogeology*. 2001.

[Fontes *et al.*, 1991] D. E. Fontes, A. L. Mills, G. M. Hornberger, and J. S. Herman. Physical and chemical factors influencing transport of microorganisms through porous media. *Applied and Environmental Microbiology*, 57(9):2473–2481, 1991.

[Foppen and Schijven, 2005] J. W A Foppen and J. F. Schijven. Transport of E. coli in columns of geochemically heterogeneous sediment. *Water Research*, 39(13):3082–3088, 2005.

[Foppen and Schijven, 2006] J W a Foppen and J F Schijven. Evaluation of data from the literature on the transport and survival of Escherichia coli and thermotolerant coliforms in aquifers under saturated conditions. *Water research*, 40(3):401–26, feb 2006.

[Foppen *et al.*, 2007] Jan Willem Foppen, Manon van Herwerden, and Jack Schijven. Measuring and modelling straining of Escherichia coli in saturated porous media. *Journal of contaminant hydrology*, 93(1-4):236–54, aug 2007.

[Foppen *et al.*, 2008] J. W A Foppen, M. van Herwerden, M. Kebtie, A. Noman, J. F. Schijven, P. J. Stuyfzand, and S. Uhlenbrook. Transport of Escherichia coli and solutes during waste water infiltration in an urban alluvial aquifer. *Journal of Contaminant Hydrology*, 95(1-2):1–16, 2008.

[Foster and Chilton, 2003] S S D Foster and P J Chilton. Groundwater: the processes and global significance of aquifer degradation. *Philosophical Transactions of the Royal Society B: Biological Sciences*, 358(1440):1957–1972, dec 2003.

[Fuller *et al.*, 2001] Mark E. Fuller, Brian J. Mailloux, Pengfei Zhang, Sheryl H. Streger, James a. Hall, Simon N. Vainberg, Andrew J. Beavis, William P. Johnson, Tullis C. Onstott, and Mary F. DeFlaun. Field-scale evaluation of CFDA/SE staining coupled with multiple detection methods for assessing the transport of bacteria in situ. *FEMS Microbiology Ecology*, 37(1):55–66, aug 2001.

[Gannon *et al.*, 1991] J. Gannon, Y H Tan, P. Baveye, and M. Alexander. Effect of sodium chloride on transport of bacteria in a saturated aquifer material. *Applied and environmental microbiology*, 57(9):2497–2501, sep 1991.

[Gelhar *et al.*, 1992] Lynn W. Gelhar, Claire Welty, and Kenneth R. Rehfeldt. A critical review of data on fieldscale dispersion in aquifers. *Water Resources Research*, 28(7):1955–1974, 1992.

[Genuchten *et al.*, 1982] MT Van Genuchten, WJ W.J. Alves, M.Th. Van Genuchten, and WJ W.J. Alves. Analytical solutions of the one-dimensional convective-dispersive solute transport equation. *Agricultural research service, Technical bulletin Number 1661*, 1661(1661):1–149, 1982.

[Ginn *et al.*, 2002] Timothy R. Ginn, Brian D. Wood, Kirk E. Nelson, Timothy D. Scheibe, Ellyn M. Murphy, and T.Prabhakar Clement. Processes in microbial transport in the natural subsurface. *Advances in Water Resources*, 25(8-12):1017–1042, aug 2002.

[Godfrey *et al.*, 2003] S Godfrey, L McCaffery, A Obika, and M Becks. The effectiveness of point-source chlorination in improving water quality in internally displaced communities in Angola. *Journal of the Chartered Institution of Water and Environmental Management*, 17(3):149–151, 2003.

[Goss *et al.*, 1998] M.J Goss, D.A.J Barry, and D.L Rudolph. Contamination in Ontario farmstead domestic wells and its association with agriculture:. *Journal of Contaminant Hydrology*, 32(3-4):267–293, aug 1998.

[Grolimund and Borkovec, 2006] Daniel Grolimund and Michal Borkovec. Release of colloidal particles in natural porous media by monovalent and divalent cations. *Journal of Contaminant Hydrology*, 87(3-4):155–175, 2006.

[Gundry *et al.*, 2004] Stephen Gundry, Jim Wright, and Ronan Conroy. A systematic review of the health outcomes related to household water quality in developing countries, 2004.

[Gupta *et al.*, 2009] Vishal Gupta, W P Johnson, P Shafieian, H Ryu, a Alum, M Abbaszadegan, S a Hubbs, and T Rauch-Williams. Riverbank filtration: comparison of pilot scale transport with theory. *Environmental science & technology*, 43(3):669–76, feb 2009.

[Hahn *et al.*, 2004] Melinda W. Hahn, Dean Abadzic, and Charles R. O'Melia. Aquasols: On the role of secondary minima. *Environmental Science and Technology*, 38(22):5915–5924, 2004.

[Hall *et al.*, 2005] J a Hall, B J Mailloux, T C Onstott, T D Scheibe, M E Fuller, H Dong, and M F DeFlaun. Physical versus chemical effects on bacterial and

bromide transport as determined from on site sediment column pulse experiments. *Journal of contaminant hydrology*, 76(3-4):295–314, feb 2005.

[Happel, 1958] John Happel. Viscous flow in multiparticle systems: Slow motion of fluids relative to beds of spherical particles. *AIChE Journal*, 4(2):197–201, 1958.

[Harvey *et al.*, 1993] Ronald W. Harvey, Nancy E. Kinner, Dan MacDonald, David W. Metge, and Amoret Bunn. Role of physical heterogeneity in the interpretation of small-scale laboratory and field observations of bacteria, microbial-sized microsphere, and bromide transport through aquifer sediments, 1993.

[Hendry *et al.*, 1999] M. J. Hendry, J. R. Lawrence, and P. Maloszewski. Effects of Velocity on the Transport of Two Bacteria Through Saturated Sand. *Ground Water*, 37(1):103–112, jan 1999.

[Hidalgo *et al.*, 2011] Gabriela Hidalgo, Michelle Chan, and Nathalie Tufenkji. Inhibition of Escherichia coli CFT073 fliC expression and motility by cranberry materials. *Applied and environmental microbiology*, 77(19):6852–7, oct 2011.

[Hijnen *et al.*, 2005] Wim A M Hijnen, Anke J. Brouwer-Hanzens, Katrina J. Charles, and Gertjan J. Medema. Transport of MS2 phage, Escherichia coli Clostridium perfringens, Cryptosporidium parvum, and Giardia intestinalis in a gravel and a sandy soil. *Environmental Science and Technology*, 39(20):7860–7868, 2005.

[Hoffmann and Chiang, 2000a] Klaus a Hoffmann and Steve T Chiang. Computational Fluid Dynamics Vol.I - Hoffmann.pdf, 2000.

[Hoffmann and Chiang, 2000b] Klaus a Hoffmann and Steve T Chiang. Computational Fluid Dynamics Vol.II - Hoffmann.pdf, 2000.

[Hornberger, 1992] GM Hornberger. Bacterial transport in porous media: evaluation of a model using laboratory observations. *Water Resources ...*, 1992.

[Hubbard *et al.*, 2001] Susan S. Hubbard, Jinsong Chen, John Peterson, Ernest L. Majer, Kenneth H. Williams, Donald J. Swift, Brian Mailloux, and Yoram Rubin. Hydrogeological characterization of the South Oyster bacterial transport site using geophysical data. *Water Resources Research*, 37(10):2431–2456, 2001.

[Hurley and Roscoe, 1983] M. A. Hurley and M.E. Roscoe. Automated Statistical analysis of microbial enumeration by dilution series. *Journal of Applied Bacteriology*, 55(1):159–164, 1983.

[James and Chrysikopoulos, 2011] Scott C. James and Constantinos V. Chrysikopoulos. Monodisperse and polydisperse colloid transport in water-saturated fractures with various orientations: Gravity effects. *Advances in Water Resources*, 34(10):1249–1255, oct 2011.

[Jean *et al.*, 2013] Kouamé Kan Jean, Jourda Jean Patrice, Saley Mahaman Bachir, Deh Serges Kouakou, Anani Abenan Tawa, Leblanc Yves, Cloutier Vincent, and Biemi Jean. Modeling of groundwater flow and drawdown evolution simulation of Abidjan aquifer. *Journal of Asian Scientific Research*, 3(4):344–364, 2013.

[Jin and Flury, 2002] Yan Jin and Markus Flury. Fate and Transport of Viruses in Porous Media. In *Advances in Agronomy*, volume 77, pages 39–102. Elsevier Inc., 2002.

[Johnson *et al.*, 2001] W. P. Johnson, P. Zhang, M. E. Fuller, T. D. Scheibe, B. J. Mailloux, T. C. Onstott, M. F. Deflaun, S. S. Hubbard, J. Radtke, W. P. Kovacik, and W. Holben. Ferrographic tracking of bacterial transport in the field at the narrow channel focus area, Oyster, VA. *Environmental Science and Technology*, 35(1):182–191, 2001.

[Johnson *et al.*, 2007a] William P. Johnson, Xiqing Li, and Shoeleh Assemi. Deposition and re-entrainment dynamics of microbes and non-biological colloids during

non-perturbed transport in porous media in the presence of an energy barrier to deposition. *Advances in Water Resources*, 30(6-7):1432–1454, jun 2007.

[Johnson *et al.*, 2007b] William P. Johnson, Meiping Tong, and Xiqing Li. On colloid retention in saturated porous media in the presence of energy barriers: The failure of α , and opportunities to predict η. *Water Resources Research*, 43(12):n/a–n/a, dec 2007.

[Kadane and Lazar, 2004] Joseph B Kadane and Nicole A Lazar. Methods and Criteria for Model Selection. *Journal of the American Statistical Association*, 99(February 2015):279–290, 2004.

[Kanti Sen and Khilar, 2006] Tushar Kanti Sen and Kartic C Khilar. Review on subsurface colloids and colloid-associated contaminant transport in saturated porous media. *Advances in Colloid and Interface Science*, 119(2-3):71–96, feb 2006.

[Keller *et al.*, 2004] Arturo A. Keller, Sanya Sirivithayapakorn, and Constantinos V. Chrysikopoulos. Early breakthrough of colloids and bacteriophage MS2 in a water-saturated sand column. *Water Resources Research*, 40(8):n/a–n/a, aug 2004.

[Kersting *et al.*, 1999] a. B. Kersting, D. W. Efurd, D. L. Finnegan, D. J. Rokop, D. K. Smith, and J. L. Thompson. Migration of plutonium in ground water at the Nevada Test Site. *Nature*, 397(6714):56–59, jan 1999.

[Kim *et al.*, 2009] Hyunjung N Kim, Scott A Bradford, and Sharon L. Walker. Escherichia coli O157:H7 Transport in Saturated Porous Media: Role of Solution Chemistry and Surface Macromolecules. *Environmental Science & Technology*, 43(12):4340–4347, jun 2009.

[Knappett *et al.*, 2011a] Peter S K Knappett, Alice Layton, Larry D. McKay, Daniel Williams, Brian J. Mailloux, M. R. Huq, M. J. Alam, Kazi Matin Ahmed, Yasuyuki Akita, Marc L. Serre, Gary S. Sayler, and Alexander Van Geen. Efficacy

of Hollow-Fiber Ultrafiltration for Microbial Sampling in Groundwater. *Ground Water*, 49(1):53–65, 2011.

[Knappett *et al.*, 2011b] Peter S.K. Knappett, Veronica Escamilla, Alice Layton, Larry D McKay, Michael Emch, Daniel E Williams, R Huq, J Alam, Labony Farhana, Brian J Mailloux, Andy Ferguson, Gary S Sayler, Kazi M Ahmed, and Alexander van Geen. Impact of population and latrines on fecal contamination of ponds in rural Bangladesh. *Science of The Total Environment*, 409(17):3174–3182, aug 2011.

[Knappett *et al.*, 2012] Peter S K Knappett, Larry D McKay, Alice Layton, Daniel E Williams, Md J Alam, Md R Huq, Jacob Mey, John E Feighery, Patricia J Culligan, Brian J Mailloux, Jie Zhuang, Veronica Escamilla, Michael Emch, Edmund Perfect, Gary S Sayler, Kazi M Ahmed, and Alexander van Geen. Implications of Fecal Bacteria Input from Latrine-Polluted Ponds for Wells in Sandy Aquifers. *Environmental Science & Technology*, 46(3):1361–1370, feb 2012.

[Knappett *et al.*, 2014] P.S.K. Knappett, J Du, P Liu, V Horvath, B.J. Mailloux, J Feighery, A van Geen, and P.J. Culligan. Importance of reversible attachment in predicting E. coli transport in saturated aquifers from column experiments. *Advances in Water Resources*, 63:120–130, jan 2014.

[Ko and Elimelech, 2000] Chun-Han Ko and Menachem Elimelech. The Shadow Effect in Colloid Transport and Deposition Dynamics in Granular Porous Media: Measurements and Mechanisms. *Environmental Science & Technology*, 34(17):3681–3689, sep 2000.

[Kurosawa *et al.*, 2006] Susumu Kurosawa, Scott C. James, Mikazu Yui, and Motomu Ibaraki. Model analysis of the colloid and radionuclide retardation experiment at the Grimsel Test Site. *Journal of Colloid and Interface Science*, 298(1):467–475, 2006.

[Lagarias *et al.*, 1998] Jeffrey C. Lagarias, James a. Reeds, Margaret H. Wright, and Paul E. Wright. Convergence Properties of the Nelder–Mead Simplex Method in Low Dimensions. *SIAM Journal on Optimization*, 9(1):112–147, 1998.

[Leber *et al.*, 2011] Jessica Leber, M Moshiur Rahman, Kazi M Ahmed, Brian Mailloux, and Alexander van Geen. Contrasting influence of geology on E. coli and arsenic in aquifers of Bangladesh. *Ground water*, 49(1):111–23, 2011.

[Leij *et al.*, 2012] F J Leij, N Toride, Mt Van Genuchten, and J Simunek. STANMOD: Model use, calibration, and Validation. *Transactions of the ASABE*, 55(4):1353–1366, 2012.

[Li and Johnson, 2005] Xiqing Li and William P Johnson. Nonmonotonic variations in deposition rate coefficients of microspheres in porous media under unfavorable deposition conditions. *Environmental science & technology*, 39(6):1658–65, mar 2005.

[Li and Logan, 1999] Qun Li and Bruce E Logan. Enhancing bacterial transport for bioaugmentation of aquifers using low ionic strength solutions and surfactants. *Water Research*, 33(4):1090–1100, mar 1999.

[Li *et al.*, 2004] Xiqing Li, Timothy D Scheibe, and William P Johnson. Apparent decreases in colloid deposition rate coefficients with distance of transport under unfavorable deposition conditions: a general phenomenon. *Environmental science & technology*, 38(21):5616–25, nov 2004.

[Li *et al.*, 2006] Xiqing Li, Chen Luh Lin, Ian D Miller, and William P Johnson. Pore-scale observation of microsphere deposition at grain-to-grain contacts over assemblage-scale porous media domains using x-ray microtomography. *Environmental Science and Technology*, 40(12):3762–3768, jun 2006.

[Li *et al.*, 2011] Zhen Li, Endalkachew Sahle-Demessie, Ashraf Aly Hassan, and George a Sorial. Transport and deposition of CeO2 nanoparticles in water-saturated porous media. *Water research*, 45(15):4409–18, oct 2011.

[Liu *et al.*, 2011] Jun Liu, Roseanne M Ford, and James a Smith. Idling time of motile bacteria contributes to retardation and dispersion in sand porous medium. *Environmental science & technology*, 45(9):3945–51, may 2011.

[Logan *et al.*, 1995] B. E. Logan, D. G. Jewett, R. G. Arnold, E. J. Bouwer, and C. R. O'Melia. Clarification of Clean-Bed Filtration Models. *Journal of Environmental Engineering*, 121(12):869–873, dec 1995.

[Logan, 2001] J. David Logan. *Transport Modeling in Hydrogeochemical Systems*, volume 15 of *Interdisciplinary Applied Mathematics*. Springer New York, New York, NY, 2001.

[Long and Hilpert, 2009] Wei Long and Markus Hilpert. A correlation for the collector efficiency of Brownian particles in clean-bed filtration in sphere packings by a Lattice-Boltzmann method. *Environmental Science and Technology*, 43(12):4419–4424, 2009.

[Long *et al.*, 2010] Wei Long, Haiou Huang, Jasmine Serlemitsos, Elizabeth Liu, Allen H. Reed, and Markus Hilpert. Pore-scale study of the collector efficiency of nanoparticles in packings of nonspherical collectors. *Colloids and Surfaces A: Physicochemical and Engineering Aspects*, 358(1-3):163–171, apr 2010.

[Loveland *et al.*, 2003] Jonathan P Loveland, Subir Bhattacharjee, Joseph N Ryan, and Menachem Elimelech. Colloid transport in a geochemically heterogeneous porous medium: aquifer tank experiment and modeling. *Journal of contaminant hydrology*, 65(3-4):161–82, sep 2003.

[Ma and Johnson, 2010] Huilian Ma and William P Johnson. Colloid retention in porous media of various porosities: predictions by the hemispheres-in-cell model. *Langmuir : the ACS journal of surfaces and colloids*, 26(3):1680–7, feb 2010.

[Ma *et al.*, 2009] Huilian Ma, Julien Pedel, Paul Fife, and William P Johnson. Hemispheres-in-cell geometry to predict colloid deposition in porous media. *Environmental science & technology*, 43(22):8573–9, nov 2009.

[Marlow *et al.*, 1991] H.J. Marlow, K.L. Duston, M.R. Wiesner, M.B. Tomson, J.T. Wilson, and C.H. Ward. Microbial transport through porous media: The effects of hydraulic conductivity and injection velocity. *Journal of Hazardous Materials*, 28:65–74, 1991.

[Massoudieh *et al.*, 2010] a Massoudieh, C Crain, E Lambertini, K E Nelson, T Barkouki, P L'amoreaux, F J Loge, and T R Ginn. Kinetics of conjugative gene transfer on surfaces in granular porous media. *Journal of contaminant hydrology*, 112(1-4):91–102, mar 2010.

[McCarthy and Zachara, 1989] John F. McCarthy and John M. Zachara. Subsurface transport of contaminants. *Environmental Science & Technology*, 23(5):496–502, may 1989.

[McClaine and Ford, 2002] JW McClaine and RM Ford. Reversal of flagellar rotation is important in initial attachment of Escherichia coli to glass in a dynamic system with high-and low-ionic-strength buffers. *Applied and Environmental Microbiology*, 68(3):1280–1289, 2002.

[McDowell-Boyer *et al.*, 1986] Laura M. McDowell-Boyer, James R. Hunt, and Nicholas Sitar. Particle transport through porous media, 1986.

[McGechan and Lewis, 2002] Mb McGechan and Dr Lewis. Transport of Particulate and Colloid-sorbed Contaminants through Soil, Part 1: General Principles. *Biosystems Engineering*, 83(3):255–273, 2002.

[Mitropoulou *et al.*, 2013] Polyxeni N. Mitropoulou, Vasiliki I. Syngouna, and Constantinos V. Chrysikopoulos. Transport of colloids in unsaturated packed columns: Role of ionic strength and sand grain size. *Chemical Engineering Journal*, 232:237–248, oct 2013.

[Molnar *et al.*, 2011] Ian L. Molnar, Denis M. O'Carroll, and Jason I. Gerhard. Impact of surfactant-induced wettability alterations on DNAPL invasion in quartz and iron oxide-coated sand systems. *Journal of Contaminant Hydrology*, 119(1-4):1–12, jan 2011.

[Molnar *et al.*, 2015] Ian L. Molnar, William P. Johnson, Jason I. Gerhard, Clinton S. Willson, and Denis M. O'Carroll. Predicting colloid transport through saturated porous media: A critical review. *Water Resources Research*, 51(9):6804–6845, sep 2015.

[Morris *et al.*, 2003] Brian Morris, A.R.L. Lawrence, John Chilton, Brian Adams, Roger Calow, and Ben Klinck. Groundwater and its susceptibility to degradation : a global assessment of the problem and options for management, aug 2003.

[Nascimento *et al.*, 2006] A.G. Nascimento, M.R. Tótola, C.S. Souza, M.T. Borges, and A.C. Borges. Temporal and spatial dynamics of blocking and ripening effects on bacterial transport through a porous system: A possible explanation for CFT deviation. *Colloids and Surfaces B: Biointerfaces*, 53(2):241–244, dec 2006.

[Nelson and Ginn, 2011] Kirk E. Nelson and Timothy R. Ginn. New collector efficiency equation for colloid filtration in both natural and engineered flow conditions. *Water Resources Research*, 47(5):W05543, may 2011.

[Neumann *et al.*, 2009] Rebecca B. Neumann, Khandaker N. Ashfaque, a. B. M. Badruzzaman, M. Ashraf Ali, Julie K. Shoemaker, and Charles F. Harvey. Anthropogenic influences on groundwater arsenic concentrations in Bangladesh. *Nature Geoscience*, 3(1):46–52, nov 2009.

[Ngueleu *et al.*, 2013] Stéphane K Ngueleu, Peter Grathwohl, and Olaf a Cirpka. Effect of natural particles on the transport of lindane in saturated porous media: Laboratory experiments and model-based analysis. *Journal of Contaminant Hydrology*, 149:13–26, jun 2013.

[O'May and Tufenkji, 2011] Che O'May and Nathalie Tufenkji. The swarming motility of Pseudomonas aeruginosa is blocked by cranberry proanthocyanidins and other tannin-containing materials. *Applied and environmental microbiology*, 77(9):3061–7, may 2011.

[Pang, 2008] Liping Pang. Microbial removal rates in subsurface media estimated from published studies of field experiments and large intact soil cores. *Journal of environmental quality*, 38(4):1531–59, 2008.

[Pazmino *et al.*, 2011] Eddy F Pazmino, Huilian Ma, and William P Johnson. Applicability of colloid filtration theory in size-distributed, reduced porosity, granular media in the absence of energy barriers. *Environmental science & technology*, 45(24):10401–7, dec 2011.

[Pei *et al.*, 2008] Jianyong Pei, John Germaine, and Patricia Culligan. Method for Visualizing Coupled Particle and Fluid Transport in Porous Media. *GeoCongress 2008 Characterization Monitoring and Modeling of GeoSystems GSP 179*, 311(May 2010):103–103, 2008.

[Petosa *et al.*, 2010] Adamo R. Petosa, Deb E B P. Jaisi, Ivan R. Quevedo, Menachem Elimelech, and Nathalie Tufenkji. Aggregation and deposition of engineered nanomaterials in aquatic environments: role of physicochemical interactions. *Environmental science & technology*, 44(17):6532–49, sep 2010.

[Prieve and Ruckenstein, 1974] Dennis C. Prieve and Eli Ruckenstein. Effect of London forces upon the rate of deposition of Brownian particles. *AIChE Journal*, 20(6):1178–1187, 1974.

[Prüss-Üstün *et al.*, 2008] A Prüss-Üstün, Robert Bos, Fiona Gore, and Jamie Bartram. *Safer water, better health: costs, benefits and sustainability of interventions to protect and promote health.* Geneva, Switzerland: World Health Organization., 2008.

[Rajagopalan and Tien, 1976] Rajamani Rajagopalan and Chi Tien. Trajectory analysis of deep-bed filtration with the sphere-in-cell porous media model. *AIChE Journal*, 22(3):523–533, may 1976.

[Redman *et al.*, 2001] Jeremy A. Redman, Mary K. Estes, and Stanley B. Grant. Resolving macroscale and microscale heterogeneity in virus filtration. In *Colloids and Surfaces A: Physicochemical and Engineering Aspects*, volume 191, pages 57–70, 2001.

[Redman *et al.*, 2004] Jeremy a Redman, Sharon L Walker, and Menachem Elimelech. Bacterial adhesion and transport in porous media: role of the secondary energy minimum. *Environmental science & technology*, 38(6):1777–85, mar 2004.

[Rezaei *et al.*, 2013] Abolfazl Rezaei, Hongbin Zhan, and Mohammad Zare. Impact of thin aquitards on two-dimensional solute transport in an aquifer. *Journal of Contaminant Hydrology*, 152:117–136, sep 2013.

[Rijnaarts *et al.*, 1996a] Huub H M Rijnaarts, Willem Norde, Edward J. Bouwer, Johannes Lyklema, and Alexan Der J B Zehnder. Bacterial deposition in porous media related to the clean bed collision efficiency and to substratum blocking by attached cells. *Environmental Science and Technology*, 30(10):2869–2876, 1996.

[Rijnaarts *et al.*, 1996b] Huub H M Rijnaarts, Willem Norde, Edward J. Bouwer, Johannes Lyklema, and Alexander J B Zehnder. Bacterial deposition in porous media: Effects of cell-coating, substratum hydrophobicity, and electrolyte concentration. *Environmental Science and Technology*, 30(10):2877–2883, 1996.

[Ryan and Gschwend, 1994] Joseph N. Ryan and Philip M. Gschwend. Effects of Ionic Strength and Flow Rate on Colloid Release: Relating Kinetics to Intersurface Potential Energy. *Journal of Colloid and Interface Science*, 164(1):21–34, apr 1994.

[Ryan *et al.*, 1999] Joseph N. Ryan, Menachem Elimelech, Rebecca a. Ard, Ronald W. Harvey, and Philip R. Johnson. Bacteriophage PRD1 and Silica Colloid Transport and Recovery in an Iron Oxide-Coated Sand Aquifer. *Environmental Science & Technology*, 33(1):63–73, jan 1999.

[Sandler, 2011] Niklas Sandler. Photometric imaging in particle size measurement and surface visualization. *International journal of pharmaceutics*, 417(1-2):227–34, sep 2011.

[Scheibe and Chien, 2003] Timothy D. Scheibe and Yi J. Chien. An evaluation of conditioning data for solute transport prediction. *Ground Water*, 41(2):128–141, 2003.

[Scheibe *et al.*, 2011] Timothy D Scheibe, Susan S Hubbard, Tullis C Onstott, and Mary F Deflaun. Lessons learned from bacterial transport research at the South Oyster Site. *Ground water*, 49(5):745–63, 2011.

[Schijven and Hassanizadeh, 2000] Jack F. Schijven and S. Majid Hassanizadeh. Removal of Viruses by Soil Passage: Overview of Modeling, Processes, and Parameters. *Critical Reviews in Environmental Science and Technology*, 30(1):49–127, jan 2000.

[Schijven and Simnek, 2002] Jack F Schijven and Jirí Simnek. Kinetic modeling of virus transport at the field scale. *Journal of contaminant hydrology*, 55(1-2):113–35, mar 2002.

[Schijven *et al.*, 1999] Jack F. Schijven, Wim Hoogenboezem, S. Majid Hassanizadeh, and Jos H. Peters. Modeling removal of bacteriophages MS2 and PRD1 by dune

recharge at Castricum, Netherlands. *Water Resources Research*, 35(4):1101–1111, 1999.

[Schijven *et al.*, 2002] Jack F. Schijven, S. Majid Hassanizadeh, and Ria H A M De Bruin. Two-site kinetic modeling of bacteriophages transport through columns of saturated dune sand. *Journal of Contaminant Hydrology*, 57(3-4):259–279, 2002.

[Sen, 2011] Tushar Kanti Sen. Processes in Pathogenic Biocolloidal Contaminants Transport in Saturated and Unsaturated Porous Media: A Review. *Water, Air, & Soil Pollution*, 216(1-4):239–256, mar 2011.

[Sgountzos *et al.*, 2006] I.N. Sgountzos, S. Pavlou, C.a. Paraskeva, and a.C. Payatakes. Growth kinetics of Pseudomonas fluorescens in sand beds during biodegradation of phenol. *Biochemical Engineering Journal*, 30(2):164–173, jun 2006.

[Shahid, 2010] Shamsuddin Shahid. Rainfall variability and the trends of wet and dry periods in Bangladesh. *International Journal of Climatology*, 30(15):2299–2313, 2010.

[Shang *et al.*, 2013] Jianying Shang, Chongxuan Liu, and Zheming Wang. Transport and retention of engineered nanoporous particles in porous media: Effects of concentration and flow dynamics. *Colloids and Surfaces A: Physicochemical and Engineering Aspects*, 417:89–98, jan 2013.

[Shen *et al.*, 2008] Chongyang Shen, Yuanfang Huang, Baoguo Li, and Yan Jin. Effects of solution chemistry on straining of colloids in porous media under unfavorable conditions. *Water Resources Research*, 44(5), 2008.

[Shen *et al.*, 2012] Chongyang Shen, Volha Lazouskaya, Hongyan Zhang, Feng Wang, Baoguo Li, Yan Jin, and Yuanfang Huang. Theoretical and experimental investigation of detachment of colloids from rough collector surfaces. *Colloids and Surfaces A: Physicochemical and Engineering Aspects*, 410:98–110, sep 2012.

[Simunek *et al.*, 2012] J Simunek, Mt Van Genuchten, and M Sejna. HYDRUS: Model use, calibration, and validation. *Transactions of the ASABE*, 55(1987):1261–1274, 2012.

[Šimnek and van Genuchten, 2008] Jirka Šimnek and Martinus Th. van Genuchten. Modeling Nonequilibrium Flow and Transport Processes Using HYDRUS. *Vadose Zone Journal*, 7:782, 2008.

[Šimnek *et al.*, 2009] J. Šimnek, M. Sejna, H. Saito, M. Sakai, and M.Th. van Genuchten. The HYDRUS-1D software package for simulating the one-dimensional movement of water, heat, and multiple solutes in variably-saturated media. Version 4.08. HYDRUS Softw. Ser. 3. *Dep. of Environ. Sci., Univ. of Calif., Riverside.*, (January):332, 2009.

[Sinton *et al.*, 2011] Lester W. Sinton, Margaret L. Mackenzie, Naveena Karki, Rod L. Dann, Liping Pang, and Murray E. Close. Transport of Escherichia coli and F-RNA Bacteriophages in a 5-M Column of Saturated, Heterogeneous Gravel. *Water, Air, & Soil Pollution*, 223(5):2347–2360, dec 2011.

[Stevik *et al.*, 2004] Tor Kristian Stevik, Kari Aa, Geir Ausland, and Jon Fredrik Hanssen. Retention and removal of pathogenic bacteria in wastewater percolating through porous media: A review, 2004.

[Swanton, 1995] SW W Swanton. Modelling colloid transport in groundwater: the prediction of colloid stability and retention behavior. *Advances in colloid and interface science*, 54(C):129–208, 1995.

[Syngouna and Chrysikopoulos, 2011] Vasiliki I. Syngouna and Constantinos V. Chrysikopoulos. Transport of biocolloids in water saturated columns packed with sand: Effect of grain size and pore water velocity. *Journal of Contaminant Hydrology*, 126(3-4):301–14, nov 2011.

[Tan *et al.*, 1994] Y. Tan, J. T. Gannon, P. Baveye, and M. Alexander. Transport of bacteria in an aquifer sand: Experiments and model simulations. *Water Resources Research*, 30(12):3243, 1994.

[Tang *et al.*, 2010] Guoping Tang, Melanie A. Mayes, Jack C. Parker, and Philip M. Jardine. CXTFIT/Excel-A modular adaptable code for parameter estimation, sensitivity analysis and uncertainty analysis for laboratory or field tracer experiments. *Computers and Geosciences*, 36(9):1200–1209, 2010.

[Tare and Venkobachar, 1985] Vinod. Tare and C Venkobachar. New conceptual formulation for predicting filter performance. *Environmental Science & Technology*, 19(6):497–499, jun 1985.

[Taylor *et al.*, 2004] Richard Taylor, Aidan Cronin, Steve Pedley, John Barker, and Tim Atkinson. The implications of groundwater velocity variations on microbial transport and wellhead protection - Review of field evidence. In *FEMS Microbiology Ecology*, volume 49, pages 17–26, 2004.

[Tian *et al.*, 2010] Yuan Tian, Bin Gao, Carlos Silvera-Batista, and Kirk J. Ziegler. Transport of engineered nanoparticles in saturated porous media. *Journal of Nanoparticle Research*, 12(7):2371–2380, apr 2010.

[Tobiason and Vigneswaran, 1994] John E. Tobiason and Balasubramaniam Vigneswaran. Evaluation of a modified model for deep bed filtration. *Water Research*, 28(2):335–342, feb 1994.

[Tong and Johnson, 2006] Meiping Tong and William P. Johnson. Excess Colloid Retention in Porous Media as a Function of Colloid Size, Fluid Velocity, and Grain Angularity. *Environmental Science & Technology*, 40(24):7725–7731, dec 2006.

[Tong and Johnson, 2007] Meiping Tong and William P Johnson. Colloid population heterogeneity drives hyperexponential deviation from classic filtration theory. *Environmental science & technology*, 41(2):493–9, jan 2007.

[Tong *et al.*, 2008] Meiping Tong, Huilian Ma, and William P Johnson. Funneling of flow into grain-to-grain contacts drives colloid-colloid aggregation in the presence of an energy barrier. *Environmental science & technology*, 42(8):2826–32, apr 2008.

[Toride *et al.*, 1995] N Toride, F J Leij, and M T Van Genuchten. The CXTFIT code for estimating transport parameters from laboratory or field tracer experiments. *Res Rep*, Research R(137):1–138, 1995.

[Torkzaban *et al.*, 2007] Saeed Torkzaban, Scott A. Bradford, and Sharon L. Walker. Resolving the coupled effects of hydrodynamics and DLVO forces on colloid attachment in porous media. *Langmuir*, 23(19):9652–9660, 2007.

[Torkzaban *et al.*, 2008] Saeed Torkzaban, Scott a Bradford, Martinus Th van Genuchten, and Sharon L Walker. Colloid transport in unsaturated porous media: the role of water content and ionic strength on particle straining. *Journal of contaminant hydrology*, 96(1-4):113–27, feb 2008.

[Tosco and Sethi, 2009] Tiziana Tosco and Rajandrea Sethi. MNM1D: A numerical code for colloid transport in porous media: Implementation and validation. *American Journal of Environmental Sciences*, 5(4):516–524, apr 2009.

[Tosco *et al.*, 2009] Tiziana Tosco, Alberto Tiraferri, and Rajandrea Sethi. Ionic strength dependent transport of microparticles in saturated porous media: Modeling mobilization and immobilization phenomena under transient chemical conditions. *Environmental Science and Technology*, 43(12):4425–4431, 2009.

[Tufenkji and Elimelech, 2004a] Nathalie Tufenkji and Menachem Elimelech. Correlation equation for predicting single-collector efficiency in physicochemical filtration in saturated porous media. *Environmental science & technology*, 38(2):529–36, jan 2004.

[Tufenkji and Elimelech, 2004b] Nathalie Tufenkji and Menachem Elimelech. Deviation from the classical colloid filtration theory in the presence of repulsive DLVO interactions. *Langmuir*, 20(25):10818–10828, 2004.

[Tufenkji and Elimelech, 2005] Nathalie Tufenkji and Menachem Elimelech. Spatial distributions of Cryptosporidium oocysts in porous media: evidence for dual mode deposition. *Environmental science & technology*, 39(10):3620–9, may 2005.

[Tufenkji *et al.*, 2002] Nathalie Tufenkji, Joseph N. Ryan, and Menachem Elimelech. Peer Reviewed: The Promise of Bank Filtration. *Environmental Science & Technology*, 36(21):422A–428A, 2002.

[Tufenkji *et al.*, 2003] Nathalie Tufenkji, Jeremy A. Redman, and Menachem Elimelech. Interpreting deposition patterns of microbial particles in laboratory-scale column experiments. *Environmental science & technology*, 37(3):616–23, feb 2003.

[Tufenkji *et al.*, 2004] Nathalie Tufenkji, Garrett F Miller, Joseph N Ryan, Ronald W Harvey, and Menachem Elimelech. Transport of Cryptosporidium oocysts in porous media: role of straining and physicochemical filtration. *Environmental science & technology*, 38(22):5932–8, nov 2004.

[Tufenkji, 2007] Nathalie Tufenkji. Modeling microbial transport in porous media: Traditional approaches and recent developments. *Advances in Water Resources*, 30(6-7):1455–1469, jun 2007.

[van Geen *et al.*, 2011] Alexander van Geen, Kazi Matin Ahmed, Yasuyuki Akita, Md Jahangir Alam, Patricia J Culligan, Michael Emch, Veronica Escamilla, John Feighery, Andrew S Ferguson, Peter Knappett, Alice C Layton, Brian J Mailloux, Larry D McKay, Jacob L Mey, Marc L Serre, P Kim Streatfield, Jianyong Wu, and Mohammad Yunus. Fecal contamination of shallow tubewells in bangladesh inversely related to arsenic. *Environmental science & technology*, 45(4):1199–205, feb 2011.

[Vasiliadou and Chrysikopoulos, 2011] Ioanna A. Vasiliadou and Constantinos V. Chrysikopoulos. Cotransport of Pseudomonas putida and kaolinite particles through water-saturated columns packed with glass beads. *Water Resources Research*, 47(2):n/a–n/a, feb 2011.

[Verwey and Overbeek, 1947] E J W Verwey and J. TH. G. Overbeek. Theory of the stability of lyophobic colloids. *The Journal of physical and colloid chemistry*, 51(3):631–636, aug 1947.

[Vigneswaran and Tulachan, 1988] S. Vigneswaran and Ravi Kumar Tulachan. Mathematical modelling of transient behaviour of deep bed filtration. *Water Research*, 22(9):1093–1100, sep 1988.

[Walker *et al.*, 2004] Sharon L. Walker, Jeremy A. Redman, and Menachem Elimelech. Role of cell surface lipopolysaccharides in escherichia coli K12 adhesion and transport. *Langmuir : the ACS journal of surfaces and colloids*, 20(18):7736–46, aug 2004.

[Walker *et al.*, 2005a] Sharon L Walker, Jane E Hill, Jeremy A Redman, and Menachem Elimelech. Influence of growth phase on adhesion kinetics of Escherichia coli D21g. *Applied and environmental microbiology*, 71(6):3093–9, jun 2005.

[Walker *et al.*, 2005b] Sharon L Walker, Jeremy a Redman, and Menachem Elimelech. Influence of growth phase on bacterial deposition: interaction mechanisms in packed-bed column and radial stagnation point flow systems. *Environmental science & technology*, 39(17):6405–11, sep 2005.

[Walshe *et al.*, 2010] Gillian E. Walshe, Liping Pang, Markus Flury, Murray E. Close, and Mark Flintoft. Effects of pH, ionic strength, dissolved organic matter, and flow rate on the co-transport of MS2 bacteriophages with kaolinite in gravel aquifer media. *Water Research*, 44(4):1255–1269, 2010.

[Weiss *et al.*, 2005] W. Joshua Weiss, Edward J. Bouwer, Ramon Aboytes, Mark W. LeChevallier, Charles R. O'Melia, Binh T. Le, and Kellogg J. Schwab. Riverbank filtration for control of microorganisms: Results from field monitoring. *Water Research*, 39(10):1990–2001, 2005.

[WHO, 2004] WHO. Water, Sanitation and Hygiene Links to Health FACTS AND FIGURES, 2004.

[Williams and Fletcher, 1996] Valerie Williams and Madilyn Fletcher. Pseudomonas fluorescens adhesion and transport through porous media are affected by lipopolysaccharide composition. *Applied and Environmental Microbiology*, 62(1):100–104, 1996.

[Wu *et al.*, 2011] Jianyong Wu, Alexander van Geen, Kazi Matin Ahmed, Yasuyuki Akita Jahangir Alam, Patricia J. Culligan, Veronica Escamilla, John Feighery, Andrew S. Ferguson, Peter Knappett, Brian J. Mailloux, Larry D. McKay, Marc L. Serre, P. Kim Streatfield, Mohammad Yunus, and Michael Emch. Increase in diarrheal disease associated with arsenic mitigation in bangladesh. *PLoS ONE*, 6(12), 2011.

[Xiao and Wiesner, 2013] Yao Xiao and Mark R Wiesner. Transport and Retention of Selected Engineered Nanoparticles by Porous Media in the Presence of a Biofilm. *Environmental Science & Technology*, 47(5):2246–2253, mar 2013.

[Xu *et al.*, 2008] Shangping Xu, Qian Liao, James E. Saiers, and New Haven. Straining of nonspherical colloids in saturated porous media. *Environmental Science and Technology*, 42(3):771–778, 2008.

[Yao *et al.*, 1971] Kuan-Mu Yao, Mohammad T. Habibian, and Charles R. O'Melia. Water and waste water filtration. Concepts and applications. *Environmental Science & Technology*, 5(11):1105–1112, nov 1971.

[Yavuz Corapcioglu and Haridas, 1984] M. Yavuz Corapcioglu and A. Haridas. Transport and fate of microorganisms in porous media: A theoretical investigation, 1984.

[Yoon *et al.*, 2006] Joon Sik Yoon, John T. Germaine, and Patricia J. Culligan. Visualization of particle behavior within a porous medium: Mechanisms for particle filtration and retardation during downward transport. *Water Resources Research*, 42:1–16, 2006.

[Yu *et al.*, 2013] Congrong Yu, Rafael Muñoz-Carpena, Bin Gao, and Oscar Perez-Ovilla. Effects of ionic strength, particle size, flow rate, and vegetation type on colloid transport through a dense vegetation saturated soil system: Experiments and modeling. *Journal of Hydrology*, 499:316–323, aug 2013.

[Zektser and Everett, 2004] I.S. Zektser and L.G. Everett. Resources of the World and Their Use, 2004.

[Zhang *et al.*, 2001] Pengfei Zhang, William P. Johnson, Timothy D. Scheibe, Keun Hyung Choi, Fred C. Dobbs, and Brian J. Mailloux. Extended tailing of bacteria following breakthrough at the Narrow Channel focus area, Oyster, Virginia. *Water Resources Research*, 37(11):2687–2698, 2001.

Appendices

Appendix A

Importance if Reversible Attachment in Predicting *E. coli* Transport in Saturated Aquifers From Column Experiments

A.1 Abstract

Drinking water wells indiscriminatingly placed adjacent to fecal contaminated surface water represents a significant but difficult to quantify health risk. Here we seek to understand mechanisms that limit the contamination extent by scaling up bacterial transport results from the laboratory to the field in a well constrained setting. Three pulses of *Escherichia coli* originating during the early monsoon from a freshly excavated pond receiving latrine effluent in Bangladesh were monitored in 6 wells and modeled with a two-dimensional (2-D) flow and transport model conditioned with measured hydraulic heads. The modeling was performed assuming three different modes of interaction of *E. coli* with aquifer sands: (1) irreversible attachment only (best-fit $ki = 7.6$ day^{-1}); (2) reversible attachment only ($ka = 10.5$ and $k_d = 0.2$

day^{-1}); and (3) a combination of reversible and irreversible modes of attachment ($k_a = 60$, $k_d = 7.6$, $ki = 5.2$ day^{-1}). Only the third approach adequately reproduced the observed temporal and spatial distribution of *E. coli*, including a 4 log 10 lateral removal distance of 9m. In saturated column experiments, carried out using aquifer sand from the field site, a combination of reversible and irreversible attachment was also required to reproduce the observed breakthrough curves and *E. coli* retention profiles within the laboratory columns. Applying the laboratory-measured kinetic parameters to the 2-D calibrated flow model of the field site underestimates the observed 4-log10 lateral removal distance by less than a factor of two. This is promising for predicting field scale transport from laboratory experiments.

A.2 Introduction

In rural areas throughout the world, aquifer filtration of pathogens and fecal bacteria has long been relied on to supply drinking water [Tufenkji *et al.*, 2002; Gupta *et al.*, 2009]. The practice has been called into question by growing evidence of widespread contamination of shallow sandy aquifers with fecal indicator bacteria (FIB) [Goss *et al.*, 1998; Leber *et al.*, 2011; van Geen *et al.*, 2011]. In developing countries, however, centralized water treatment or point-of-use disinfection of water from wells affected by infiltration of microbially contaminated surface water remains technically and economically unrealistic for the foreseeable future [Godfrey *et al.*, 2003; Gundry *et al.*, 2004]. In rural Bangladesh in particular, microbial contamination of shallow groundwater is of concern for tens of millions of households relying on shallow tubewells because of the combination of an extremely high population density and generally poor sanitation [Knappett *et al.*, 2011b; Escamilla *et al.*, 2013]. A recent analysis of household-level data collected over several years within the ICCDDR,B's (International Center for Diarrheal Disease Research, Bangladesh) study area of Matlab upazilla has shown that shallow aquifers that are vulnerable to mi-

crobial contamination are, indeed, associated with a significant increase in diarrheal disease in children under five [Wu *et al.*, 2011]. It is therefore particularly important in such settings to distinguish wells that are likely to be contaminated with microbial pathogens from those that are not.

Theoretical advances and a considerable number of laboratory and field experiments conducted in recent years have contributed to an improved understanding of pore-scale microbial removal processes [Ginn *et al.*, 2002; Bradford *et al.*, 2006b; Choi *et al.*, 2007] but some significant puzzles remain [Dong *et al.*, 2006]. For example, microbial removal efficiencies across distance (D^{-1}) observed in field experiments [Schijven *et al.*, 1999; Weiss *et al.*, 2005; Schijven and Simnek, 2002; Knappett *et al.*, 2012] are usually lower than measured with columns in the laboratory [Hijnen *et al.*, 2005; Feighery *et al.*, 2013]. This has tentatively been attributed to preferential flow paths in the field that are not reproduced within sediment columns [Taylor *et al.*, 2004]. Columns, moreover, are typically run under steady-state flow conditions whereas transient flow predominates in the field. Further, irreversible bacterial attachment is implicitly assumed to operate when up-scaling column results to field settings [Pang, 2008] and are frequently calculated directly from steady-state peak breakthrough concentrations (D1) rather than modeling the entire breakthrough curve with reversible attachment and detachment rates.We hypothesize that kinetic attachment and detachment rates (T^{-1}) may be less sensitive to scale of measurement than irreversible attachment alone and may therefore allow more accurate predictions.

The impact of transient flow on microbial transport resulting, for example, from pulses of recharge due to heavy monsoonal rains has also rarely been studied systematically at the field scale [Derx *et al.*, 2013]. This is important because microbial removal efficiencies (D^{-1} and T^{-1}) are sensitive to pore velocity and more bacteria may enter the saturated water table as the soil zone becomes more saturated. In the present study, we seek to understand the reason for the apparently more restricted movement of bacteria in column experiments relative to the field. Kinetic interaction

parameters modeled on laboratory column experiments packed with sand from the base of a freshly excavated pond in Bangladesh are compared with those obtained from modeling a previously documented breakthrough of *Escherichia coli* through the bottom of the pond following an induced rise in pond water level.

Previous studies reported on widespread fecal contamination in private tubewells in sandy villages and identified ponds dug recently into the unconfined aquifer as point sources of fecal contamination during the early monsoon [Knappett *et al.*, 2012]. The field component of the present study was previously reported and carried out in the village of Char Para in Araihazar upazilla where the local sandy aquifer extends to the surface and is therefore vulnerable to microbial contamination [Knappett *et al.*, 2011a]. The vulnerability of the shallow aquifer was locally intensified by artificially raising the water level in a recently excavated pond whose base was not protected by the fine-grained sediments that tend to accumulate on pond bottoms over time. Under these conditions, simulating a recharge pulse to the aquifer during monsoonal rains, *E. coli* penetration into the aquifer over the course of several days was documented along a transect of 6 previously installed piezometers radiating from the pond. Here, we combine an expanded *E. coli* time series, including 5 post-pulse sampling events, and a more detailed reconstruction of the pond water recharging the aquifer to reproduce observed *E. coli* concentrations and hydraulic heads using the 2-D finite element model HYDRUS 2D. We present new column experiments with sand from the base of the pond. From these, kinetic attachment/detachment rates are derived and substituted into the calibrated 2-D flow model to predict *E. coli* transport under transient flow conditions.

A.3 Setting

A.3.1 Pond infiltration field experiment

The Bangladeshi village of Char Para lies within Araihazar upazilla, 25 km east of Dhaka (see Fig. 1 in [Knappett *et al.*, 2012]). Pond 1 is a freshly excavated, sandy bottom pond located in the northeast corner of the village. A transect of five shallow monitoring wells 5.5 m deep, and one 8.5 m deep well were placed orthogonal to the edge of Pond 1 (Fig. A.1). The first well was placed 2.5 m from the edge of Pond 1 and they were spaced 1 m apart. The wells had a screened interval length of 1.5 m. The construction details of these wells are described in [Knappett *et al.*, 2012]. Throughout this paper, the wells are named in the following way. Transects and the wells within them are labeled according to $\Delta x, y, \delta$, where Δ is either T or W, referring to the transect or well, respectively, x and y numerically reference the pond (1-4) and the transect adjacent to pond x (1-3), respectively, and d is a letter referring to a well in transect y ((a)-(e) for shallow wells, and z for the single deeper well) (Fig. A.1).

Of the four ponds studied in detail in [Knappett *et al.*, 2012] only the bottom of Pond 1 was not lined with silt, and consequently was the only pond where an increase in *E. coli* concentrations in adjacent observation wells were measured in response to artificial filling and subsequent rainfall. Pond 1 penetrates a local 1.5 m thick silt layer and terminates in a medium sand aquifer used for drinking water. Neighboring Pond 3, used to artificially fill Pond 1, is a shallower pond that does not penetrate the local silt layer and receives effluent from surrounding latrines.

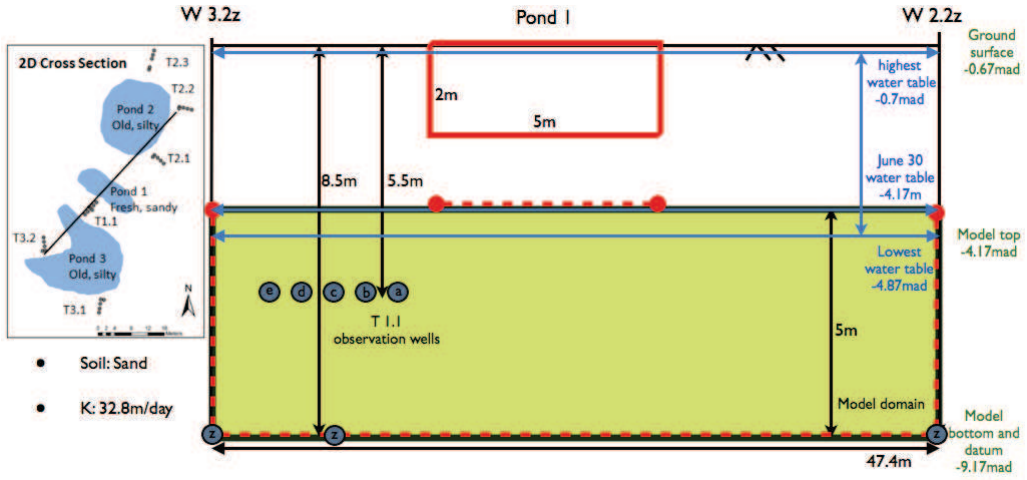

Figure A.1: 2-D model set up with boundary conditions. All elevations are relative to an established Site K datum22. Blue lines indicate minimum and maximum observed limit of local water table during the years 2007-2009. The solid red line demarcates the dimensions of Pond 1 and the dashed red lines indicates the permeable boundaries of the model. The shaded yellow area shows the modeled region within the saturated aquifer. Model boundaries are indicated by red dashed lines. The bottom of wells 3.2z (W3.2z) and 2.2z (W2.2z) are located at the southwestern (left) and northeastern (right) varying head boundaries, respectively. Head observations from well 1.1z (W1.1z) defined the lower varying head boundary. Elevations of the different surfaces are listed in small print and are relative to a local datum (meters above datum).

A.4 Methods

A.4.1 Pond infiltration field experiment

This study focuses on five days between July 1 and 6 in 2009 referred to herein as the experimental period [Knappett *et al.*, 2012]. During this time, hydraulic head (Fig. A.2) and *E. coli* concentrations (Fig. A.3) were monitored at least once every two days in adjacent observation wells. The base of Pond 1 was perched approximately 1.5 m above the local saturated water table on June 30 before the artificial filling with contaminated latrine water began (Fig. A.2). There were three major inputs of water through the base of Pond 1. The first, and largest, of these pulses was caused by the artificial filling of Pond 1 with contaminated latrine pond water from neighboring Pond 3. The second pulse resulted from several natural rainfall events spaced closely together over 24 h, and the third resulted from a single rainfall event.

The chemistry of the water in Pond 1 and that in the adjacent shallow transect wells were very similar (Fig. S2 in [Knappett *et al.*, 2012]). Specific conductance was typically low and similar in ponds and their adjacent shallow transect wells during the wet season (¡400 μS/ cm). Specific conductance in shallow transect wells tends to increase during the end of the dry season (1,000 μ S/cm), whereas ponds tend to remain low year round.

The level of the water in Pond 1 was not measured immediately after all rainfall events, however the level of Pond 4,200 m south of Pond 1 (Fig. 1 in [Knappett *et al.*, 2012]), was measured every 20 min using a pressure transducer (Model 3001 Levelogger Edge, Solinst Canada Ltd., Georgetown, Ontario, Canada) during this period and was used to determine the timing and relative magnitude of rainfall events. In Bangladesh hourly precipitation amounts during the monsoon often vary over short distances [Shahid, 2010]. Therefore, daily rainfall measured in Dhaka (Bangladesh Meteorological Department, www.bmd.gov), 25 km to the west, was used to only to confirm the occurrence of rainfall on the days indicated by the transducer in Pond 4

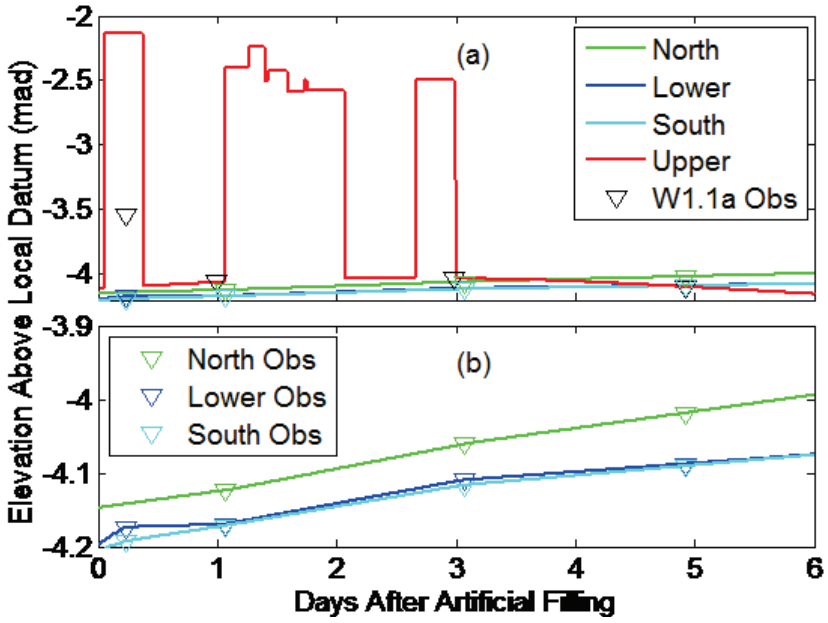

Figure A.2: Hydraulic head boundary conditions input into the 2-D Hydrus model. (a) The upper boundary was simulated by combining a record of rainfall events at Site K and a record of observations on Pond 1 levels. Head loss across the 1.5 m space between the base of the pond and the top of the model was calculated using Darcy's Law. Black grad symbols represent observed water table level in W1.1a. (b) Expanded view of the slowly varying head boundaries and the observations from which they were calculated.

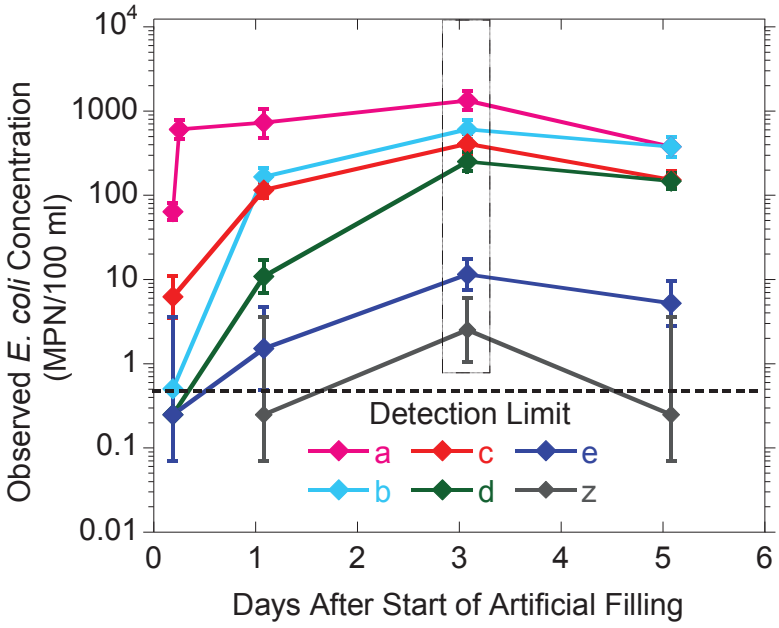

Figure A.3: Observed *E. coli* concentrations in transect 1.1 wells following artificial pond filling on July 1, 2009. Prior to artificial filling of Pond 1, <20 MPN/100 ml *E. coli* was found in W1.1a, and was at or below detection limit in all the other wells. At any point *E. coli* was only detected at very low concentrations once in the 8.5 m deep well (W1.1z). The error bars represent 95% confidence intervals and the horizontal dashed line represents the detection limit of 0.5 MPN/100 ml based on duplicate 100 ml water samples37. The data in the box on day 3 has been published previously in [Knappett et al. (2012)] and was used to extrapolate the source concentration within the saturated aquifer (Fig. A.6).

within Char Para.

The porosity and bulk density of the aquifer were measured to be 0.4 (-) and 1500 (kg/m^3), respectively, using the water displacement method outlined in [Brush *et al.*, 1999]. Longitudinal and transverse dispersivities were estimated from to be 0.5 and 0.1 m, respectively based on broad scale-dependent dispersitivities presented in [Gelhar *et al.*, 1992]. Continuous 1.5 cm diameter direct push cores were taken in the middle of T1.1 at 0.3 m intervals from 3 to 5.5 m below ground surface to log the lithology in detail. With the exception of four ¡1 cm thick silt layers, the aquifer is homogeneous with respect to grain size distribution [Knappett *et al.*, 2012]. Excluding the silt layers, the average values of d_{10}, d_{50} and d_{60}, determined by log-linear interpolation with standard deviations in parentheses are 0.13 ($\pm$0.03), 0.33 ($\pm$0.01) and 0.36 ($\pm$0.01) mm, respectively, corresponding to a uniformity coefficient (d_{60}/d_{10}) of 2.8. The terms d_{10}, d_{50} and d_{60} refer to the grain sizes for which 10%, 50% and 60% of the sample was finer by mass, respectively. Grain size distributions were also measured on sand taken from the base of Pond 1 for the laboratory column experiments, and matched the cored sand to within the error tolerance. Based on visual inspection the sand was determined to be sub-angular to sub-rounded in texture. No silt was observed in the sand taken from the base of Pond 1. The horizontal hydraulic conductivity (K_h) was assumed to be the middle of the narrow range (26.8 38.9 m/day) of hydraulic conductivities determined by triplicate slug tests in the 6 wells in T1.1 (Supplementary Table 2 in [Knappett *et al.*, 2012]).

A.4.2 2-D modeling of field experiment

A.4.2.1 Governing transport equations

Hydrus 2D-lite version 2.01.1080 [Šimnek and van Genuchten, 2008] was used to model the transient flow and transport conditions in the saturated aquifer below Pond 1. The model solves Richard's equation for water flow and uses the Fickian-based advection-dispersion model for contaminant transport in saturated porous media us-

ing a finite element grid with 7,378 nodes. The model can fit both kinetic irreversible and reversible attachment parameters. The governing equations for bacterial transport in one dimension with both irreversible and reversible attachment are [Schijven and Simnek, 2002]:

$$\frac{\partial c}{\partial t} + \frac{\rho_b}{\theta}\frac{\partial s_r}{\partial t} + \frac{\rho_b}{\theta}\frac{\partial s_i}{\partial t} = D\frac{\partial^2 c}{\partial z^2} - v\frac{\partial c}{\partial z} - \mu c \tag{A.1}$$

$$\frac{\rho_b}{\theta}\frac{\partial s_r}{\partial t} = k_a c - \frac{\rho_b}{\theta}k_d s_r - \mu s_r \tag{A.2}$$

$$\frac{\rho_b}{\theta}\frac{\partial s_i}{\partial t} = k_i c - \mu s_i \tag{A.3}$$

where c is the concentration of bacteria in free suspension (cells/L^3), θ is the effective porosity (-), v is the advective velocity of the water (L/T), D is the hydrodynamic dispersion coefficient (L^2/T) which is equal to λv where λ is the dispersivity (L), z is the distance along the flow path (L), ρ_b is the dry bulk density of the porous media (M/L^3), s_r is the concentration of bacteria at reversible sites (cells/M), and s_i is the concentration of bacteria at irreversible sites (cells/M). k_a is the forward attachment rate at reversible sites (T^{-1}), k_d is the reverse detachment rate at reversible sites (T^{-1}), and k_i is the irreversible forward attachment rate (T^{-1}). μ is the first-order inactivation rate of bacteria (T^{-1}). This model assumes there are two different attachment modes (reversible and irreversible) taking place at constant rates simultaneously throughout the saturated sand. A more complex model than this is employed in this study, which assumes one population of bacteria interacting as the first model describes, and a second equal-sized population attaching at a unique irreversible attachment rate (Eqs. (S1) (S4)).

A.4.2.2 Hydraulic head modeling

The upper boundary of the 2-D model is located directly below Pond 1. Steep hydraulic gradients observed in the adjacent T1.1 wells (Fig. A.2) located 2.5 m laterally

from the edge of Pond 1 (Fig. A.1) led to the assumption that the filling of the pond created a temporary groundwater mound resulting in a saturated flow path between the pond and the local water table. Hydraulic head for the upper model boundary was simulated using the available observations on the water level in Pond 1, rainfall events recorded in Pond 4, and hydraulic head measurements made in T1.1 (Fig. A.2). Peak water levels in Pond 1 are calibrated to synoptic peak water levels in Pond 4 following two different rainfall events. Three "off-peak" (when Pond 1 had no water in it) dry pond observation time points are used to constrain the drainage time of Pond 1, found to be approximately 8 h. Off-peak groundwater levels were measured on 3 occasions by manual hydraulic head measurements in T1.1 monitoring wells. The pond surface is assumed to represent the pressure head of the upper boundary subtracting head loss across the 1.5m of sediment between the bottom of the pond and the top of the model. This head loss is calculated using Darcy's Law assuming a Darcy flux of 1.86 m/day; consistent with the disappearance of 0.62 m of standing water in Pond 1 in approximately 8 h.

Slowly varying, specified hydraulic head boundaries are imposed along the northeast, southwest and bottom of the model and heads at these boundaries are set to the observed heads in wells W2.2z, W3.2z and W1.1z, respectively (Fig. A.1). The model domain is 47.4 m long and 5 m thick. It extends from a depth of 8.5 m below the local ground surface along T1.1, coinciding with the bottom of W1.1z, to 3.5 m below ground surface, coinciding with the saturated water table at the start of the experimental period (Fig. A.1). The base of Pond 1 is approximately 2 m below the local ground surface.

A.4.2.3 Bacterial transport modeling

Pond water *E. coli* concentrations ranged from 100,000 to 200,000 MPN/100 ml. Pond water *E. coli* concentrations were substantially higher than observed in the aquifer and the spatial concentration trends in the saturated aquifer indicated *E. coli*

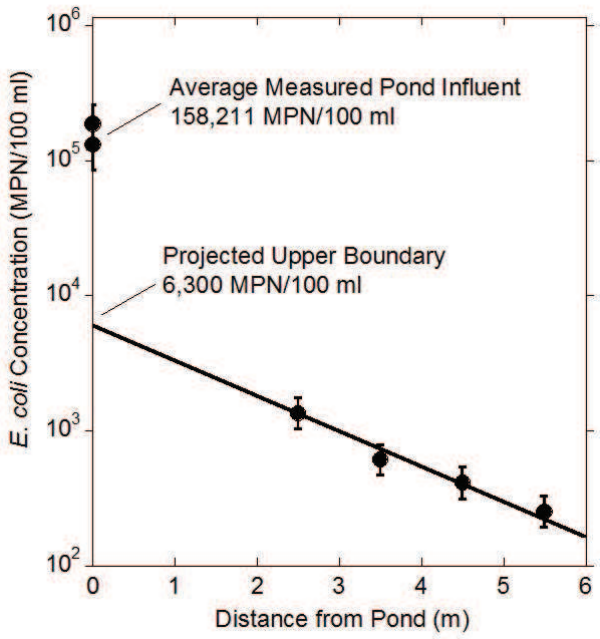

Figure A.4: Estimation of *E. coli* input concentration at upper model boundary 1.5 m below the base of Pond 1. Concentrations at distances > 0 m were measured in shallow transect 1.1 wells on day three after artificial filling of Pond 1, when the plume had reached the outer well. Error bars represent 95% confidence intervals

concentrations were substantially reduced across the 1.5 m of vertical flow between the base of Pond 1 and the upper boundary of the model. The log-linear relationship between *E. coli* concentration and lateral distance from the edge of Pond 1 in the saturated aquifer on day 3 of the experimental period (Fig. 4(a) in [Weiss *et al.*, 2005]) was used to determine the influent *E. coli* concentration at the model's upper boundary of 6300MPN/100 ml (Fig. A.4). Day 3 after artificial filling was chosen since it represents the first observed time that the *E. coli* plume penetrated the entire T1.1 (Fig. A.3).

A.4.3 Column experiments

A.4.3.1 Experimental measurements

Four replicate column experiments were conducted to compare laboratory modeled attachment/detachment rates to those modeled at the 2-D field-scale. The column experiment methodology exactly followed that in [Feighery *et al.*, 2013] for unwashed sands with one modification. *E. coli* ATCC strain 700891, which is resistant to Streptomycin and Ampicillin, was used in the present study, whereas [Feighery *et al.*, 2013] used ATCC strain 700609, a nalidixic acid resistant strain of *E. coli*.

Plastic columns 10-cm long with an inner diameter of 1.7 cm were dry packed with sand taken from the base of Pond 1 (see Section 3.1). All four columns were packed with sand from the same homogenized 2 kg bag of sand from the base of Pond 1. After slowly saturating the sand by upward flow, *E. coli* was injected in the top of the column at a concentration of approximately 300,000 MPN/100 ml, to ensure that effluent concentrations would be well above detection limit, and a volumetric flow rate of 0.5 ml/min using a multi-channel peristaltic pump (Gilson MiniPuls, Middleton, WI). A fraction collector (LKB-Bromma, Sweden) was used to collect samples in 15 ml polypropylene tubes (Fischer Scientific, Pittsburg, PA). This volumetric flow rate resulted in an advective velocity of approximately 8 m/day. An artificial groundwater solution (AGW) containing 3.5 mM KCl was used throughout the entire experiment. Each column was flushed for approximately 15 pore volumes with AGW while effluent pH and specific conductivity was monitored to ensure stabilization. Without stopping the pump, the influent water was switched over to contaminated groundwater solution containing *E. coli* and 20 mg/L KBr (0.17 mM) and appropriately adjusted KCl concentration to maintain the same ionic strength as the AGW. The contaminated water was run for 10 pore volumes before switching back to pristine AGW for 30 pore volumes. Within 8 h of sampling, *E. coli* was analyzed by diluting samples in 100 ml sterile bottles and adding Colilert^{TM} reagent (IDEXX, Westbrook, ME).

The 100 ml bottles were poured into a Quanti-Tray 2000^{TM} and incubated for 24 h after which the compartments fluorescing under a UV light were enumerated and the number converted to a Most Probable Number (MPN) of cultured *E. coli* [Hurley and Roscoe, 1983].

To determine the attached *E. coli* profile, the two columns used for the last two experiments were sectioned into 8 equal lengths with a flame-sterilized knife immediately upon completion of the experiments. *E. coli* was extracted from the sand initially by vortexing for 5 s in 20 ml of sterile deionized water in 50 ml polypropylene tubes (Fischer Scientific, Pittsburg, PA). The tubes were then placed on an orbital shaker at 37 C for 30 min. After this 5 ll were transferred via pipette from the 50 ml tubes to a 100 ml sterile Colilert bottle and processed exactly as the effluent samples. The sediment remaining in each 50 ml tube was dried at 80 C overnight and weighed to obtain the bulk density of the packed sand at each interval (g/ml).

The inactivation rate of the laboratory-grown *E. coli* at room temperature was determined in [Feighery *et al.*, 2013] to be 0.067 ln/day. This is comparable to a study that measured *E. coli* inactivation of 0.15 ln/day at 20 C [Foppen *et al.*, 2008] and that reported in a review paper by [Foppen and Schijven, 2006] of 0.5 ln/day with a range of 0.1 to 1.0 ln/day. In slightly warmer groundwater in Bangladesh (26 C), multi-day measurements made on *E. coli* concentrations in shallow wells adjacent to Ponds 1 and 2 during stagnant flow periods when no new *E. coli* was introduced to the well suggest a inactivation rate of 0.11 ln/day. Thus inactivation rates of 0.067 and 0.11 ln/day were assumed for the 1-D column and 2-D field model, respectively. These inactivation rates are so low that removing inactivation from the 2-D model has negligible impact on the modeled kinetic interaction parameters.

A.4.3.2 1-D modeling of column experiments

Modeling of the Br breakthrough curve was performed with CXTFIT [Toride *et al.*, 1995; Tang *et al.*, 2010] a 1-D numerical advection-dispersion model, to determine the

porosity and dispersivity of the packed sand. *E. coli* kinetic interaction parameters were determined by inversion using a 1-D Finite Element flow and transport model programmed in Matlab operating on the same governing equations as the 2-D model (Eqs. A.1 A.3). The 1-D model was run at a constant 8 m/day advective flow velocity, which corresponds to peak advection in the saturated aquifer indicated by the 2-D flow model underlying Pond 1 during peak filling events.

The *E. coli* concentration retained in the sand was normalized according to the equation (Eq. A.4):

$$\frac{s}{C_0} = \frac{\frac{\rho_b}{\theta}\frac{\#C_s}{m_s}}{C_0} \tag{A.4}$$

where ρ_b is the bulk density of the dry sand (g/cm^3), θ is porosity (-), $\#C_s$ is the cells extracted per gram of dry sand in each segment (cells/g), m_s is dry mass of the sand in the each segment (g), and C_0 (cells/cm3) is the influent concentration during the pulse phase. This method of normalizing retained cell densities is useful since it represents multiples of the injected concentration found in the pore space volume of each segment [Feighery *et al.*, 2013; Basha and Culligan, 2010].

A.5 Results

A.5.1 Observations

A.5.1.1 *E. coli* time series in the field

Concentrations of *E. coli* in all but two of the monitoring wells were at or below the detection limit of 0.5 MPN/100 ml on the day before the level of Pond 1 was artificially raised (Fig. A.3). In the well closest to the pond (W1.1a), the concentration of *E. coli* measured in duplicate samples was 60 MPN/100 ml. Within a day of filling Pond 1, *E. coli* increased to greater than two orders of magnitude above detection limit in the 3 monitoring wells closest to the pond. In the single monitoring well at 8.5 m

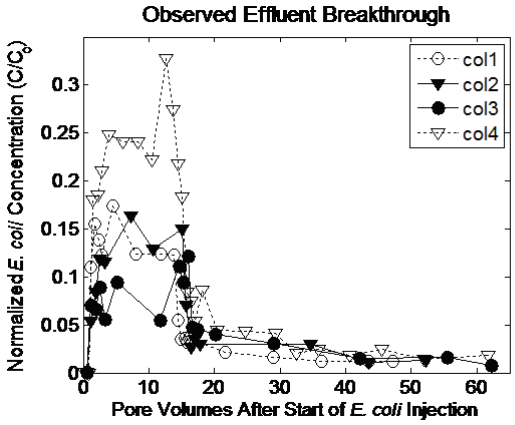

Figure A.5: Observed effluent breakthrough curves from four replicate column experiments. Retention curves were only available for columns 3 and 4, which represent the lowest and highest peak breakthrough concentrations among the four replicates.

depth, *E. coli* was detected only once, on day three, and barely detectable on that single occasion (2 MPN/100 ml).

A.5.1.2 *E. coli* breakthrough in columns

The plateau in effluent *E. coli* concentrations reached during column experiments corresponds to only 10 to 25% of the influent concentrations which ranged from 1.7 3.7×10^5 MPN/100 ml for the 4 replicate columns (Fig. A.5). After switching the influent back to AGW, effluent concentrations of *E. coli* remained detectable for an additional 40 pore volumes of flushing. Retained concentrations of *E. coli* decreased within the first few cm but remained detectable through the length of the two columns. Summing total *E. coli* measured in the effluent with total retained *E. coli* on the sand corresponds to 60 70% of the total *E. coli* injected into the column.

A.5.2 Modeling

A.5.2.1 Hydraulic forcing in the field

Observed hydraulic heads were used to constrain the hydraulic anisotropy K_h/K_v in the 2-D flow model, where K_v is vertical hydraulic conductivity. With the boundary conditions set (see above), hydraulic anisotropy is determined by manually minimizing the root mean squared error (RMSE) between the modeled and observed heads by entering anisotropies between 1 and 20 into the numerical model. Four sets of hydraulic head observations were available immediately after filling (day 0) and on days 1, 2, and 5 of the experimental period, but only one of these events represent peak filling conditions (Fig. A.2(a)). Hydraulic heads from this event had the greatest influence on determining the best fit for aquifer anisotropy. The best fit between observed and modeled hydraulic heads was found with an anisotropy of 4. This was insensitive to varying K_h across the measured range in the six monitoring wells of T1.1 (Table A.1).

A.5.2.2 E. coli transport in the field

A total of 21 observations (4 sampling events in five wells plus an additional sampling event for well 1.1a) constrain the interactions of *E. coli* with aquifer sands. All three models (Irreversible, Reversible and Two Attachment Mode) can reproduce the rapid increase in *E. coli* soon after the filling of Pond 1. Irreversible attachment only, however, predicts a sharp drop-off in *E. coli* towards the end of the experimental period that was not observed (RMSE = 1,158 MPN/100 ml) (Fig. A.6(a)). Reversible attachment only does not generate the full range of *E. coli* concentrations maintained throughout the experimental period along the length of the transect (RMSE = 826 MPN/100 ml) (Fig. A.6(b)). Applying both irreversible and irreversible attachment to an arbitrary equal division of sites reduces the RMSE in *E. coli* by almost an order of magnitude lower to 99 MPN/100 ml (Fig. A.6(c)). The RMSE value is stable

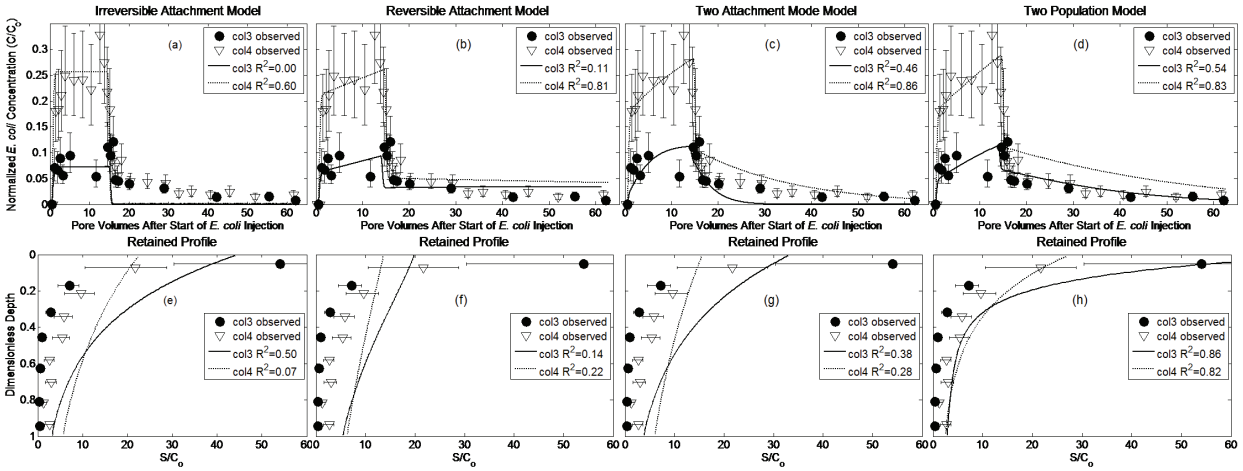

Figure A.6: Modeled effluent breakthrough curves (a-d) and retained profiles (e-h) of *E. coli* in saturated 10 cm duplicate columns of packed sand taken from the base of Pond 1. Solid and dashed lines represent results of 1-D inversion modeling which put equal weight on the effluent breakthrough and retained concentration profile. Error bars represent 95% confidence intervals

across a broad range of parameter values and the minimum is maintained as long as the k_a/k_d ratio remains close to 8 (Table A.2).

The anisotropy calibrated to hydraulic heads is consistent with the modeled *E. coli* concentrations in the transect wells (Table A.1). For example, the 2-D model shows that *E. coli* would have been detected in abundance on day three of the field experiment with a hydraulic anisotropy of 1 and would have never been detected for an anisotropy of 10 (Fig. A.8(a)).

The distribution of hydraulic heads that constrained anisotropy did not constrain Kh (Table A.1). Triplicate slug tests, however, on each of the six transect wells measured a narrow range of Kh from 26.8 to 38.9 m/d representing approximately ±20% difference of advective velocity using Darcy's Law. The midpoint of this range was assigned to the entire modeled aquifer.

A.5.2.3 E. coli transport in the columns

Column experiments 3 and 4 (Fig. A.5) span the full range of steady-state breakthrough concentrations of *E. coli* measured in all four laboratory experiments. Two types of models were used to describe the movement of water and *E. coli* through repacked sand columns. Bromide breakthrough was modeled with CXTFIT to obtain a dispersivity and advective velocity of 0.003 m and 8 m/day, respectively. These conditions represent a Peclet number of 0.11. A 1-D 101 node finite difference transport model was developed using Crank-Nicholson and central difference weighting to obtain kinetic interaction terms between *E. coli* and the sand. Similar to the field modeling, the observations were fitted to four different models of interaction between *E. coli* and aquifer sands. Irreversible attachment only cannot reproduce the measured *E. coli* concentrations up to 40 pore volumes after the effluent has been switched back to AGW only (Fig. A.7(a)). Reversible attachment only, on the other hand, does not reproduce the observed build-up of *E. coli* in the near the column inlet. As in the field, the combination of irreversible and reversible attachment provides a better fit to the observations than single attachment mode models (Fig. A.7(c) and (g)), however even this model was unable to reproduce the very high deposition rates near the column inlet. The model that fit the data best assumed an equal proportion of two populations of *E. coli*, one that attached irreversibly and one that attached both irreversibly and reversibly (Fig. A.7(d) and (h)). Model fits tend to overestimate *E. coli* concentrations since the experimental recovery in each column was lower than that expected based on the mass balance calculations which included the very low measured inactivation rates in the influent reservoir.

The kinetic attachment/detachment rates for the two population models from columns 3 and 4 were applied to the calibrated 2-D flow model to obtain expected transport distances in the saturated aquifer underneath Pond 1. The predicted 4-log10 removal distance for *E. coli* in the saturated water table directly below Pond 1, was 3.5 m for rates obtained from column 3 and 6.9 m for column 4 rates (Fig.

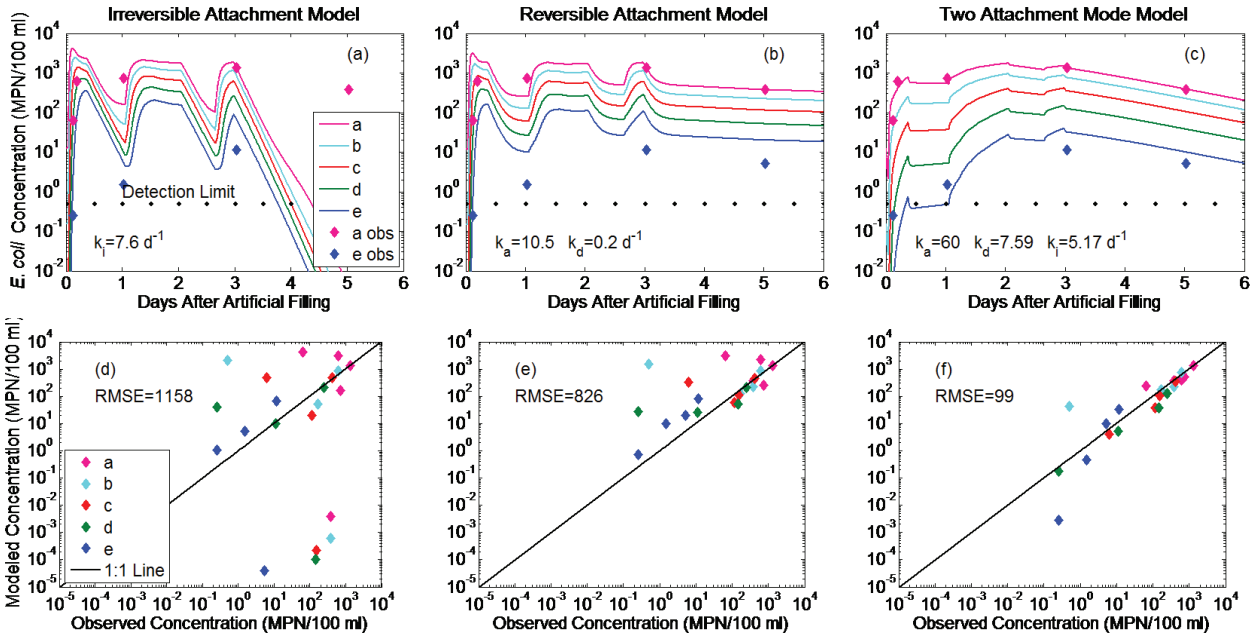

Figure A.7: Modeled breakthrough of *E. coli* in transect 1.1 shallow wells during the experimental period (a-c). Input concentration at the upper boundary of the model was 6,300 MPN/100 ml. Observed concentrations in the closest (W1.1a) and furthest (W1.1e) wells from Pond 1 are displayed for comparison (a-c). The lower three panels represent observed versus predicted *E. coli* concentrations for each of the three model types with the root mean squared error (RMSE) (d-f).

A.8(b)).

A.6 Discussion

A.6.1 Influence of hydraulic anisotropy on spatial extent of *E. coli* movement

Hydraulic anisotropy controls the relative proportion of horizontal to vertical groundwater flow. This aquifer property is not always measured during field transport studies, and thus may have gone unnoticed in its potential influence on field-scale bacterial transport. Modest changes in hydraulic anisotropy within the calibrated 2-D model strongly influence the depth of *E. coli* penetration into the aquifer. The sensitivity analysis indicated that if the aquifer was isotropic the deeper well (W1.1z) would have contained abundant *E. coli* (Fig. A.8(a)). Anisotropy restricts this vertical movement into the aquifer. In the present 2-D numerical model, hydraulic anisotropy influences the flow paths along which bacteria are advected but assumes the aquifer is homogeneous with respect to grain size distribution. Thus kinetic parameters are spatially uniform. In this floodplain aquifer, however, thin silt layers were present and bacterial attachment rates (T1) in fine material is much higher than in medium sand. The saturated aquifer underlying Pond 1 has few silt layers and the medium sand is homogeneous across the cored depth in the middle of the adjacent transect. Approximately 20 m northeast of T1.1, however, transect 2.1 contained numerous 1 2cm thick, and one 20 cm thick, silt layer indicating a higher local hydraulic anisotropy (Fig. 2(b) in [Knappett *et al.*, 2012]). This may explain why, in our previous study, the deeper well in transect 2.1 (W2.1z) was found to contain little FIB DNA, whereas the deeper well in T1.1 (W1.1z), less protected by silt layers, contained abundant FIB DNA [Knappett *et al.*, 2012].

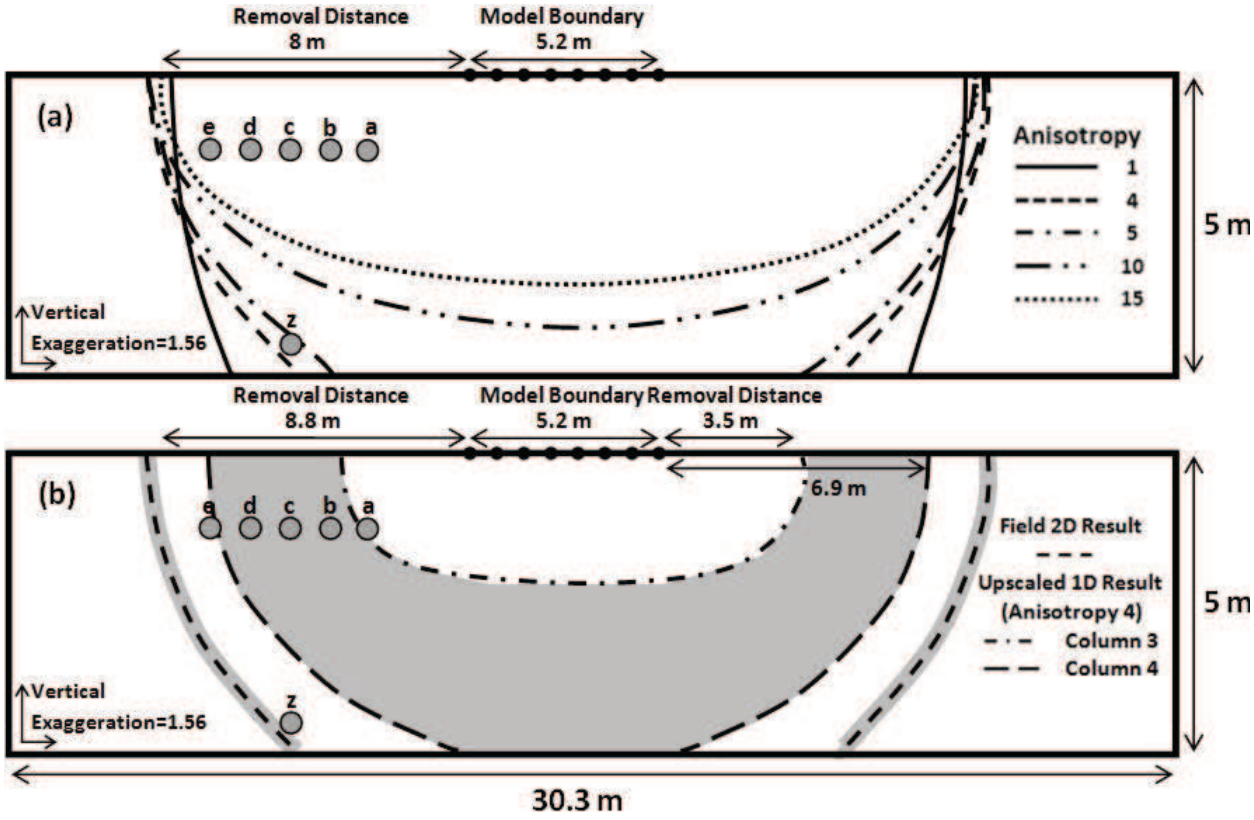

Figure A.8: Modeled and predicted *E. coli* 4-log10 removal distance representing the maximum transport distance on day 3 after the start of artificial pond filling. (a) As a function of hydraulic anisotropy. The long-dashed line represents the fitted 4-log10 *E. coli* removal distance based on the optimal anisotropy of 4. The other lines show the predicted 4-log10 removal distances for different hydraulic anisotropies. (b) Comparison of 4-log10 *E. coli* removal distances between 2-D model fitted to *E. coli* concentrations from the field and predictions made from substituting kinetic attachment/detachment rates derived from 1-D column experiments into the calibrated 2-D flow model. The shaded areas represent the estimated uncertainty in each method. The uncertainty band for the 2-D model was obtained by substituting the range of possible values of k_a , k_d and k_i into the model (Table A.1).

A.6.2 Importance of irreversible and reversible attachment

Microbial attachment modes operating at the column scale impact the observed transport distances at the field scale. In contrast to classic colloid filtration theory [Yao *et al.*, 1971; Logan *et al.*, 1995] irreversible attachment alone is not able to reproduce the spatial-temporal distribution of *E. coli* in the field characterized by its delayed arrival at the wells more distal to Pond 1 (Fig. A.6(a)). Reversible attachment alone was also inadequate (Fig. A.6(b)). The observed concentration convergence in the five shallow monitoring wells, indicative of a slowly arriving plume over 3 days (Fig. A.2), can only be reproduced by the model that assumes both reversible and irreversible modes of attachment.

Attachment and detachment rates vary dynamically with pore velocity [Hendry *et al.*, 1999; Tong and Johnson, 2006]. In the present 2-D model, however, these rates are assumed to be static. This limits the ability of the simpler, single attachment mode models to predict *E. coli* transport under transient flow conditions. The sharp decrease in modeled *E. coli* concentration after the end of each hydraulic input pulse in single attachment mode reversible and irreversible attachment models (Fig. A.6(a) and (b)) is the result of fixed rates. In the more complex two attachment mode model, the high detachment rate (11.4 d^{-1}) maintains elevated *E. coli* concentrations in the aquifer independent of flow velocity. Classic colloid filtration theory, valid for uniform-sized particles traveling through uniform-size spherical beads, predicts a positive linear relationship between k_i and pore velocity [Yao *et al.*, 1971; Logan *et al.*, 1995]. This relationship is qualitatively the same in natural heterogeneously-sized sand since empirical researchers find a linear relationship between k_a, k_d, k_i and pore velocity. This means that when pore velocity stagnates, k_a, k_d, and k_i, decrease and pore concentrations would remain more stable than in the single attachment mode models presented here. These simpler models would perform better if Hydrus 2-D allowed attachment and detachment rates to vary with pore velocity.

Detachment has been demonstrated at the laboratory column [Logan *et al.*, 1995;

Fontes *et al.*, 1991] (Fig. A.7) scale, and at the field scale [Zhang *et al.*, 2001] by extended tailing after a bacterial plume has passed. Temporary attachment has been attributed to particles attracted to like-charged grain surfaces in the secondary energy minimum [Hahn *et al.*, 2004]. Empirical evidence and theory shows that under repulsive bacteria-grain conditions, typical in nature, temporary attachment may in fact be a slow rolling of the bacteria along the surface until they either detach back into the flow stream or come to rest in flow stagnation zones downstream of a sand grain [Johnson *et al.*, 2007a]. Although it is typically studied at the pore and column scale, the present study shows that detachment cannot be ignored at the field scale.

Pore velocity did not only vary transiently in the 2-D model, it also varied spatially during filling events, from 8 m/d near the upper model boundary to ¡0.1 m/d at the outer model boundaries (data not shown). Modeled pore velocities are linearly dependent on Kh, which ranges ±20% from the midpoint, however this uncertainty in K_h has a minor impact on model fit (Table A.1). Substituting the lower and upper extremes of measured K_h while keeping kinetic parameters derived for the midpoint Kh constant caused RSME to increase by 59 and 33%, respectively.

There was uncertainty in longitudinal dispersivity in the 2-D model (λ), since published values range from 0.1 to 2.5 m for studies at the 10 m scale. Varying λ across this range while keeping kinetic parameters derived for $\lambda = 0.5m$ constant caused RMSE to increase by 73% and 46%, respectively. This indicates that the model is similarly sensitive to λ and K_h. If these were permitted to vary with the kinetic parameters in the 2-D model, it is likely the fits of the field measured *E. coli* concentrations would have improved, but not enough to negate the need for all three kinetic parameters, since the RSME for the three parameter (two attachment mode) model was an order of magnitude better than the reversible attachment model (Fig. A.6).

A.6.3 Potential confounding factors comparing columns to aquifers

The differences in attachment rates between columns and aquifers could be partly due to differences in bacterial metabolic state, background water chemistry, and geochemistry of the sand. The water recharging through the base of Pond 1 contained potentially older *E. coli*i that may have lost some of its surface coatings that enhance adsorption. [Hijnen *et al.*, 2005] reported greater transport of indigenous thermotolerant coliforms in river water flowing through saturated columns packed with gravel than *E. coli* grown in the laboratory. In the present study, freshly grown *E. coli* was injected into the column, possibly leading to higher attachment rates and under prediction of field transport. Dissolved organic matter has been shown to enhance bacterial transport, in some cases coating positively charged metal oxides which attract the negatively charged bacteria [Ryan *et al.*, 1999; Hall *et al.*, 2005], but this depends on the type of organic matter. Ponds in Bangladesh contain substantial DOC [Neumann *et al.*, 2009] and water recharging through Pond 1 had a low reduction potential (Eh) (data not shown) and its dark brown color and high *E. coli* concentrations were the product of human and animal organic waste. In contrast, no organic matter was co-injected into the columns with *E. coli*. Lastly, the sand taken from the base of Pond 1 for columns appeared oxidized being light brown in color and the transition to grey sand occurred at 2.5 m below the base of the pond, near the level of the lowest water table level during the time period September 2008 December 2009. The higher irreversible attachment rate modeled on the column data may have been due to the presence of more positively charged metal oxides in the sand from the base of Pond 1 [Abudalo *et al.*, 2005].

A.6.4 Scaling microbial transport with kinetic interaction parameters

At the column scale, *E. coli* effluent breakthrough and retention curves can be modeled with simple or more complex numerical models (Table A.3). For the two attachment mode, single population model, reversible attachment rates are similar to that modeled on field data, but irreversible attachment rates are an order of magnitude higher in the columns (Table A.3). When the kinetic parameters derived from the two population models are substituted into the calibrated 2-D model, the predicted spatial extent of the *E. coli* plume is shorter than observed in the field (Fig. A.8(b)). The rates from columns 3 and 4 predict that 4-log10 removal would occur after 3.5 and 6.9 m, respectively. Clearly, variability between small columns can result in large differences in predicted transport distances in the field (Fig. A.8(b)). But in each column the best model, assessed by goodness of fit to the column breakthrough and retention curves (Two Population Model), most accurately predicted field scale transport (Table A.3). Therefore, quantification of attachment and detachment mechanisms, in 10 cm column experiments, are required to predict the movement of *E. coli* into the aquifer.

Researchers tend to apply overly simplistic models when upscaling column experiments to the field scale. Often only irreversible attachment is accounted for in keeping with classic colloid filtration theory. The assumption of irreversible attachment operating in the context of steady-state flow biases predicted field transport distances. As a result column experiments are perceived to vastly over predict removal rates in sand aquifers, although the degree to which they over predict removal has rarely been quantified even with simple models. Where this has been quantified assuming irreversible attachment only, columns over predict removal by one or more orders of magnitude. Our findings contrast with this general perception exemplified by Table 1 in [Pang, 2008]. Removal efficiency can be described spatially (D1) or kinetically (T1). But a simple translation between the two can only be performed when steady-

state flow conditions are assumed. In the present study, if the column data is modeled based on the peak breakthrough concentration assuming irreversible attachment and steady-state flow, as in [Pang, 2008] the predicted 4-log10 removal distances are less than 1 m (Table A.3). When those same irreversible attachment rates were applied to the 2-D transient flow model 4-log10 removal distances were higher, partly due to high modeled pore velocities close to the base of Pond 1 (Table A.3).

The inclusion of reversible and irreversible attachment in the up-scaled 2-D model produced much more realistic transport distances. The model that was complex enough to accurately describe transport and retention in columns also made reasonable predictions at the field scale (Table A.3). Even amongst 1-D models presented here that include reversible attachment, the goodness of fit and the predicted transport distances vary (Table A.3). The only model that is able to adequately describe both column breakthrough concentrations and retention profile, however, is the two population model (Fig. A.4(h)). This model assumes that there are two populations of *E. coli* present, differing in their attachment characteristics [Foppen *et al.*, 2007]. These underlying mechanisms result in transport that cannot be accounted for by a simple first-order removal process, neither can their impact at the field scale be predicted by a spatial removal rate from snap-shots in time at the column scale [Pang, 2008].

A.6.5 Predicting field-scale transport from ex situ measurements

Differences in filtration rates in the vertical and lateral directions, in the presence of fine layers, are expected to be substantial. [Feighery *et al.*, 2013] demonstrated substantially higher kinetic removal rates for *E. coli* flowing through intact vertical cores, with the horizontal silt layers preserved, than in columns packed with homogenized sediment from the same site. The utility of column experiments in making predictions at the field scale could therefore be improved if fine layers were explicitly

rendered in the field-scale model to account for the impact of both spatially varying flow field and filtration rates.

Transient flow conditions are typical in aquifers under the influence of surface water. In the present study, column experiments were run at constant high advective velocity (8 m/day). This velocity was derived from the simulated peak advective velocity in the 2-D calibrated flow model on the saturated aquifer immediately below the upper boundary when Pond 1 was full, and is not representative of the modeled aquifer. Much lower peak velocities predominated through most of the 2-D model domain, even when Pond 1 was full. This may be why higher kinetic attachment rates were modeled on columns than on the aquifer. In future experiments, therefore parallel column experiments should be conducted across the range of those velocities encountered at the field site and these empirical relationships should be incorporated into the predictive field scale model.

A.7 Conclusions

Reproducing the movement of *E. coli* in a well-studied shallow sandy aquifer required a 2-D model that assumed both reversible and irreversible modes of bacterial attachment. Anisotropy of hydraulic conductivity was also shown to greatly influence the depth that microbial contamination emanating from a latrine pond can negatively impact groundwater quality. Kinetic attachment rates for *E. coli* measured in 10 cm columns were somewhat higher than modeled at the field scale, yielding a shorter 4-log10 removal distance even when hydraulic anisotropy and multiple rainfall events are accounted for. The underestimate in the maximum transport distance in the field predicted by the columns was only 39 78%, however, suggesting that predicting field-scale transport from laboratory studies could be within reach once the dependency of kinetic attachment and detachment rates upon temporally and spatially varying flow field and sediment size distribution are accounted for. This is important because non-

steady state conditions with multiple pulses of water are more typical of the natural environment, especially in places with extreme rainfall events.

A.8 Acknowledgments

This study was supported by Grant 5 R01 TW008066 from the NIH/FIC Ecology of Infectious Disease program, Grant W911NF-10-1-0123 from the Army Research Office, and in part by NIEHS Superfund Research Program Grant P42 ES010349. Thank you also to J. Simunek for guidance with Hydrus 2-D Lite and to S. Bradford for critical feedback. Four anonymous reviewers are thanked for contributing greatly to the improvement of this work.

A.9 Tables

Table A.1: Sensitivity analysis for K_h and anisotropy (K_h/K_v). Interaction parameters (k_a, k_d, k_i) were derived for Anisotropy = 4, K_h = 32.8 m/d. The lower and upper range of K_h was substituted into the model, while keeping k_a, k_d, k_i constant and the goodness of fit was calculated (RMSE). The same was done for horizontal dispersivity (λ).

Anisotropy	RMSE hydraulic head (m)	$K_h = 26.8m/day$	$K_h = 32.8m/day$	$K_h = 38.9m/day$	$\lambda = 0.1m$	$\lambda = 0.5m$	$\lambda = 2.5m$
		RMSE E.coli (MPN/100ml)					
1	47						
4	11.6	157	99	132	171	99	145
5	12.8						
10	18						
15	17						

Table A.2: Manual Optimization of the attachment/detachment kinetic parameters for the 2-D flow and transport model.

k_a	k_d	k_i	RMSE	k_a/k_d
110	13.9	5.32	113.6	7.91
100	12.64	5.3	110.7	7.91
90	11.38	5.28	108.0	7.91
80	10.12	5.28	104.9	7.91
70	8.85	5.23	102.1	7.91
60	7.59	5.17	99.4	7.91
50	6.32	5.15	100.3	7.91
40	5.06	5.12	109.7	7.91
30	3.79	5.09	142.9	7.91

Table A.3: Best-fit Model Parameters for E. coli in Column Experiments performed using Sand from Base of Pond 1. The analytical model type refers to that extracted simply based on the peak steady-state breakthrough concentration which was taken to be the average normalized concentration (C/C_0) along the flat plateau. Assuming the advective flow regime was steady-state flow of 8 m/day, used in the column experiment, k_i was used to obtain the 4-log10 removal distance. The 1-D numerical modeling results were up-scaled by substitution into the calibrated, transient flow 2-D model. The results from the 2-D modeling are shown for comparison.

			Population 1			Population 2			Field Scale	
Experiment	Model Name	Model Type	$k_a(d^{-1})$	$k_d(d^{-1})$	$k_i(d^{-1})$	$k_i(d^{-1})$	BTC R^2	Retained R^2	Flow Regime	Removal Distance (m)
Column 3	Irreversible, Peak C/C_0	Analytical			197.7				Steady-State	0.4
	Irreversible	Numerical			227.1		0	0.5	Transient	1
	Reversible	Numerical	240.1	1.2			0.11	0.14	Transient	3.4
	Two mode	Numerical	159.1	43.9	184.1		0.46	0.38	Transient	2.4
	Two population	Numerical	130.2	7.3	71.4	842.5	0.54	0.86	Transient	3.4
Column 4	Irreversible, Peak C/C_0	Analytical			117.5				Steady-State	0.6
	Irreversible	Numerical			115.7		0.6	0.07	Transient	2.1
	Reversible	Numerical	132.6	0.9			0.81	0.22	Transient	4.3
	Two mode	Numerical	69.3	5.7	78.3		0.86	0.28	Transient	3.8
	Two population	Numerical	96.9	4.1	0	276.5	0.83	0.82	Transient	6.9
Field 2-D	Irreversible	Numerical			7.6		115.8		Transient	
	Reversible	Numerical	10.5	0.2			826		Transient	
	Two mode	Numerical	60	7.6	5.2		99		Transient	8.8